REPORT DOCUMENTATION PAGE

Form Approved
OMB No. 0704-0188

1. AGENCY USE ONLY *(Leave blank)*	2. REPORT DATE	3. REPORT TYPE AND DATES COVERED
	9 JUN 97	

4. TITLE AND SUBTITLE
LOOKING -FREE MIXED hp FINITE ELEMENT METHODS FOR LINEAR AND GEOMETRICALLY NONLINEAR ELASTICITY

5. FUNDING NUMBERS

6. AUTHOR(S)
LAWRENCE K CHILTON

7. PERFORMING ORGANIZATION NAME(S) AND ADDRESS(ES)
UNIVERSITY OF MARYLAND BALTIMORE COUNTY

8. PERFORMING ORGANIZATION REPORT NUMBER
97-013D

9. SPONSORING/MONITORING AGENCY NAME(S) AND ADDRESS(ES)
DEPARTMENT OF THE AIR FORCE
AFIT/CI
2950 P STREET
WRIGHT-PATTERSON AFB OH 45433-7765

10. SPONSORING/MONITORING AGENCY REPORT NUMBER

11. SUPPLEMENTARY NOTES

12a. DISTRIBUTION AVAILABILITY STATEMENT

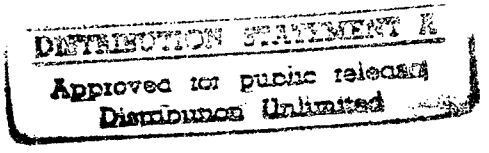

12b. DISTRIBUTION CODE

13. ABSTRACT *(Maximum 200 words)*

19970613 018

14. SUBJECT TERMS	15. NUMBER OF PAGES
	107
	16. PRICE CODE

17. SECURITY CLASSIFICATION OF REPORT	18. SECURITY CLASSIFICATION OF THIS PAGE	19. SECURITY CLASSIFICATION OF ABSTRACT	20. LIMITATION OF ABSTRACT

LOCKING-FREE MIXED *hp* FINITE ELEMENT METHODS FOR LINEAR AND GEOMETRICALLY NONLINEAR ELASTICITY

by
Lawrence K. Chilton

Dissertation submitted to the Faculty of the Graduate School
of the University of Maryland in partial fulfillment
of the requirements for the degree of
Doctor of Philosophy
1997

Lawrence K. Chilton
Department of Mathematics and Statistics

University of Maryland Baltimore County [redacted], 410-455-2412 (W)
Catonsville, MD 21228 email : lkchilt@math.umbc.edu

Personal Data

[redacted]

Education

Ph.D. Applied Mathematics, University of Maryland Graduate School Baltimore, 1997
M.S. Applied Mathematics, University of Illinois, Urbana-Champaign, 1988
Bachelor of Electrical Engineering, Auburn University, 1983

Professional Experience

1997 Assistant Professor, Department of Mathemetics and Statistics, Air Force Institute of Technology, Dayton, OH

1992-1994 Chief, Electronic Imaging Lab, NSA, Ft Meade, MD

1988-1992 Assistant Professor, Department of Mathemetical Sciences, United States Air Force Academy, Colorado Springs, CO

1983-1987 Avionic Systems Engineer, Foreign Technology Division, US Air Force Systems Command, Dayton, OH

Research Interests

The solution of partial differential equations by the finite element method. Particular areas of interest : *hp* versions, mixed methods, nearly incompressible materials, curvilinear domains, nonlinear elasticity.

Publications

L. Chilton and M. Suri, *On the selection of a locking-free hp element for elasticity problems*, International Journal for Numerical Methods in Engineering, Volume 40, 2045-2062, Springer-Verlag, 1997.

Conference Presentations

Finite Element Semi-Annual Conference, New York City, NY, *Mixed hp elements for linear and geometrically nonlinear elasticity*, April 1997.

Graduate Student Research Day, Baltimore, MD, *Numerical stability of finite element methods*, May 1996.

Finite Element Semi-Annual Conference, Baltimore, MD, *Computational Analysis of finite element methods for nearly incompressible linear easticity*, October 1995.

ABSTRACT

Title of Dissertation: Locking-free mixed *hp* finite element methods for linear and geometrically nonlinear elasticity.

Lawrence K. Chilton, Doctor of Philosophy, 1997

Dissertation directed by: Dr. Manil Suri, Professor
Department of Mathematics and Statistics
University of Maryland Baltimore County

We consider the mixed formulation of the linear elasticity problem. We identify stable families of mixed finite element spaces for both curvilinear quadrilateral and triangular elements. We give conditions under which these elements converge at asymptotically optimal (or near-optimal) rates, both in terms of the mesh width h and polynomial degree p. We validate these findings computationally. Finally, we identify a mixed formulation for the geometrically nonlinear elasticity problem and experimentally investigate the stability of our mixed finite element spaces for this problem.

ACKNOWLEDGMENTS

I am extremely grateful to Professor Manil Suri for his guidance, encouragement and friendship throughout my graduate education. I wish to thank those who kindly agreed to serve on my dissertation committee, Dr. Thomas Seidman, Dr. Vadim Korneev, Dr. Sonia Garcia and Dr. Rouben Rostamian for their time and helpful comments. Thanks also go to Professors Thomas Armstrong, Muddappa Gowda, and the late Søren Jensen, for their inspired instruction. Finally, I thank my family for their unwaivering support.

Contents

Chapter 1

Introduction

Finite element methods use polynomials to approximate the solution to boundary value problems over some subdivision (mesh) of the domain. The traditional method, called the h version, involves keeping the degree of the approximating polynomial fixed, usually at a low level, and achieves accuracy by properly refining the mesh. A more recent method is the p version, where the mesh is fixed and accuracy is achieved by increasing the degree of the polynomial approximation. The hp version is a combination of these two approaches.

Currently, there are several commercial finite element codes available or under development including RASNA, PHLEX, STRESSCHECK, and IBM-POLYFEM that offer these new p and hp methods. Moreover, codes well established in industry, such as MSC/NASTRAN, are being equipped with p/hp technology.

Codes with hp capabilities allow the user to selectively employ a combination of h-

refinement and p-refinement to achieve accuracy. For example, a highly refined mesh with low p may be used near corners, while large elements with high p may be used in the interior. The selection of h and p may also be done *adaptively.*

The increased flexibility afforded by such hp codes puts increased demands on the underlying variational method and elements being used. The code must now be robust with respect to *both* h-refinement and p-refinement. Various quantities of engineering interest, in particular the displacements and stresses, should be calculated robustly and optimally for the type of refinement chosen. The correct design of elements and underlying method is therefore crucial.

For many materials and geometries, this level of robustness is easily realized by using the standard finite element method (SFEM). However, in the case of isotropic linear elasticity, if the material is *almost incompressible* (Poisson ratio ν close to $\frac{1}{2}$), the SFEM can lead to dilational (or Poisson ratio) locking (see e.g. [1, 6, 13, 25]). Locking is when the rate of convergence decreases as $\nu \to \frac{1}{2}$. In severe cases the method may not converge to the correct solution at all. This is an important exception since almost incompressible materials are commonly used in industry. Natural rubber is almost incompressible and materials that undergo plastic deformations may also be considered almost incompressible [23]. Certain biological tissues are also considered nearly incompressible. Also, the limiting case of $\nu = \frac{1}{2}$ reduces to Stokes problem, which is obviously of great importance in fluid flow problems.

In the context of isotropic linear elasticity under conditions of *plane strain*, it

is well known from computational experience that locking occurs in various finite element schemes. For example, with ν close to 0.5, the h version using piecewise linear polynomials on triangular meshes produces a very poor approximation of the displacements. However, in 1985, Scott and Vogelius (see [18] and [19]) showed that the h version is locking free for both displacements and pressures [1] when polynomials of degree $k \geq 4$ are used on certain triangular meshes. [2] They showed that locking can also be avoided for $k < 4$ if very specialized meshes can be constructed. In 1992, Babuška and Suri [1] characterized displacement locking for $k < 4$, which was shown to depend not only on k but also on the mesh. They also showed that for two types of rectangular elements, locking cannot be avoided for any k.

The p version has long been known to be locking-free for displacements. In 1983, Vogelius [26] showed that for computing displacements on triangular meshes, the p version converges uniformly in ν, with optimal rate up to an arbitrary $\varepsilon > 0$. Babuška and Suri [1] removed the dependence on ε in the locking-free rate of convergence for the p version. They also showed this applies to parallelogram elements as well. However, the references cited here do not guarantee the pressures will be locking free for the p version (though results exist for the h version).

[1] We use the term "pressures" in place of stresses here because the quantity that suffers most due to locking is the sum of the normal stresses, which reduces to a multiple of the pressure in Stokes problem, i.e. in the limit $\nu = \frac{1}{2}$. (See equation(2.6).) We use the two terms interchangeably in the sequel.

[2] Since p will be used to denote *pressure*, we use k to denote polynomial degree.

Mixed methods have also been used to avoid locking. In these methods, an auxiliary variable related to the stresses is introduced, and the solution is found as a saddle point, rather than the minimum of the energy functional. Several mixed p-type elements have been studied for the Stokes problem in the context of the spectral element method[4]. If chosen appropriately they converge well in both displacements and pressures. This is also true for h version mixed methods. The difficulty lies in choosing the mixed method spaces correctly. As shown in [10], if the spaces are not properly balanced, mixed methods may converge at less than optimal rates, or they may may not converge at all. It is well known [6] that mixed method spaces must satisfy an inf-sup (Babuška - Brezzi) condition to be stable and that choosing such spaces can be difficult. More specifically, identifying spaces and proving that they are both stable and nearly optimal can be difficult.

The problem of hp mixed methods has been addressed by Stenberg and Suri[20]. They identify sufficient conditions for selecting mixed method spaces on parallelogram elements that produce nearly optimal and stable methods. Using these conditions, they identify several mixed methods. They show that these mixed method elements are optimal in both displacements and pressures for h-refinement, and that p-refinement produces at worst $O(k^{\varepsilon})$ locking in displacements and $O(k^{\frac{1}{2}+\varepsilon})$ locking in pressures. However, this study did not include any numerical verification of these methods.

In the p version, since the element size remains fixed, curved elements are essential for practical problems. In [22], some experiments with curved elements showed that

both the h and p versions of SFEM show increased locking in the displacements when curved elements are used. For mixed h version methods, the $Q_2 - \mathcal{P}_0$ element (see [6]) is known to be stable for curved elements, as are some other elements.

Our goal in this dissertation is to identify finite element methods that compute both displacements and stresses with uniform, near optimal accuracy for any $\nu \in [0, \frac{1}{2})$, when either h- or p-refinement is used. In addition, the methods should provide nearly optimal performance on domains of practical interest, which include curvilinear domains.

Several definitions and descriptions are needed throughout this dissertation; these are given in Chapter 2. We describe the differential and variational forms of linear elasticity and the associated finite element methods. We then define locking and related issues.

In Chapter 3 we do a computational study of finite element methods on parallelogram elements. We summarize the available theory mentioned above so we can compare this with our computational results. We examine the mixed methods from [20] to see how they perform numerically. In [20], it was stated that the inf $-$ sup constant for these methods decayed at a rate no worse than $k^{-\frac{1}{2}}$ — we validate this numerically. The conditions used in [20] to define mixed methods indicate that a traditional spectral element, $Q^k - Q^{k-2}$, is not an optimal choice. This is because the polynomial space for pressures should be one degree less than the displacements, and not two. We computationally compare this element with mixed methods from [20]

and show that the $Q^k - Q^{k-2}$ element is indeed less than optimal. We also show that for a model problem these methods work well for computing both displacements and pressure. The SFEM is also compared with these mixed methods .

We turn our attention to straight sided triangular elements in Chapter 4. The results in [26] imply that the divergence-stability constant for the p version SFEM on triangular elements is $k^{-\alpha}$ for some unknown $\alpha > 0$. Since triangular elements are used extensively in several hp commercial codes, we investigate their performance computationally as $\nu \to 0.5$. We find that the stresses can be extracted fairly accurately, which suggests that α in the estimate from [26] is small. However, when we evaluate curved triangular elements, we find that stress extraction is less satisfactory. We therefore seek mixed methods for which a better characterization of the $\inf - \sup$ constant can be made. These mixed triangular elements are formulated to satisfy the conditions outlined for parallelograms in [20]. One of these elements was analyzed in [17], where a lower bound of k^{-3} was obtained on the $\inf - \sup$ constant. We show that this bound of k^{-3} is quite pessimistic in the range of k used in practice by (a) computing the $\inf - \sup$ constant numerically and (b) testing the rate of convergence computationally for some test problems. Let us mention that the elements we consider use discontinuous pressures. In the case of a continuous pressure space, Boillat [5] showed that the divergence-stability constant behaves like $k^{-2}\left(\sqrt{\ln k}\right)^{-1}$ for the p version based on Taylor-Hood elements.

Since curved elements are essential for p version meshes, in Chapter 5 we invest-

igate locking on curved elements. We prove that on a single curved element, the displacement error behaves like $(k-\alpha)^{-r}$ where α depends on the mapping from a reference element to the curvilinear element. Next, we consider the mixed methods from [20] on curved elements and show how the stability constant can be estimated for curvilinear meshes. We use this result to compute inf $-$ sup constants for several maps and show that they are stable for practical elements. We also formulate a new curvilinear quadrilateral element and show that the inf-sup constant for this element is bounded below by $Ck^{-\frac{1}{2}}$. This is the same bound as for parallelogram elements.

When the pressure is of interest, we show that the p version SFEM shows significant deterioration when curved elements are used. We show experimentally that this effect is worse when elements are curved at the boundary as opposed to having curved interior edges. We also perform experiments to show that the mixed methods from Chapters 3 and 4 are robust for a model problem.

As a final test, in Section 5.4, we use a benchmark problem from [25] to investigate the performance of SFEM and a mixed method for computing point values of stresses. In [25], Szabo, Babuška and Chayapathy showed that SFEM is ineffective for computing point values of the sum of normal stress and proposed a post-processing method to overcome this shortcoming. We demonstrate that curvilinear mixed method elements can be used to accurately extract these point values.

Recently, Noël and Szabo [16] proposed a spatial formulation for geometrically nonlinear elasticity. They showed that their SFEM works well on many problems when

ν is not close to 0.5. In Chapter 6, we reformulate this problem with a mixed method and investigate locking of the standard and the mixed method. We find that while the standard method produces erratic results when computing point values of stresses, the mixed method eliminates the oscillations. This result mirrors that of Section 5.4 for a linear problem. Our results therefore suggest that the mixed methods discussed here can be applied to eliminate locking in such non-linear problems as well.

The overall conclusion of this thesis is that the mixed methods investigated here are excellent candidates for *hp* implementation when a robust code is desired.

Notation

In this dissertation, we shall denote the n-dimensional Euclidean space by $\mathbb{R}^n$, with $\mathbf{x} = (x_1, x_2)$ or $\mathbf{x} = (x, y)$ and $|\mathbf{x}| = (x^2 + y^2)^{1/2}$. We also denote the set of non-negative integers by $\mathbb{N}$. If Q is any one- or two-dimensional set, $\overline{Q}$ denotes its closure. By Ω we denote a domain in $\mathbb{R}^2$ with boundary $\partial\Omega$. By $H^r(\Omega)$ we denote the Sobolev space of functions on Ω with square integrable generalized derivatives of order $\leq r$ $(r \geq 0)$ furnished with the norm

$$\|u\|^2_{H^r(\Omega)} := \|u\|^2_{r,\Omega} = \sum_{0 \leq |\alpha| \leq r} \|D^\alpha u\|^2_{L^2(\Omega)},$$

where $\alpha = (\alpha_1, \alpha_2)$, $\alpha_i \geq 0$, $i = 1, 2$ integers, $|\alpha| = \alpha_1 + \alpha_2$, and

$$D^\alpha u = \frac{\partial^{|\alpha|} u}{\partial x_1^{\alpha_1} \partial x_2^{\alpha_2}}.$$

As usual, $H^0(\Omega) = L^2(\Omega)$. For functions $u, v \in L^2(\Omega)$, (u, v) will denote the usual L^2 inner product. We denote

$$L_0^2(\Omega) = \left\{ u \in L^2(\Omega) : \int_\Omega u \, dx = 0 \right\}.$$

Also,

$$H_0^1(\Omega) = \left\{ u \in H^1(\Omega) : u = 0 \text{ on } \partial\Omega \right\},$$

and we will further use the semi-norm notation

$$|u|_{r,\Omega}^2 = \sum_{|\alpha|=r} \|D^\alpha u\|_{0,\Omega}^2 .$$

Throughout this dissertation, the letter C will be used to denote generic positive constants, possibly not the same in each occurrence. Finally, K will refer to an element in a finite element mesh C_h on a domain Ω.

Chapter 2

Preliminaries

2.1 The Standard and Mixed Methods for Linear Elasticity

The differential form of the equations of isotropic linear elasticity consists of three relationships. They include the *equilibrium* equations

$$-\sigma_{ij,j} = f_i \quad \text{on} \quad \Omega, \tag{2.1a}$$

the *constitutive* relation for isotropic plane strain

$$\sigma_{ij} = \lambda \,\mathrm{div}\mathbf{u}\, \delta_{ij} + 2\mu\epsilon_{ij}(\mathbf{u}), \tag{2.1b}$$

and the *deformation* (strain) tensor

$$\epsilon_{ij}(\mathbf{u}) = \frac{1}{2}(u_{i,j} + u_{j,i}), \tag{2.1c}$$

which relates the displacement $\mathbf{u} = (u_1, u_2)$ to the strain. We let $\mathbf{u} = 0$ on Γ_0 and $\sigma_{ij} n_j = g_i$ on Γ_1, where $\partial\Omega = \Gamma_0 \cup \Gamma_1$ and $\Gamma_0 \cap \Gamma_1 = \emptyset$. Let $0 \leq \nu < 0.5$ be the Poisson ratio and E the modulus of elasticity, and define the Lamé constants

$$\lambda = \frac{E\nu}{(1+\nu)(1-2\nu)}, \quad \mu = \frac{E}{2(1+\nu)}. \tag{2.2}$$

Then the variational form of our problem is: Find $\mathbf{u} \in \mathbf{V}$ such that for all $\mathbf{v} \in \mathbf{V}$,

$$2\mu(\varepsilon(\mathbf{u}), \varepsilon(\mathbf{v})) + \lambda(\operatorname{div} \mathbf{u}, \operatorname{div} \mathbf{v}) = F(\mathbf{v}), \tag{2.3}$$

where

$$F(\mathbf{v}) = \iint_\Omega \mathbf{f} \cdot \mathbf{v}\, dx + \int_{\Gamma_1} \mathbf{g} \cdot \mathbf{v}\, ds$$

and $\mathbf{V} = [H^1(\Omega)]^2$. For the case $\Gamma_0 = \emptyset$, we assume that $F(\mathcal{R}) = 0$ for any rigid body motion $\mathcal{R}$. This ensures that (2.3) has a unique solution (modulo rigid body motions — these are assumed eliminated in computations by suitable constraints).

Given a sequence of finite element subspaces $\{\mathbf{V}_N\}$, $\mathbf{V}_N \subset \mathbf{V}$, we define the standard finite element approximation to (2.3) as: Find $\mathbf{u}_N \in \mathbf{V}_N$ such that for all $\mathbf{v} \in \mathbf{V}_N$,

$$2\mu(\varepsilon(\mathbf{u}_N), \varepsilon(\mathbf{v})) + \lambda(\operatorname{div} \mathbf{u}_N, \operatorname{div} \mathbf{v}) = F(\mathbf{v}). \tag{2.4}$$

We identify the parameter N with the dimension of the subspace $\mathbf{V}_N$. Associated with this standard method, we define the *energy norm*

$$\|\mathbf{u}\|_{E,\nu} = \left(2\mu\|\varepsilon(\mathbf{u})\|_0^2 + \lambda\|\operatorname{div}(\mathbf{u})\|_0^2\right)^{\frac{1}{2}}. \tag{2.5}$$

Next, we describe the mixed formulation. We define the new independent unknown

$$p = -\lambda \operatorname{div} \mathbf{u}, \tag{2.6}$$

which is a multiple of the sum of the normal stresses, i.e. $p = \frac{-\lambda}{2(\lambda+\mu)}(\sigma_{11} + \sigma_{22}) = \frac{-\lambda}{2(\lambda+\mu)}(\sigma_x + \sigma_y)$ [1]. (As $\lambda \to \infty$, this corresponds to the *pressure* in the limiting Stokes equations.) Then (2.3) is written in the Herrmann variational form [9]: Find $(\mathbf{u}, p) \in \mathbf{V} \times W$ such that for all $(\mathbf{v}, q) \in \mathbf{V} \times W$,

$$2\mu\left(\varepsilon\left(\mathbf{u}\right), \varepsilon\left(\mathbf{v}\right)\right) - \left(p, \operatorname{div} \mathbf{v}\right) = F\left(\mathbf{v}\right) \tag{2.7}$$

$$\left(\operatorname{div} \mathbf{u}, q\right) + \frac{1}{\lambda}\left(p, q\right) = 0 \tag{2.8}$$

where $W = L^2\left(\Omega\right)$.

For the mixed finite element method, we assume we are given a sequence of finite element subspaces $(\mathbf{V}_N \times W_N) \subset \mathbf{V} \times W$ and find $(\mathbf{u}_N, p_N) \in (\mathbf{V}_N \times W_N)$ such that

$$2\mu\left(\varepsilon\left(\mathbf{u}_N\right), \varepsilon\left(\mathbf{v}\right)\right) - \left(p_N, \operatorname{div} \mathbf{v}\right) = F\left(\mathbf{v}\right) \tag{2.9}$$

$$\left(\operatorname{div} \mathbf{u}_N, q\right) + \frac{1}{\lambda}\left(p_N, q\right) = 0 \tag{2.10}$$

for all $(\mathbf{v}, q) \in \mathbf{V}_N \times W_N$. The correct analog of the "energy norm" for mixed methods should be

$$\|u\|_{E,\nu} = \left(2\mu\|\varepsilon\left(\mathbf{u}\right)\|_0^2 + \lambda^{-1}\|p\|_0^2\right)^{\frac{1}{2}}. \tag{2.11}$$

As is well known [6], the accuracy of this method will not only depend upon how well $\mathbf{V}_N, W_N$ *approximate* $\mathbf{V}, W$ respectively, but also the *stability* of the pair

[1] Note that $\sigma_{11} = \sigma_x$ and $\sigma_{22} = \sigma_y$.

$(\mathbf{V}_N, W_N)$ (i.e., the inf-sup or Babuška-Brezzi condition satisfied by them). This is made precise in the following.

Theorem 2.1 *[6] Suppose* $(\mathbf{V}_N \times W_N) \subset (\mathbf{V} \times W)$ *and let* $(\mathbf{u}, p)$ *satisfy (2.7) and (2.8) and let* $(\mathbf{u}_N, p_N)$ *satisfy (2.9) and (2.10). If there exists* $\beta > 0$ *such that*

$$\inf_{q \in W_N} \sup_{\mathbf{v} \in \mathbf{V}_N} \frac{|(q, \operatorname{div} \mathbf{v})|}{\|q\|_0 \|\mathbf{v}\|_1} \geq \beta \tag{2.12}$$

then

$$\|\mathbf{u} - \mathbf{u}_N\|_1 + \|p - p_N\|_0 \leq C \left(\inf_{\mathbf{v} \in \mathbf{V}_N} \|\mathbf{u} - \mathbf{v}\|_1 + \inf_{q \in W_N} \|p - q\|_0 \right).$$

2.2 Locking

Before we give the formal definitions relative to locking, we explain the practical meaning by way of an example. In (2.4) we see that if $\lambda \to \infty$, the term $(\operatorname{div} \mathbf{u}_N, \operatorname{div} \mathbf{v})$ must approach zero for the equation to have meaning. This forces $\operatorname{div} \mathbf{u}_N \to 0$. When the finite element space is not rich enough to simultaneously satisfy this constraint and approximate $\mathbf{u}$ well, we can expect poor performance. In linear elasticity, $\lambda \to \infty$ has physical meaning; it is the case of nearly incompressible materials.

We illustrate what can happen as $\lambda \to \infty$ in Figure 2.1, which duplicates Figure 4.2. This shows the results of using the h version SFEM to solve (2.4) on a uniform triangular mesh. Recall that λ is related to ν by (2.3), and $\lambda \to \infty$ is equivalent to $\nu \to \frac{1}{2}$. We see that when $k = 2$ the rate of convergence in energy norm changes from $O(h^2)$ when $\nu = 0.3$ to $O(h)$ when $\nu = 0.4999$. In contrast, when $k = 4$, the energy

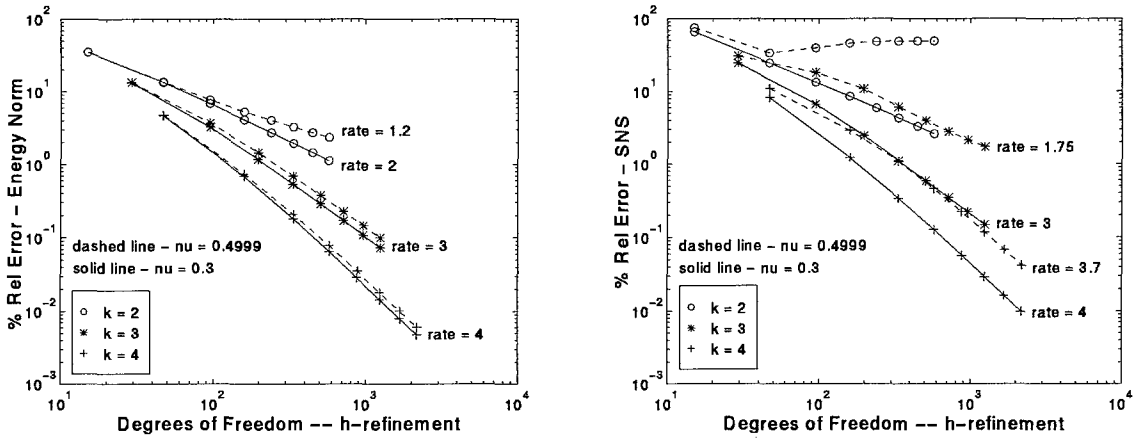

Figure 2.1: ST, h-refinement, Smooth Solution.

norm error curves for $\nu = 0.3$ and 0.4999 are nearly identical. This deterioration in the energy norm rate of convergence as $\nu \to \frac{1}{2}$ is known as *locking.* Notice that locking also occurs when $k = 2$ for the SNS (sum of normal stresses) relative error. When $\nu = 0.4999$ the error curve actually increases as h decreases. Another important effect is observed when $k = 4$ for the SNS error. The curves for $\nu = 0.3$ and 0.4999 have the same slope, but the $\nu = 0.4999$ curve is shifted up relative to $\nu = 0.3$ curve. This shift at a given level of refinement is referred to as the *locking ratio.* A desirable feature of a finite element method is to be free of locking and to have a locking ratio near unity over the range of discretizations of interest.

We now make these concepts more precise. We will need the following ingredients for our definitions [22].

1. Solution space $\mathbf{H}_\nu$. We assume that our exact solutions $\mathbf{s}_\nu$ lie in some sets $\mathbf{H}_\nu$, which characterize the smoothness of $\mathbf{s}_\nu$. For solutions $\mathbf{s}_\nu$ of comparable

smoothness we expect comparable results, so we will define locking with respect to the family $\{\mathbf{H}_\nu\}$. We assume that $\|\cdot\|_{\mathbf{H}_\nu}$ is a norm on $\mathbf{H}_\nu$ and define for any $B > 0$, the set

$$\mathbf{H}_\nu^B = \{\mathbf{s}_\nu \in \mathbf{H}_\nu : \|\mathbf{s}_\nu\|_{\mathbf{H}_\nu} \leq B\}.$$

2. Error functional E_ν. Next, we assume we are interested in a certain functional $E_\nu : \mathbf{s}_\nu \to \mathbb{R}$. We will be interested in the H^1 norm of the displacement and the L^2 norm of the sum of normal stresses. We should point out that locking is closely coupled to the error functional. A method may be locking free in one error measure but show significant locking in another.

3. Extension procedure $\mathcal{E}$. We assume there is a sequence of finite element spaces $\mathcal{E} = \{\mathbf{V}_N\}$. Then $\mathcal{E}$ gives an *extension procedure*, i.e. a rule on how to increase the dimension N (e.g. by the h version, p version, etc.). We assume here that N ranges over a set $\mathcal{N}$. As we shall see, locking is strongly dependent on $\mathcal{E}$.

4. Parameter set S. Our parameter here is ν, the Poisson ratio, which we assume varies over the set $S = \{\nu : 0 \leq \nu < 0.5\}$. (In computations, we will often take $S = \{0.3, 0.4999\}$.

We first define locking ratio.

Definition 2.1 *The function $L(\nu, N)$, called the locking ratio for $(\nu, N) \in S \times \mathcal{N}$, is*

given by

$$L(\nu, N) = \frac{\sup_{\mathbf{u}_\nu \in \mathbf{H}_\nu^B} E_\nu(\mathbf{u}_\nu - \mathbf{u}_\nu^N)}{\inf_{\nu \in S_\alpha} \sup_{\mathbf{w}_\nu \in \mathbf{H}_\nu^B} E_\nu(\mathbf{w}_\nu - \mathbf{w}_\nu^N)}, \tag{2.13}$$

where $S_\alpha = S \cap (-\infty, \alpha]$ for some $\alpha < 0.5$ such that $S_\alpha \neq \emptyset$.

Obviously, L also depends on $\mathbf{H}_\nu, E_\nu, \mathcal{E}$ and S_α. It compares the performance of the method at Poisson ratio ν to the best possible performance for *reasonable* values of ν, characterized by $\nu \leq \alpha$.

Let us now present the definition of locking ([2], [1]), for the case that $\alpha > 0$.

Definition 2.2 *The extension procedure $\mathcal{E}$ is locking free for $\nu \in [0, 0.5)$, with respect to the solution sets $\mathbf{H}_\nu$, and error measures E_ν, if and only if*

$$\limsup_{N \to \infty} \left(\sup_{\nu \in [0, 0.5)} L(\nu, N) \right) = C < \infty.$$

$\mathcal{E}$ shows locking of order $f(N)$ if and only if

$$0 < \limsup_{N \to \infty} \left(\sup_{\nu} L(\nu, N) \frac{1}{f(N)} \right) = C < \infty$$

where $f(N) \to \infty$ as $N \to \infty$.

The denominator in (2.13) can be replaced by $F_0(N)$, the *asymptotic rate of best approximation* in $H^1(\Omega)$ of functions in $H^k(\Omega)$ by functions in V_N,

$$F_0(N) = \sup_{w \in (H^k)^B} \inf_{v \in V_N} \|w - v\|_{1,\Omega},$$

which represents the smallest error which could be achieved using V_N to approximate the most unfavorable w in $(H^k)^B$. For example, for the h version, $F_0(N) = O(h^\mu) =$

$O(N^{-\frac{\mu}{2}})$ where $\mu = \min\{k-1, p\}$, while for the p version, $F_0(N) = O(p^{-(k-1)}) = O(N^{-\frac{k-1}{2}})$.

For the standard method, we are interested in two error functionals:

1. The H^1 norm of the displacement error (which is equivalent to the energy norm (2.5)).

2. The L^2 norm of the error in the sum of normal stresses, SNS (which is computed by differentiating the displacement).

For the mixed method, we use the same error measures, but we compute the energy norm using (2.11) and we compute SNS directly, since it is a scalar multiple of the independent variable p.

Chapter 3

Parallelogram Elements

We describe the SFEM and several mixed methods [20] on parallelogram elements. We show experimentally that for these mixed methods the inf $-$ sup constant does indeed decay like $k^{-\frac{1}{2}}$. We then summarize the rates of convergence for these methods. For a model problem, we show that these methods are locking free for computing both displacements and pressure. We also compare the SFEM with these mixed methods.

3.1 Approximation Spaces

3.1.1 General conditions for stability and approximability

We begin with the notation and definitions needed to define the finite element spaces we will use. We do this here not only for parallelogram elements, but for the other elements considered in this thesis as well.

Assume that a sequence of meshes $\{\mathcal{C}_h\}$ consisting of (curvilinear) quadrilaterals and/or triangles is defined on Ω, which is regular in the following sense [7]:

i) The intersection of two elements in $\mathcal{C}_h$ consists of one point (a vertex), one entire common edge or the empty set,

ii) There exists a constant σ such that

$$\forall K \in \mathcal{C}_h, \ \frac{h_K}{\rho_K} \leq \sigma.$$

Here, h_K is the diameter of K and ρ_K is the diameter of the largest inscribed ball in K. $\mathcal{C}_h$ does not have to be quasi-uniform (see Remark 3.3 below). For $K \in \mathcal{C}_h$, we denote $\mathcal{F}_K$ to be the smooth invertible mapping from the reference element $\hat{K}$ onto K, where $\hat{K} = [-1,1]^2$ when K is a quadrilateral and $\hat{K} = \{(x,y) : -1 \leq x \leq 1, -1 \leq y \leq -x\}$ when K is a triangle. (Further restrictions on $\mathcal{F}_K$ will be imposed in the chapter on curvilinear elements.)

Let $\mathbf{V}_k(\hat{K})$ and $W_k(\hat{K})$ be, respectively, the spaces for $\mathbf{u}$ and p on $\hat{K}$, consisting of polynomials of degree related to k. Define for any $K \in \mathcal{C}_h$,

$$\begin{aligned} \mathbf{V}_k(K) &= \left\{\mathbf{v} = \hat{\mathbf{v}} \circ \mathcal{F}_K^{-1} : \hat{\mathbf{v}} \in \mathbf{V}_k(\hat{K})\right\}, \\ W_k(K) &= \left\{p = \hat{p} \circ \mathcal{F}_K^{-1} : \hat{p} \in W_k(\hat{K})\right\}. \end{aligned} \tag{3.1}$$

Then with $N = N(h,k)$, the finite element spaces are defined as

$$\begin{aligned} \mathbf{V}_N &= \left\{\mathbf{v} \in \mathbf{V} : \mathbf{v}_{|K} \in \mathbf{V}_k(K) \ \forall K \in \mathcal{C}_h\right\}, \\ W_N &= \left\{p \in W : p_{|K} \in W_k(K) \ \forall K \in \mathcal{C}_h\right\}, \end{aligned} \tag{3.2}$$

where $\mathbf{V}$ and W are the solution spaces for (2.7) and (2.8). We will denote by $\mathcal{P}_k(\hat{K})$ the set of polynomials of *total* degree k on $\hat{K}$, while $Q_k(\hat{K})$ will be the set of polynomials of degree k in *each* variable. The serendipity or trunk space $Q'_k(\hat{K})$ will be span $\left\{\mathcal{P}_k(\hat{K}), x^k y, x y^k\right\}$.

As noted earlier, the mixed method spaces we consider are based on [20]. In that paper, six conditions are given for selecting mixed method spaces $\mathbf{V}_k, W_k$ on parallelogram elements.[1] These conditions motivate the choice of the mixed finite element spaces, and are central to arguments developed in later chapters. Since we are interested in extending the mixed methods of [20] to more general meshes, (including straight sided triangular and curvilinear triangular and quadrilateral meshes), we will list a more general form of two of these conditions.

The first condition in [20] is that identical subspaces are used for both displacement components, i.e.,

(A1) $\quad \mathbf{V}_k(\hat{K}) = [V_k(\hat{K})]^2.$

Let $V_k^0(\hat{K}) = V_k(\hat{K}) \cap H_0^1(\hat{K})$ denote the set of internal shape functions used for all components of the displacement, so that $\mathbf{V}_k^0(\hat{K}) = \mathbf{V}_k(\hat{K}) \cap [H_0^1(\hat{K})]^2 = [V_k^0(\hat{K})]^2$. We note that there exists a space $X_k(\hat{K})$ such that

$$V_k^0(\hat{K}) = \{v | v = b_{\hat{K}} w,\ w \in X_k(\hat{K})\},$$

where $b_{\hat{K}}$ is the lowest degree "bubble function" on $\hat{K}$, the reference element (square

[1] The conditions from [20] are given for both $\mathbb{R}^2$ and $\mathbb{R}^3$. We restrict our presentation to $\mathbb{R}^2$.

or triangle). The second condition is that the space for the pressure satisfies the following.

(A2) $\nabla q \in [X_k(\hat{K})]^2 \ \forall \ q \in W_k(\hat{K})$.

Due to the definitions of the spaces V_k^0 and $X_k(\hat{K})$, we can define a weighted L^2 projection $\mathcal{T}_k : H_0^1(\hat{K}) \to V_k^0(\hat{K})$ by

$$(v - \mathcal{T}_k v, w)_{\hat{K}} = 0 \ \ \forall w \in X_k(\hat{K}). \tag{3.3}$$

The third condition is that the projection operator $\mathcal{T}_k$ satisfies

(A3) $\|\mathcal{T}_k u\|_{1,\hat{K}} \leq Ck^{\gamma}\|u\|_{1,\hat{K}}$ for some $\gamma > 0$.

Note that in [20], instead of a general γ, condition (A3) is stated with $\gamma = \frac{1}{2}$, since for parallelogram elements considered there, this can be proven.

Conditions (A1)-(A3) give a local stability condition for any element K for which $\mathcal{F}_K$ is linear. The following lemma follows from Lemma 5.1 of [20].

Lemma 3.1 *Let the spaces $\mathbf{V}_k(\hat{K}), W_k(\hat{K})$ satisfy conditions (A1)-(A3). Let $K = \mathcal{F}_K(\hat{K})$, where $\mathcal{F}_K$ is an affine mapping. Then for every $q^* \in W_k(K) \cap L_0^2(K)$ there exists $\mathbf{v}^* \in \mathbf{V}_k(K) \cap [H_0^1(K)]^2$ such that*

$$(\operatorname{div} \mathbf{v}^*, q^*)_K \geq C_1 k^{-\gamma}\|q^*\|_{0,K}^2 \text{ and } |\mathbf{v}^*|_{1,K} \leq C_2\|q^*\|_{0,K}, \tag{3.4}$$

where C_1, C_2 are positive constants independent of K, h, k and q^*.

Note that γ in (3.4) may be different over different K. In this case, the value chosen in (3.4) is the maximum.

Remark 3.1 *Let us remark that if (A1) and (A2) hold, then we can always define* $\mathcal{T}_k$ *by (3.3). For* $V_k^0(\hat{K}) \neq \emptyset$, *we will always have*

$$\|\mathcal{T}_k u\|_{1,\hat{K}} \leq C(k)\|u\|_{1,\hat{K}}$$

for some $C(k) < \infty$. *Then Lemma 3.1 holds with* $k^{-\gamma}$ *replaced by* $(C(k))^{-1}$. *Hence, (A1), (A2) are sufficient to ensure a unique solution to (2.9)-(2.10).*

As we shall see in later chapters, the best theoretical estimate available for γ *in (A3) is pessimistic for triangular elements, and unavailable for most curvilinear elements. In order to investigate such elements, we will estimate the local inf-sup condition (3.4) computationally. Once this local inf-sup constant has been estimated for all elements in a given mesh, the remaining theory developed in [20] is still applicable.*

We therefore formulate the following alternative condition to (A1)-(A3).

(LS) For every $K \in \mathcal{C}_h$, given $q^* \in W_k(K) \cap L_0^2(K)$, there exists $\mathbf{v}^* \in \mathbf{V}_k(K) \cap [H_0^1(K)]^2$ such that (3.4) holds.

Let $q \in W_N$ be arbitrary and write $q = \bar{q} + q^*$ with $\bar{q}$ being the L^2 projection of q onto the space of piecewise constants:

$$\bar{W}_N = \{q \in W_N : q_{|K} \in \mathcal{P}_0(K) \quad \forall K \in \mathcal{C}_h\}.$$

To have a global condition we need the following.

(A4) The pair $(\tilde{\mathbf{V}}_N, \bar{W}_N)$ is stable,

where $\tilde{\mathbf{V}}_N = \{\mathbf{v} : \mathbf{v}_{|K} = \hat{\mathbf{v}} \circ F_K^{-1} \text{ for some } \hat{\mathbf{v}} \in \mathbf{E}_2(\hat{K}) \ \ \forall K \in \mathcal{C}_h\}$, where $\mathbf{E}_2(\hat{K}) = [Q_2(\hat{K})]^2$ if $\hat{K}$ is the reference square and $\mathbf{E}_2(\hat{K}) = [\mathcal{P}_2(\hat{K})]^2$ if $\hat{K}$ is the reference triangle. Then we have the following, see [20, Theorem 5.1].

Theorem 3.1 *Let the spaces $\mathbf{V}_N, W_N$ satisfy conditions (A1)-(A4) or (LS),(A4). Then*

$$\sup_{\mathbf{v} \in \mathbf{V}_N \setminus \{\mathbf{0}\}} \frac{(\operatorname{div} \mathbf{v}, q)}{\|\mathbf{v}\|_1} \geq C k^{-\gamma} \|q\|_0 \ \forall q \in W_N, \tag{3.5}$$

where the constant C is independent of h, k and q.

The proof is similar to that of Theorem 5.2.

Finally, we will take the spaces $\mathbf{V}_k(\hat{K})$ and $W_k(\hat{K})$ to contain polynomials of degree k and $k-1-n$, respectively. Note that in order to get the optimal convergence rate in both h and k, we require $n = 0$. More precisely, we need the following conditions.

(A5) $[Q_k'(\hat{K})]^2 \subset \mathbf{V}_k(\hat{K})$ if $\hat{K}$ is the reference square,

$[\mathcal{P}_k(\hat{K})]^2 \subset \mathbf{V}_k(\hat{K})$ if $\hat{K}$ is the reference triangle.

(A6) $\mathcal{P}_{k-1-n}(\hat{K}) \subset W_k(\hat{K}), \ \ n \geq 0.$

We will assume that $k \geq 2$, i.e. we exclude the case with piecewise constant pressure.

3.1.2 Choice of Parallelogram Spaces

We now define our methods by fixing the choices of $V_k(\hat{K})$ and $W_k(\hat{K})$, when $\hat{K}$ is a parallelogram. We define the polynomial spaces

$\tilde{Q}_k(\hat{K}), Q_k^*(\hat{K}) \subset Q_k(\hat{K})$ by

$\tilde{Q}_k(\hat{K}) = Q_k(\hat{K}) \cap \mathcal{P}_{k+2}(\hat{K})$, and

$Q_k^*(\hat{K}) = Q_k(\hat{K})$ augmented by all bubble functions of degree $k+1$, i.e. $Q_k(\hat{K})$ together with functions in $Q_{k+1}(\hat{K})$ that vanish on $\partial\hat{K}$.

We then define the following methods[20]:

MQ1: $V_k(\hat{K}) = \left[\tilde{Q}_k(\hat{K})\right]^2$, $W_k(\hat{K}) = \mathcal{P}_{k-1}(\hat{K})$.

MQ2: $V_k(\hat{K}) = \left[Q_k(\hat{K})\right]^2$, $W_k(\hat{K}) = \mathcal{P}_{k-1}(\hat{K})$.

MQ3: $V_k(\hat{K}) = \left[Q'_{k+2}(\hat{K})\right]^2$, $W_k(\hat{K}) = \mathcal{P}_{k-1}(\hat{K})$.

MQ4: $V_k(\hat{K}) = \left[Q_k^*(\hat{K})\right]^2$, $W_k(\hat{K}) = Q_{k-1}(\hat{K})$.

MQ5: $V_k(\hat{K}) = \left[Q_k(\hat{K})\right]^2$, $W_k(\hat{K}) = Q_{k-2}(\hat{K})$.

MQ6: $V_k(\hat{K}) = \left[Q_k(\hat{K})\right]^2$, $W_k(\hat{K}) = Q_{k-2}(\hat{K}) \cup \mathcal{P}_{k-1}(\hat{K})$.

In addition, we define

SQ: $V_k(\hat{K}) = \left[Q'_k(\hat{K})\right]^2$.

The mixed method spaces MQ1 and MQ5 are illustrated for $k = 5$ in Figure 3.1, where spanning sets for $W_5(\hat{K})$ and one component of $V_5(\hat{K})$ are shown.

We note that given $W_k(\hat{K}) = \mathcal{P}_{k-1}(\hat{K})$ the minimal displacement space satisfying (A2) is $\left[\tilde{Q}_k(\hat{K})\right]^2$, the displacement space for MQ1. Comparing MQ2 or MQ3 with MQ1, we see that the only difference is that this minimal space has been replaced by a larger space. This increases the number of degrees of freedom without increasing

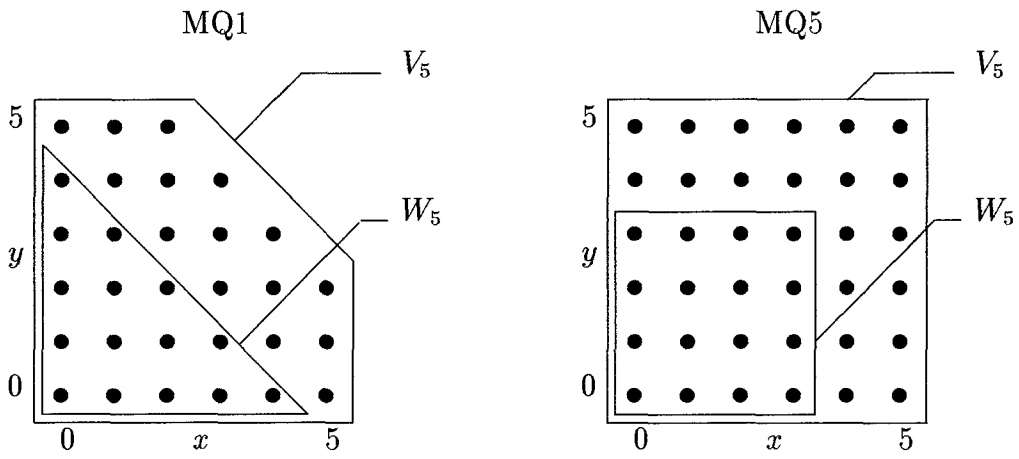

Figure 3.1: Polynomial spaces for MQ1 and MQ5 when $k = 5$.

the asymptotic approximation rate. (For instance, $Q_k(\hat{K})$ has dimension $(k+1)^2$ compared to $(k^2+7k)/2$ for $\tilde{Q}_k(\hat{K})$.)

On the other hand, MQ6 can be regarded as an optimized version of MQ5, where $V_k(\hat{K})$ has been kept fixed and the *maximal* space chosen for $W_k(\hat{K})$. This only involves adding two extra degrees of freedom per element, but, as Theorem 3.4 below shows, leads to an extra order in the asymptotic rate of h convergence. Similarly, in MQ4, the *minimal* space has been selected for $V_k(\hat{K})$ with the choice $W_k(\hat{K}) = Q_{k-1}(\hat{K})$, which again leads to an improved error estimate. (Note that $Q_K^*(\hat{K})$ contains extra bubble functions compared to $Q_k(\hat{K})$, but condensing out bubble functions is relatively cheap, see [24].)

We note that for SQ, MQ1-2,4-6, the displacement space has been chosen to satisfy

$$\left[Q_k'(\hat{K})\right]^2 \subset \mathbf{V}_k(\hat{K}),\ \left[Q_{k+1}'(\hat{K})\right]^2 \not\subset \mathbf{V}_k(\hat{K}).$$

This ensures that all the displacement spaces have the same $O(h^k)$ asymptotic approximability in the $\mathbf{H}^1(\Omega)$ norm with respect to the h version, thus facilitating the easy comparison of the various methods. While MQ3 does not have this property, it is useful for comparisons with SQ, since their displacement spaces are directly comparable.

The following corollary follows from Theorem 3.1 applied to parallelograms and shows that the above choices of spaces lead to mixed methods that satisfy a common inf-sup condition.

Corollary 3.1 [20] *Let the mappings $\mathcal{F}_K$ be affine, i.e. the elements are all parallelograms. For (V_N, W_N) defined as in MQ1-6 above,*

$$\inf_{q \in W_N} \sup_{\mathbf{v} \in V_N} \frac{(q, \operatorname{div} \mathbf{v})}{\|q\|_0 \, \|\mathbf{v}\|_1} = \rho_N \geq C k^{-\frac{1}{2}}, \tag{3.6}$$

where the constant C is independent of h and k.

Corollary 3.1 shows that the above combinations are stable with respect to h as $h \to 0$. Moreover, the spaces are almost stable with respect to k as $k \to \infty$, with the stability constant behaving like $Ck^{-\frac{1}{2}}$. (This loss is unavoidable, at least for MQ5, [4]).

3.2 Numerical Investigation of Inf-Sup Condition

For a given mixed method, we want to verify computationally that inequality (3.6) holds and since it is a lower bound, see if the bound is approached. We proceed

as in [10]. Let $\{\phi_i\}_{i=1}^m$ be a basis for $W_N(\Omega)$ and $\{\boldsymbol{\psi}_i\}_{i=1}^n$ be a basis for $\mathbf{V}_N(\Omega)$. Then $q \in W_N(\Omega)$ can be written $q = \sum_{i=1}^m \lambda_i \phi_i$ and $\mathbf{v} \in \mathbf{V}_N(\Omega)$ can be written $\mathbf{v} = \sum_{i=1}^n \alpha_i \boldsymbol{\psi}_i$. Then

$$(q, \operatorname{div} \mathbf{v}) = (\sum_{i=1}^m \lambda_i \phi_i, \sum_{j=1}^n \alpha_j \operatorname{div} \boldsymbol{\psi}_j) = \boldsymbol{\lambda}^T (\phi_i, \operatorname{div} \boldsymbol{\psi}_j) \boldsymbol{\alpha} = \boldsymbol{\lambda}^T \mathbf{B} \boldsymbol{\alpha},$$

where $\mathbf{B} = [(\phi_i, \operatorname{div} \boldsymbol{\psi}_j)]$ is $m \times n$, $\boldsymbol{\lambda}$ is $m \times 1$ and $\boldsymbol{\alpha}$ is $n \times 1$. Also

$$\|q\|_0^2 = (\sum_{i=1}^m \lambda_i \phi_i, \sum_{j=1}^m \lambda_j \phi_j) = \boldsymbol{\lambda}^T (\phi_i, \phi_j) \boldsymbol{\lambda} = \boldsymbol{\lambda}^T \mathbf{D} \boldsymbol{\lambda},$$

where $\mathbf{D} = [(\phi_i, \phi_j)]$ is $m \times m$. And

$$\|\mathbf{v}\|_1^2 = (\sum_{i=1}^n \alpha_i \boldsymbol{\psi}_i, \sum_{j=1}^n \alpha_j \boldsymbol{\psi}_j) + (\sum_{i=1}^n \alpha_i \boldsymbol{\psi}_{i,1}, \sum_{j=1}^n \alpha_j \boldsymbol{\psi}_{j,1}) + (\sum_{i=1}^n \alpha_i \boldsymbol{\psi}_{i,2}, \sum_{j=1}^n \alpha_j \boldsymbol{\psi}_{j,2}) = \boldsymbol{\alpha}^T \mathbf{C} \boldsymbol{\alpha},$$

where

$$\mathbf{C} = [(\boldsymbol{\psi}_i, \boldsymbol{\psi}_j) + (\boldsymbol{\psi}_{i,1}, \boldsymbol{\psi}_{j,1}) + (\boldsymbol{\psi}_{i,2}, \boldsymbol{\psi}_{j,2})]$$

is $n \times n$. The discrete $\inf - \sup$ constant ρ_N in (3.6) can then be characterized as

$$\min_{\substack{\boldsymbol{\lambda} \in \mathbb{R}^m \\ \boldsymbol{\lambda} \neq 0}} \max_{\substack{\boldsymbol{\alpha} \in \mathbb{R}^n \\ \boldsymbol{\alpha} \neq 0}} \frac{\boldsymbol{\lambda}^T \mathbf{B} \boldsymbol{\alpha}}{(\boldsymbol{\lambda}^T \mathbf{D} \boldsymbol{\lambda})^{\frac{1}{2}} (\boldsymbol{\alpha}^T \mathbf{C} \boldsymbol{\alpha})^{\frac{1}{2}}} = \rho_N > 0.$$

Since $\mathbf{C}$ and $\mathbf{D}$ are symmetric positive definite, we let

$$\boldsymbol{y} = \mathbf{D}^{\frac{1}{2}} \boldsymbol{\lambda}, \quad \boldsymbol{x} = \mathbf{C}^{\frac{1}{2}} \boldsymbol{\alpha}.$$

Then, the $\inf - \sup$ constant ρ_N can be written

$$\rho_N = \min_{\substack{\boldsymbol{y} \in \mathbb{R}^m \\ \boldsymbol{y} \neq 0}} \max_{\substack{\boldsymbol{x} \in \mathbb{R}^n \\ \boldsymbol{x} \neq 0}} \frac{\boldsymbol{y}^T \mathbf{D}^{-\frac{1}{2}} \mathbf{B} \mathbf{C}^{-\frac{1}{2}} \boldsymbol{x}}{(\boldsymbol{y}^T \boldsymbol{y})^{\frac{1}{2}} (\boldsymbol{x}^T \boldsymbol{x})^{\frac{1}{2}}}.$$

For a given $\boldsymbol{y}$, the maximum over $\boldsymbol{x}$ occurs when $\boldsymbol{y}^T\mathbf{D}^{-\frac{1}{2}}\mathbf{B}\mathbf{C}^{-\frac{1}{2}}$ and $\boldsymbol{x}$ are colinear, or

$$\gamma\mathbf{C}^{-\frac{1}{2}}\mathbf{B}^T\mathbf{D}^{-\frac{1}{2}}\boldsymbol{y} = \boldsymbol{x}.$$

Then

$$\rho_N = \min_{\substack{\boldsymbol{y}\in\mathbb{R}^m \\ \boldsymbol{y}\neq 0}} \frac{\gamma\boldsymbol{y}^T\mathbf{D}^{-\frac{1}{2}}\mathbf{B}\mathbf{C}^{-1}\mathbf{B}^T\mathbf{D}^{-\frac{1}{2}}\boldsymbol{y}}{(\boldsymbol{y}^T\boldsymbol{y})^{\frac{1}{2}}(\gamma^2(\boldsymbol{y}^T\mathbf{D}^{-\frac{1}{2}}\mathbf{B}\mathbf{C}^{-1}\mathbf{B}^T\mathbf{D}^{-\frac{1}{2}}\boldsymbol{y}))^{\frac{1}{2}}}$$

and

$$\rho_N^2 = \min_{\substack{\boldsymbol{y}\in\mathbb{R}^m \\ \boldsymbol{y}\neq 0}} \frac{\boldsymbol{y}^T\mathbf{D}^{-\frac{1}{2}}\mathbf{B}\mathbf{C}^{-1}\mathbf{B}^T\mathbf{D}^{-\frac{1}{2}}\boldsymbol{y}}{\boldsymbol{y}^T\boldsymbol{y}}$$

which is a Rayleigh quotient. This is minimized when

$$\mathbf{D}^{-\frac{1}{2}}\mathbf{B}\mathbf{C}^{-1}\mathbf{B}^T\mathbf{D}^{-\frac{1}{2}}\boldsymbol{y}_m = \rho_N^2\boldsymbol{y}_m$$

or

$$\mathbf{B}\mathbf{C}^{-1}\mathbf{B}^T\boldsymbol{u}_m = \rho_N^2\mathbf{D}\boldsymbol{u}_m \tag{3.7}$$

and ρ_N^2 is the smallest positive generalized eigenvalue of $(\mathbf{B}\mathbf{C}^{-1}\mathbf{B}^T, \mathbf{D})$. To verify (3.6) for a given mixed method we construct the matrices $\mathbf{B}$, $\mathbf{C}$ and $\mathbf{D}$ and solve (3.7) for the minimum positive eigenvalue.

In Figure 3.2, we show the results of numerically estimating the inf-sup constant ρ_N for MQ1 and MQ5. The finite element spaces are defined on a square of side 2, with four equal square elements of side 1 (with natural boundary conditions). The $O(k^{-\frac{1}{2}})$ deterioration is clearly observed for both elements, showing that the stability of MQ1 and MQ5 is similar. For the given mesh, the inf-sup constant for MQ5 is slightly larger, about 1.09 times the size of the inf-sup constant for MQ1. Similar computations were

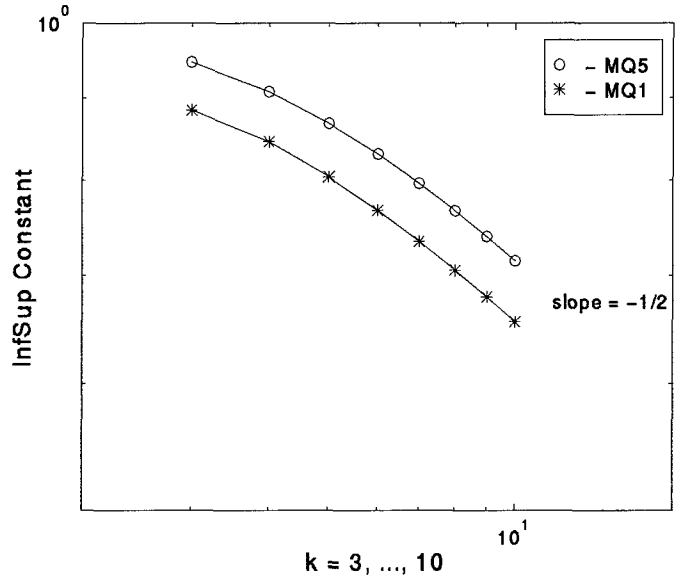

Figure 3.2: The inf-sup constant for MQ1 and MQ5

performed in [14] where they considered the homogeneous Dirichlet problem. The decay rate they found was less than what we show here. When comparing the actual magnitude, their inf-sup constant estimates are significantly less than our estimates, which is to be expected since the displacement space for the Dirichlet problem is a subspace of the displacement space of the Neumann problem.

3.3 Asymptotic Convergence Rates

We note that in SQ, the space $\mathbf{V}_k(\hat{K}) = \left[Q'_k(\hat{K})\right]^2$ is the minimal conforming space of polynomials of degree $\leq k$. This means that the asymptotic convergence rate in

terms of the $\mathbf{H}^1(\Omega)$ norm for SQ is

$$\|\mathbf{u}-\mathbf{u}_N\|_1 \leq C_1(\nu)\, h^{\min(k,r-1)} k^{-(r-1)} \|\mathbf{u}\|_r , \tag{3.8}$$

assuming the solution $\mathbf{u} \in \mathbf{H}^r(\Omega)$, $r > 1$. This is the asymptotic rate of best approximation referred to in Section 2.2. A method that produces this rate for all $\nu \in \left[0, \frac{1}{2}\right)$ is locking-free. The same rate will also be observed in the energy norm (2.5) of the error

$$\|\mathbf{u}-\mathbf{u}_N\|_{E,\nu} = \left(2\mu\|\varepsilon(\mathbf{u}-\mathbf{u}_N)\|_0^2 + \lambda\|\mathrm{div}\,(\mathbf{u}-\mathbf{u}_N)\|_0^2\right)^{\frac{1}{2}},$$

which is equivalent to the $\mathbf{H}^1(\Omega)$ norm for ν bounded away from 1/2. Also, defining for SQ

$$p_N = -\lambda\ \mathrm{div}\ \mathbf{u}_N, \tag{3.9}$$

we see that

$$\|p-p_N\|_0 \leq C_2(\nu)\, h^{\min(k,r-1)} k^{-(r-1)} \|\mathbf{u}\|_r . \tag{3.10}$$

The upper bound in (3.8),(3.10) represents the *optimal* asymptotic convergence rate for polynomials of degree k. Unfortunately, both constants C_1 and C_2 blow up as $\nu \to \frac{1}{2}$ $(\lambda \to \infty)$, so that this rate is not uniform if ν is allowed to vary in $[0, \frac{1}{2})$. The following theorem gives the best possible estimate *independent* of ν for the special case of a uniform rectangular mesh.

Theorem 3.2 [1] *Let* $\mathbf{u} \in H^r(\Omega)$, $r > 1$, *be the solution of* (2.3) *and let* $\mathbf{u}_N$ *be the solution obtained by SQ, using parallelogram elements. Then there exists a constant*

C independent of $\mathbf{u}$, h, k *and* $\nu \in [0, \frac{1}{2})$ *such that*

$$\|\mathbf{u} - \mathbf{u}_N\|_1 \leq C h^{\min(k-\alpha, r-1)} k^{-(r-1)} \|\mathbf{u}\|_r , \tag{3.11}$$

where $\alpha = 1$ *for* $k = 1, 2$ *and* $\alpha = 2$ *for* $k > 2$. *Moreover, this is the sharpest estimate that is uniform in* ν *for* $\nu \in [0, \frac{1}{2})$.

The same estimate in equation (3.11) also holds in the energy norm defined by (2.5). For results on other meshes, see [1].

We see from the above theorem that if the h version is used, the rate deteriorates by $O(h^2)$ as $\nu \to \frac{1}{2}$ ($O(h)$ if $k = 1, 2$). In terms of Definition 2.2 h-refinement for SQ has $O(h^{-2})$ locking for $k > 2$ and $O(h^{-1})$ locking for $k = 1, 2$ in the displacement. For the p version, there is no deterioration in the asymptotic convergence rate, i.e., p-refinement for SQ is locking-free in the displacements in the sense of Definition 2.2.

Remark 3.2 *The statement that there is no locking with the p version for displacements is somewhat misleading. Even though there is no deterioration in the* asymptotic rate *of convergence, the actual observed error does deteriorate, particularly with curved elements. In other words, the locking ratios defined in Definition 2.1 increase. See [22] and Chapter 5.*

Let us mention that if in SQ we take $V_k(\hat{K}) = \left[Q_k(\hat{K})\right]^2$ instead, then $\alpha = 1$ for all k in (3.11), so that this choice has $O(h)$ locking for h-refinement for all k.

Turning now to the mixed methods, we have the following theorems, which follow from Theorem 3.1.

Theorem 3.3 [20] *Let* $(\mathbf{u}, p)$ *the solution of (2.7)-(2.8) be in* $\mathbf{H}^r(\Omega) \times H^{r-1}(\Omega)$, $r > 1$. *Let* $(\mathbf{u}_N, p_N)$ *be the solution of MQ5 solving equations (2.9)-(2.10) with parallelogram elements. Then for any* $\varepsilon > 0$, *there exists a constant* C_ε *independent of* $\mathbf{u}$, h, k *and* $\nu \in [0, \frac{1}{2})$ *such that*

$$\|\mathbf{u} - \mathbf{u}_N\|_1 \leq C_\varepsilon h^{\min(k-1,r-1)} k^{-(r-1-\varepsilon)} \left(\|\mathbf{u}\|_r + \|p\|_{r-1} \right), \tag{3.12}$$

$$\|p - p_N\|_0 \leq C_\varepsilon h^{\min(k-1,r-1)} k^{-(r-\frac{3}{2}-\varepsilon)} \left(\|\mathbf{u}\|_r + \|p\|_{r-1} \right). \tag{3.13}$$

Theorem 3.4 [20] *Let* $(\mathbf{u}, p)$ *be as in Theorem 3.3 and* $(\mathbf{u}_N, p_N)$ *be the solution of MQ1-4,6 solving equations (2.9)-(2.10) with parallelogram elements. Then for any* $\varepsilon > 0$, *there exists a constant* C_ε *independent of* $\mathbf{u}$, h, k *and* $\nu \in [0, \frac{1}{2})$ *such that*

$$\|\mathbf{u} - \mathbf{u}_N\|_1 \leq C_\varepsilon h^{\min(k,r-1)} k^{-(r-1-\varepsilon)} \left(\|\mathbf{u}\|_r + \|p\|_{r-1} \right), \tag{3.14}$$

$$\|p - p_N\|_0 \leq C_\varepsilon h^{\min(k,r-1)} k^{-(r-\frac{3}{2}-\varepsilon)} \left(\|\mathbf{u}\|_r + \|p\|_{r-1} \right). \tag{3.15}$$

From the above, we observe that in terms of the p version, all the mixed methods are (like SQ) asymptotically free of locking in displacement (except for an $O(k^\varepsilon)$ factor, which comes in due to a technicality in the proof). In terms of the h version, MQ5 shows an $O(h^{-1})$ loss in the displacement rate of convergence when compared to the optimal estimate (3.8) (for $r \geq k+1$). Similarly, MQ3 shows an $O(h^{-2})$ loss in the displacement rate, since with Q'_{k+2} elements, we would expect $O(h^{k+2})$ convergence in the displacements for smooth solutions. However, these losses are *not* manifestations of locking, since the loss is observed for any ν. Rather, this is an *approximability* problem, since the space for p_N should be of one degree lower than that for $\mathbf{u}_N$ (and

not two degrees lower). Hence, all these methods are free of locking in displacement for h-refinement, and, in addition, MQ1,2,4,6 are correctly balanced.

Turning to the stresses, for the h version, the conclusions for locking are the same as those for displacements. For the p version, if we compare (3.13), (3.15) with the optimal rate in (3.10), we see a loss of $O(k^{\frac{1}{2}+\epsilon})$. Hence, we conclude that p-refinement gives rise to stress locking of order $O(k^{-(\frac{1}{2}+\epsilon)})$ for all the above mixed methods. As we see in the next section, this is a rather mild amount of locking, and does not show up in the model problems for the practical ranges of k used by us, giving a method that is essentially locking-free.

Let us mention that (3.12),(3.14) will not hold with $\|\mathbf{u}-\mathbf{u}_N\|_1$ replaced by the error $\|\mathbf{u}-\mathbf{u}_N\|_{E,\nu}$ defined by (2.5). The correct analog of the "energy norm error" for mixed methods is given in (2.11). With this definition of the energy norm, (3.12),(3.14) will hold once again.

Remark 3.3 *With proper mesh-degree selection, exponential rates of convergence may be obtained using the hp version. The estimates in Theorems 3.2 - 3.4 would then be improved, reflecting these exponential rates. Exponential convergence requires highly refined meshes in parts of the domain (e.g. at corners). Such meshes may be constructed even if the elements are all parallelograms by using "hanging nodes." See [11] for a discussion of a fully adaptive hp method (with hanging nodes) for the Stokes problem, based on MQ4. Also, see [17] where the hp-FEM is constructed by using both triangular and parallelogram elements to give such exponential rates of convergence*

on polygonal domains.

Remark 3.4 *The mixed methods described here may be generalized to three-dimensional parallelepiped elements, see [20]. The best stability constant in the 3-d case is* Ck^{-1}.

Remark 3.5 *In [20], Theorems 3.1, 3.3 and 3.4 above have actually been established for the more restrictive case of homogeneous* Dirichlet *boundary conditions. In that case, the spaces for the displacements are further restricted, so we can expect the locking to be more severe. In subsequent sections, it is shown that the MFEMs perform much better than SFEM with respect to locking, using test problems involving Neumann (traction) boundary conditions. For the case of a clamped boundary, we expect the difference in performance to be even more significant.*

3.4 Numerical Experiments

In this section, we investigate the computational performance of the methods SQ, MQ1-5, both with h- and p-refinement. Our results support the theoretical evidence in Section 3.3, i.e. that only appropriately balanced mixed methods provide near-optimal performance both for displacements and stresses calculated either by h- or p-refinement. Although we did not perform computations with MQ6, we expect its numerical behavior to be similar to MQ1-4, as suggested by Theorems 3.1 and 3.4.

3.4.1 Model Problem

In our numerical experiments, we use a model problem that we refer to as SING, having reference to the movable singularity in the displacement **u**. For this problem, we solve (2.4) or (2.9) - (2.10) on $\Omega = \{(x,y) : -1 \le x \le 1, -1 \le y \le 1\}$, with $\mathbf{f} = 0$ and tractions **g** specified on the boundary by

$$\begin{aligned} g_1(x,y) &= \frac{8(x-x_0)(y-y_0)\left[(y-y_0)^2-(x-x_0)^2\right]}{\left[(x-x_0)^2+(y-y_0)^2\right]^3} n_2 + \\ &\quad \frac{4(x-x_0)^2\left[3(y-y_0)^2-(x-x_0)^2\right]}{\left[(x-x_0)^2+(y-y_0)^2\right]^3} n_1, \\ g_2(x,y) &= \frac{8(x-x_0)(y-y_0)\left[(y-y_0)^2-(x-x_0)^2\right]}{\left[(x-x_0)^2+(y-y_0)^2\right]^3} n_1 + \\ &\quad \frac{4(y-y_0)^2\left[(y-y_0)^2-3(x-x_0)^2\right]}{\left[(x-x_0)^2+(y-y_0)^2\right]^3} n_2. \end{aligned}$$

Here (n_1, n_2) is the outward unit normal on $\partial\Omega$. The exact solution is given by [15]

$$u_1(x,y) = \frac{(x-x_0)\left[(\lambda+2\mu)(x-x_0)^2-\lambda(y-y_0)^2\right]}{\mu(\lambda+\mu)\left[(x-x_0)^2+(y-y_0)^2\right]^2}, \tag{3.16}$$

$$u_2(x,y) = \frac{(y-y_0)\left[\lambda(x-x_0)^2-(\lambda+2\mu)(y-y_0)^2\right]}{\mu(\lambda+\mu)\left[(x-x_0)^2+(y-y_0)^2\right]^2} \tag{3.17}$$

(from which the stresses can be calculated). In the above, λ and μ are defined in terms of E and ν by (2.2). We take $E = 1$ and let ν vary.

As seen in (3.16) - (3.17) the solution has a movable singularity at (x_0, y_0). By taking $(x_0, y_0) = (-2, -2)$, we get the case of a *smooth* solution. We also consider the case $(x_0, y_0) = (-1.1, -1.1)$, to see how well these methods handle a *near-singular* solution.

3.4.2 Computational Considerations

Implementation of our mixed method is relatively easy. Since no inter-element continuity is imposed on p_N, we simply solve (2.10) locally over each element for p_N in terms of $\mathbf{u}_N$, and then substitute this in (2.9). This gives a positive definite system for $\mathbf{u}_N$, which can then be solved by a direct solver. For the range of ν's tested ($0.3 \leq \nu \leq 0.4999$), round-off error was not a problem.

The MFEMs do cost more than the SFEMs to compute. This increase is due to the pressure variable, which increases the size of the element stiffness matrix. For example, for MQ1 the increased cost ranges from 36% when $k = 2$ to 75% when $k = 10$, up to 125% as $k \to \infty$. However, the overall cost of the two methods is more difficult to compare. Since the pressures are discontinuous, they can be condensed out on each element. Similarly, if a frontal solver is used[24], the pressure degrees of freedom do not contribute to the size of the front. Another factor is the size of the problem. For problems with few elements, the MFEM cost may be significant. But when solving large problems, the cost of solving the global system, which is the same for MFEM and SFEM, may dominate. On a parallel machine, cost comparisons become even less obvious.

For these reasons, rather than comparing the error obtained via different methods with N the sum of $\dim(V_N)$ and $\dim(W_N)$, we compare it with $n = \dim(V_N)$, which represents the total number of variables in the global system to be solved. Of course, our choice n is just one possible (incomplete) measure of the actual cost, which is very

implementation dependent. The SFEM will definitely be cheaper when locking is not an issue. The MFEMs are more robust, but are cheaper only when ν is sufficiently close to 0.5.

The mesh $\mathcal{C}_h$ is a uniform partition of Ω into square elements of side h. Then it is easily seen that the number of degrees of freedom N satisfies

$$N(h,k) \approx Ch^{-2}k^2,$$

so that the asymptotic rates of Section 3.2 could be re-written (for comparison) in terms of N, using the equivalence $h \approx CN^{-1/2}$ for h-refinement (k fixed) and $k^{-1} \approx CN^{-1/2}$ for p-refinement (h fixed).

3.4.3 Computational Convergence Results

Comparison of SQ and MQ1 - h version

Figures 3.3 - 3.5 show the results of h-refinement with SQ and MQ1 (smooth solution). The number of elements ranges from 1 to 64. We have plotted the percentage relative errors in the energy norm of the displacement (defined by (2.5) and (2.11)), and the L^2 norm of the sum of the normal stresses (SNS), vs n, the number of degrees of freedom. (Recall that the energy norm satisfies the same error estimate as the $\mathbf{H}^1$ norm of the displacement.) On these h-refinement plots "*rate*" is the exponent of h, i.e. the rate of convergence.

For SQ, the energy norm error shows good correlation with the asymptotic rates predicted in Equation 3.8 — the optimal rate of $O\left(h^k\right)$ for $k = 2,3,4$ is observed

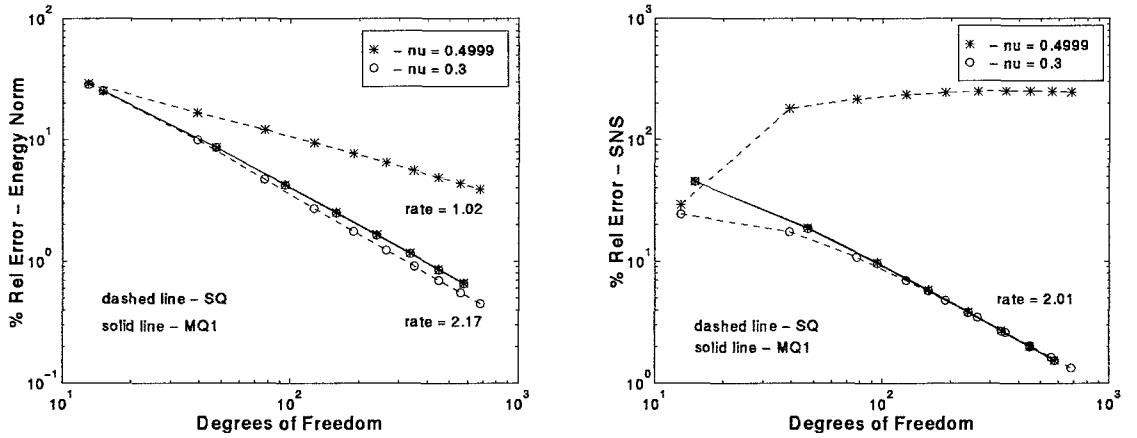

Figure 3.3: SQ vs MQ1, h-refinement, Smooth solution, k = 2.

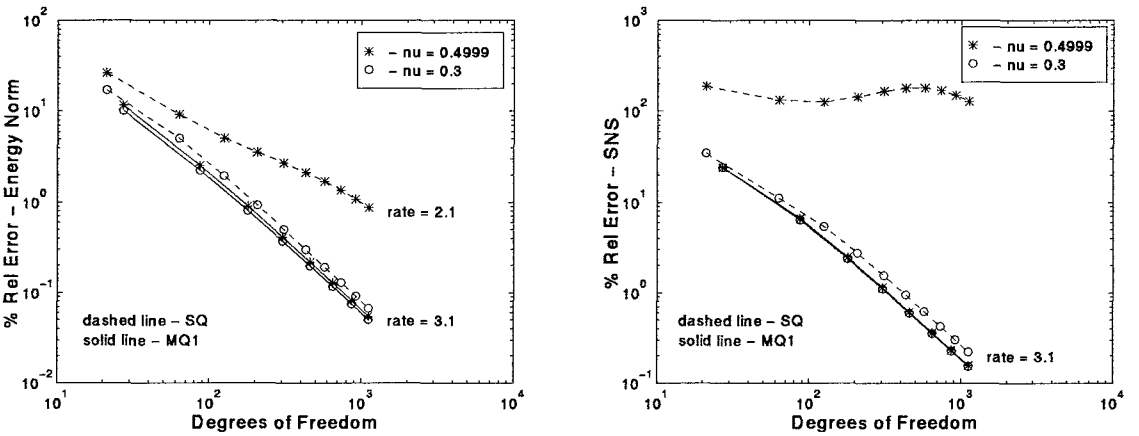

Figure 3.4: SQ vs MQ1, h-refinement, Smooth solution, k = 3.

when $\nu = 0.3$, while the "locked" rate of $O\left(h^{k-1}\right)$ for $k = 2, 3$ is observed when $\nu = 0.4999$. When $k = 4$, we observe the predicted locking of order $O(h^{-2})$ on this model problem. The energy norm locking ratios [2] (L_E) in Table 3.4.3 emphasize that the locking ratio increases gradually as N increases (h decreases). In contrast, MQ1

[2]The locking ratio $L_E(0.4999, N)$ is the observed error at $\nu = 0.4999$ divided by the observed error at $\nu = 0.3$.

exhibits the asymptotic rate of best approximation in energy norm for $k = 2, 3$ and 4 , and is locking-free. The locking ratios (not shown) remain bounded by 1.15.

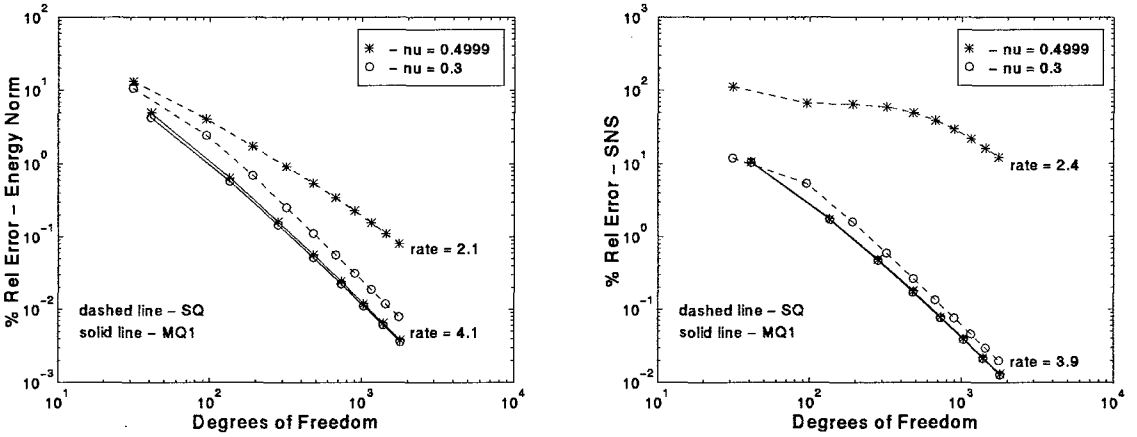

Figure 3.5: SQ vs MQ1, h-refinement, Smooth solution, k = 4.

For SQ, the deterioration in SNS is worse, since there is no observed convergence for $k = 2$ when $\nu = 0.4999$. The error is just beginning to decrease for $k = 3$ in the range of h we use. When $k = 4$, SQ begins to converge for stresses with a rate of $O(h^{2.4})$. The stress locking ratios [3] (L_S) in Table 3.4.3 show dramatic increase with N. On the other hand, we see that MQ1 produces the same near-optimal results for both $\nu = 0.3$ and 0.4999. The stress locking ratios (not shown for MQ1) remain bounded by 1.04.

	N									
$k = 2$	13	39	77	127	189	263	349	447	557	679
$L_E(0.4999, N)$	1.0	1.7	2.6	3.5	4.0	5.3	6.2	7.0	7.8	8.7
$L_S(0.4999, N)$	1.2	10.3	20.0	33.6	50.9	71.7	95.8	122.9	152.5	184.5
	N									
$k = 3$	21	63	125	207	309	431	573	735	917	1119
$L_E(0.4999, N)$	1.5	1.8	2.6	3.8	5.4	7.2	8.9	10.5	11.8	13.0
$L_S(0.4999, N)$	5.4	11.9	23.4	52.1	106.4	188.4	290.2	396.7	494.8	578.7
	N									
$k = 4$	31	95	191	319	479	671	895	1151	1439	1759
$L_E(0.4999, N)$	1.3	1.7	2.5	3.6	4.9	6.2	7.3	8.4	9.3	10.2
$L_S(0.4999, N)$	9.3	12.3	40.4	100.0	189.6	293.7	394.1	481.2	554.7	618.0

Table 3.1: Locking Ratios, SQ, h-refinement, $k = 2$, 3, 4.

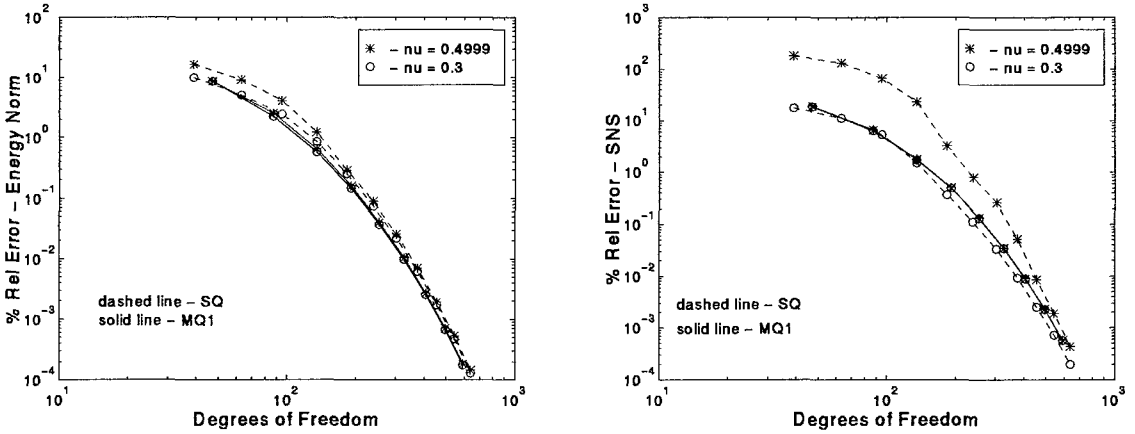

Figure 3.6: SQ vs MQ1, p-refinement, Smooth solution.

Comparison of SQ and MQ1 - p version

Next, in Figures 3.6 and 3.7 we see the performance of SQ and MQ1 with p-refinement on a four element mesh. We observe no locking with either method where the displacement is concerned, since the curves for $\nu = 0.3$ and $\nu = 0.4999$ are very close. (Here, and for all mixed method calculations, the "energy" norm used is the one defined in (2.11).) If one looks at the stresses for the smooth solution, there is a marked decrease in accuracy with SQ when we go from $\nu = 0.3$ to $\nu = 0.4999$. This decrease in accuracy is even more apparent for the unsmooth solution, see Table 3.4.3

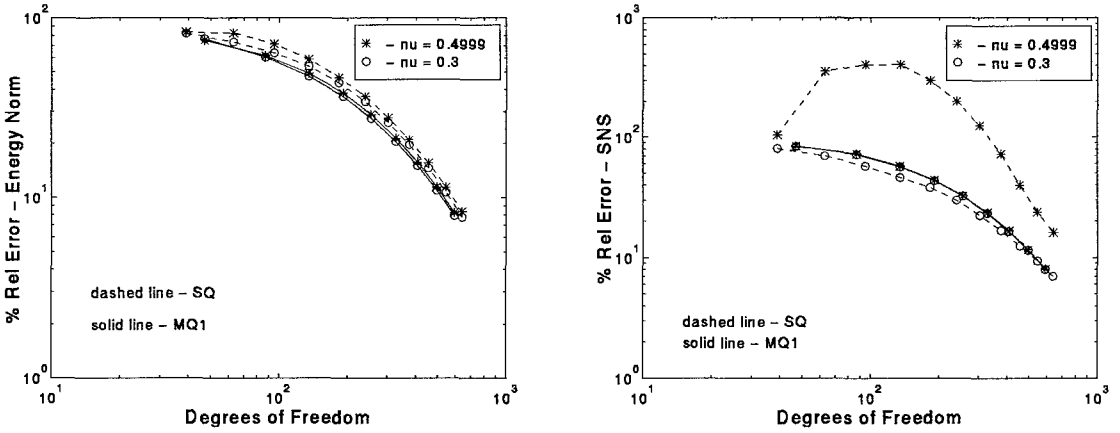

Figure 3.7: SQ vs MQ1, p-refinement, Unsmooth solution.

On the other hand, MQ1 shows no change as $\nu \to 0.5$, either in the smooth or non-smooth case. Hence, **no** locking can be seen in these results for MQ1, not even the $O\left(k^{1/2+\varepsilon}\right)$ predicted by Theorem 3.4. The results with the other mixed methods

[3]The locking ratio $L_S(0.4999, N)$ is the observed error at $\nu = 0.4999$ divided by the observed error at $\nu = 0.3$.

	N									
Smooth	39	63	95	135	183	239	303	375	455	543
$L_E(0.4999, N)$	1.7	1.8	1.7	1.4	1.1	1.2	1.2	1.1	1.1	1.1
$L_S(0.4999, N)$	10.3	11.9	12.3	15.3	8.7	7.1	7.9	5.6	3.5	2.6
	N									
Unsmooth	39	63	95	135	183	239	303	375	455	543
$L_E(0.4999, N)$	1.0	1.1	1.1	1.1	1.1	1.1	1.1	1.1	1.1	1.1
$L_S(0.4999, N)$	1.3	5.1	7.1	8.9	7.9	6.7	5.6	4.3	3.2	2.5

Table 3.2: Locking Ratios, SQ, p-refinement, Smooth, Unsmooth.

are similar, showing that stresses are accurately recovered by the p version mixed method. (Let us remark, however, that even though the $O\left(k^{1/2+\varepsilon}\right)$ loss is not seen for this problem, it could appear in other problems, depending upon the nature of the exact solution.)

Comparison of MQ1-5 - h- and p-refinement

Next, we compare MQ1-5, by seeing how well they perform with h-refinement. As mentioned in the introduction, for an hp code, optimality with respect to h as well is highly desirable. In Figures 3.8 and 3.9, we plot the displacement and stress errors of MQ1-5 when the solution is smooth, for $k = 2$ and 4. These have been plotted for $\nu = 0.4999$ (the figures do not change appreciably for ν closer to $\frac{1}{2}$ or for $\nu = 0.3$).

We see clearly the superiority of MQ1-4, which have $O(h^k)$ convergence in both

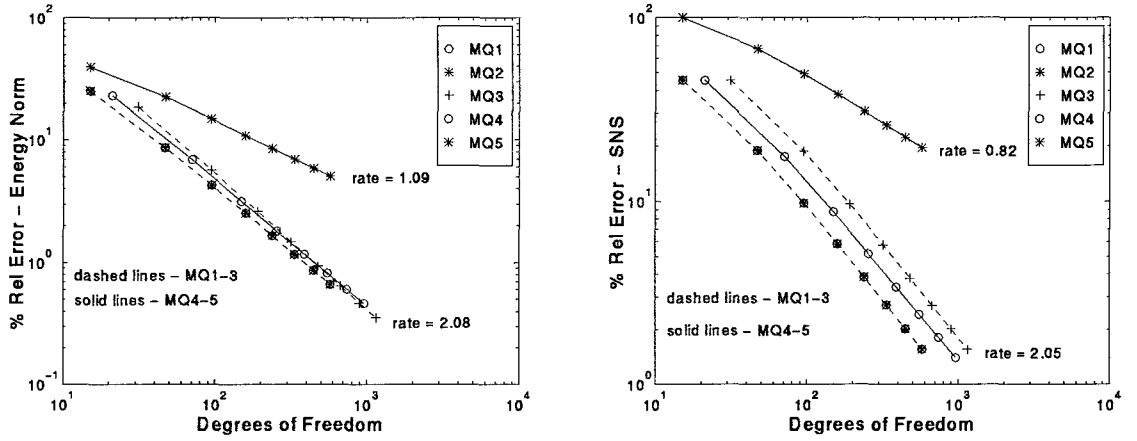

Figure 3.8: MQ1-5, h-refinement, Smooth solution, $k = 2$.

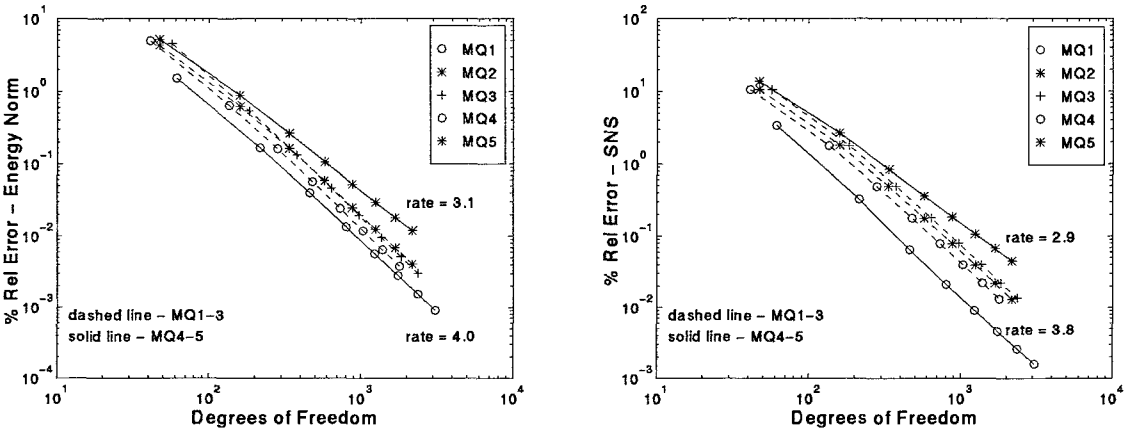

Figure 3.9: MQ1-5, h-refinement, Smooth solution, $k = 4$.

energy norm and SNS, which is the optimal rate for MQ1,2,4,5. The reason MQ5 gives a sub-optimal rate ($O(h^{k-1})$) is *not* due to locking, since the rate is the same for $\nu = 0.3$ and $\nu = 0.4999$. Rather, it is due to the polynomial degree used for p_N being 2 degrees lower than that for $\mathbf{u}_N$, i.e. it is an *approximability* issue. One could, of course, compare MQ1-4 with degree k to MQ5 with degree $k+1$, but then the optimal

rate expected for the displacements from MQ5 would be one order higher, and would still not be attained. Note that the optimal rate for MQ3 is $O(h^{k+2})$ convergence. It fails to achieve this rate for the same reason MQ5 does, because the pressure spaces is 3 degrees lower than the displacement space. This emphasizes the importance of considering both stability and approximability when constructing mixed method spaces.

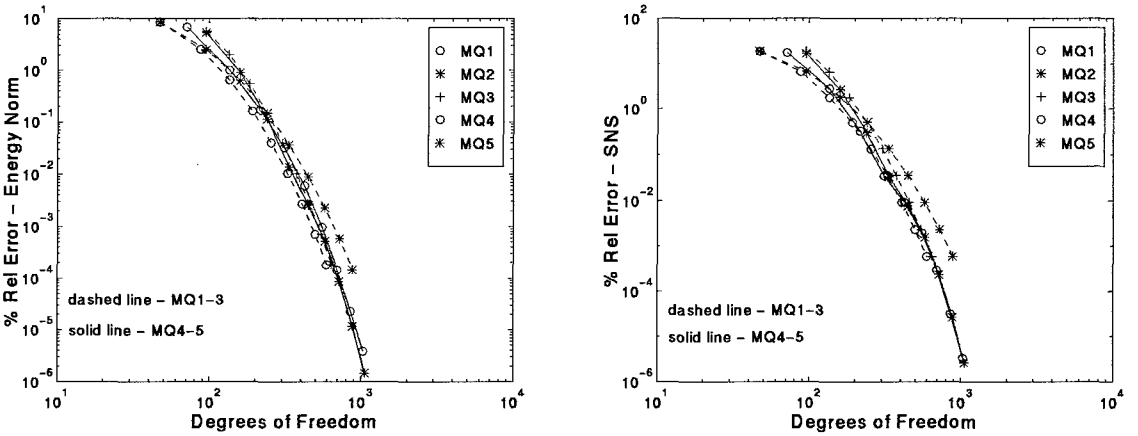

Figure 3.10: MQ1-5, p-refinement, Smooth solution.

For completeness, we also compare MQ1-5 under p-refinement (for four elements). These results (Figures 3.10 and 3.11) show the mixed methods perform about equally well. Since we have not taken $\dim(W_N)$ into account in the comparisons, the method with the minimal degrees of freedom for W_N, i.e. MQ1, may be preferable overall.

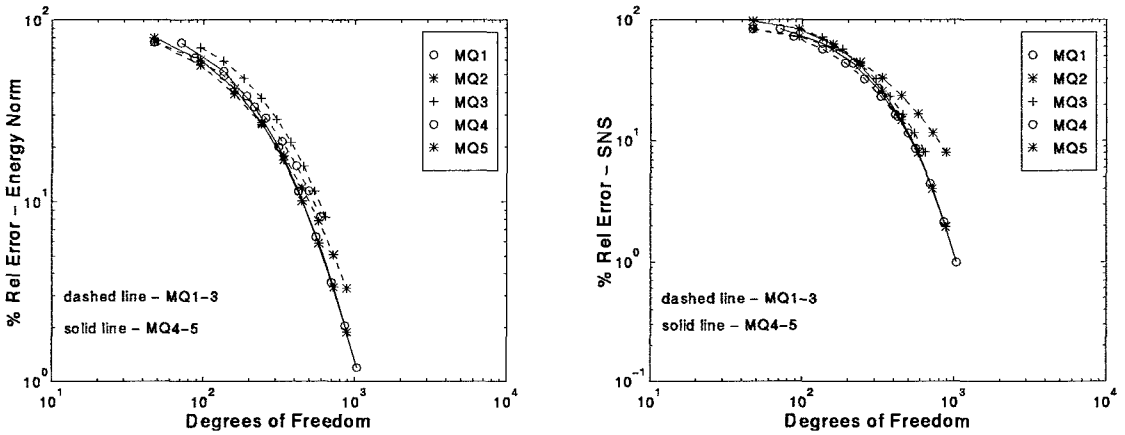

Figure 3.11: MQ1-5, p-refinement, Unsmooth solution.

Chapter 4

Straight-Sided Triangular Elements

From the results in [26], it follows that the inf $-$ sup constant for the p version SFEM on triangular elements is $O(k^{-\gamma})$ for some unknown γ. Many commercial codes rely heavily on automatic mesh generation using triangular elements. For these codes to have reliable hp capability, triangular elements with known stability characteristics are necessary. In this chapter, we look at mixed method triangular elements for which a better characterization of stability can be made. These mixed triangular elements are based on conditions (A1)-(A6) outlined in Chapter 3. The pair of spaces that was analyzed by Schwab and Suri [17] satisfy these conditions. They showed that the inf $-$ sup constant is no worse than Ck^{-3}. We provide evidence that the inf $-$ sup constant for this mixed triangular element is better by computing it for a single element for a practical range of k, and then invoking Theorem 3.1. We also propose and investigate an optimized version of this element. We then perform experiments on

triangular meshes with both SFEM and our mixed triangular elements and compare their performance for a model problem.

4.1 Spaces and Stability

As in section 3.1, we use the same definition of V_N and W_N, with the exception that now the reference element $\hat{K} = \{(x, y) : 0 \leq x \leq 1, 0 \leq y \leq 1 - x\}$ is a triangle. We use conditions (A1)-(A6) (see section 3.1) to select displacement and pressure spaces for two mixed triangular elements.

We identify the first triangular element as MT1, and begin by letting $\mathbf{V}_k(\hat{K}) = \left[\mathcal{P}_k(\hat{K})\right]^2$. Then (A1) is satisfied and (A2) requires $W_k(\hat{K}) \subseteq \mathcal{P}_{k-2}(\hat{K})$, so we let $W_k(\hat{K}) = \mathcal{P}_{k-2}(\hat{K})$. Condition (A3) is verified in [17] for these spaces with $\gamma = 3$. Condition (A4) is satisfied if $\mathcal{P}_2(\hat{K}) \subset V_k(\hat{K})$. Finally, (A5) is satisfied and (A6) is satisfied with $n = 1$. We point out that $n \geq 1$ in (A6) implies less than optimal approximation. Thus we define

$$\text{MT1:} \qquad \mathbf{V}_k(\hat{K}) = [\mathcal{P}_k(\hat{K})]^2, \;\; W_k(\hat{K}) = \mathcal{P}_{k-2}(\hat{K}),$$

and expect MT1 to have inf-sup constant no worse than $O(k^{-3})$ and less than optimal approximability.

Another approach is to set $W_k(\hat{K}) = \mathcal{P}_{k-1}(\hat{K})$ and determine the smallest space $\mathbf{V}_k(\hat{K})$ that satisfies conditions (A1) - (A6). The lowest order triangular bubble function $b_{\hat{K}} \in \mathcal{P}_3(\hat{K})$, and $\forall q \in \mathcal{P}_{k-1}(\hat{K}) = W_k(\hat{K})$ we have $\nabla q \in \mathcal{P}_{k-2}(\hat{K})$. Then (A2)

requires that $\{\text{bubble functions in } \mathcal{P}_{k+1}(\hat{K})\} \subset V_k(\hat{K})$. This leads to the following mixed triangular element

MT2: $$\mathbf{V}_k(\hat{K}) = [\mathcal{P}_k(\hat{K}) \cup \{\mathcal{P}_{k+1}(\hat{K}) \text{ bubble functions}\}]^2,$$

$$W_k(\hat{K}) = \mathcal{P}_{k-1}(\hat{K}).$$

The analysis of local stability for MT1 also applies to MT2, so the inf-sup constant will be no worse than $O(k^{-3})$. Note that in contrast to MT1, the polynomial degree of the displacement and pressure spaces for MT2 differs by only 1, so MT2 should have optimal approximability.

For SFEM, we define

ST: $$V_k(\hat{K}) = \mathcal{P}_k(\hat{K}).$$

This is equivalent to SQ, since for a given k, both SQ and ST are the minimal space of polynomials of degree k that produces C^0 continuity on a regular mesh. As mentioned earlier, the inf-sup constant for ST is $O(k^{-\gamma})$ for some unknown γ [26].

To characterize the stability of MT1 and MT2, we would like to use Theorem 3.1. Both MT1 and MT2 satisfy (A1) and (A2). They also satisfy (A3) with $\gamma = 3$ (computations indicate this is pessimistic). Condition (A4) is met by both MT1 and MT2 (see [6]). To gain a practical description of the inf-sup constant for these mixed methods we turn to the computational approach of the next section.

4.2 Numerical Investigation of Inf-Sup Condition

Recall from Chapter 3 that the global inf-sup constant in Theorem 3.1 can be established if either (A1)-(A4) hold or if (LS),(A4) hold. Just like we estimated the global inf-sup constant by an eigenvalue computation in section 3.2, so also we can estimate the *local* inf-sup constant in (LS) instead. Once γ in (LS) has been estimated computationally, we can expect the estimate in Theorem 3.1 to hold for the range of k tested, since (A4) holds.

We therefore estimate, for both MT1 and MT2, the value of γ in (LS) over the reference triangle $\hat{K}$. The results are given in Figure 4.2. We see that for $k \leq 11$ the slope is -0.3 and for $k > 11$ the slope is -1.1. This significant shift in the slope may indicate that the $k > 11$ region reflects the asymptotic rate. This suggests that the inf-sup constant for MT1 is about $O(k^{-1})$.

Most commercial codes limit p-refinement, using an upper bound on polynomial degree that is usually much less than 20. For practical purposes therefore, the $O(k^{-1})$ computational estimation we have obtained will govern the globally observed inf-sup constant.

Remark 4.1 *Let us remark that ST could also be put in the form of a mixed method, i.e. in the form (2.7)-(2.8), by taking* $W_N = div(\mathbf{V}_N)$, *which gives [19]* $W_k(\hat{K}) = \mathcal{P}_{k-1}(\hat{K})$. *We could then attempt to numerically estimate the global inf-sup constant by the local one as done here, since Theorem 3.1 will again hold. Unfortunately, the local inf-sup constant is 0 in this case, even though the global one is positive. This*

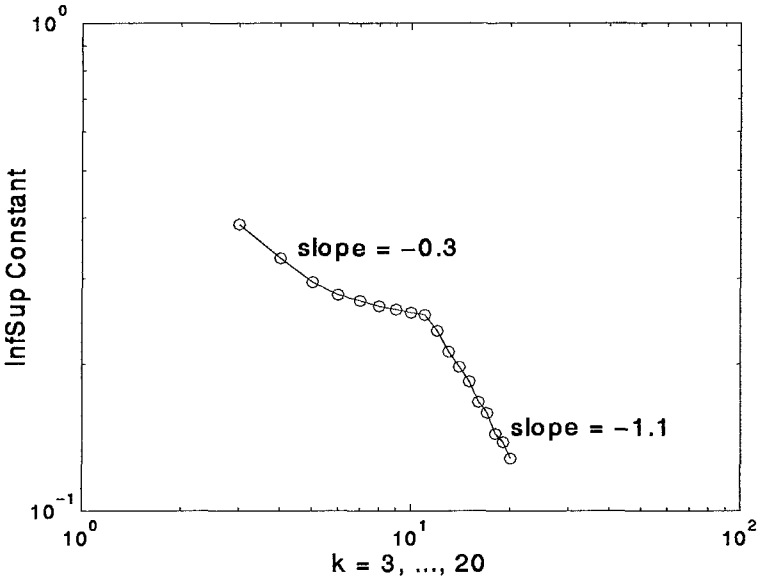

Figure 4.1: The local inf-sup condition for MT1 and MT2.

discrepancy occurs since condition (A2) is not satisfied here.

4.3 Asymptotic Convergence Rates

Recall that the space $\mathbf{V}_k(\hat{K}) = \left[\mathcal{P}_k(\hat{K})\right]^2$ used in ST is the minimal conforming space of polynomials of degree $\leq k$. As in Section 3.2, this means that in the absence of locking (ν fixed and not close to 1/2), the asymptotic rate of best approximation in terms of the $\mathbf{H}^1(\Omega)$ norm for ST is given by (3.8), assuming the solution $\mathbf{u} \in \mathbf{H}^r(\Omega)$, $r > 1$. The same rate will also be observed in the energy norm (2.5). Also, the inequality given in (3.10) holds for the pressure. The upper bounds in (3.8),(3.10) represent the *optimal* asymptotic convergence rate for polynomials of degree k.

Keeping h fixed in (3.8), we get the rate for the displacement error for ST un-

der p-refinement for any $\nu \in [0, \frac{1}{2})$. Hence p-refinement is free of locking for the displacements (but not necessarily the pressures).

Under h-refinement with $k \leq 3$, $O(h)$ energy norm locking is the best rate independent of ν. However, for $k \geq 4$, the rate of convergence in displacement *and* pressure for ST is $O(h^{\min(k,r-1)})$ independent of ν, where the solution $\mathbf{u} \in \mathbf{H}^r$.

For the mixed methods, we have the following result for the case of straight sided triangles.

Theorem 4.1 *Let* $\mathbf{V}_N(\Omega), W_N(\Omega)$ $(k \geq 2)$ *satisfy (LS),(A4). Then for any* $\varepsilon > 0$, *there exists a constant* C_ε *independent of* $\mathbf{u}, h, k$ *and* $\nu \in [0, \frac{1}{2})$ *such that*

$$\|\mathbf{u} - \mathbf{u}_N\|_1 \leq C_\varepsilon h^l k^{-s+1+\varepsilon}(\|\mathbf{u}\|_s + \|p\|_{s-1}),$$

$$\|p - p_N\|_0 \leq C_\varepsilon h^l k^{-s+1+\gamma+\varepsilon}(\|\mathbf{u}\|_s + \|p\|_{s-1}),$$

where

$$l = \min\{s-1, k-n\}, \quad n = 0 \text{ for } MT2, n = 1 \text{ for } MT1.$$

and γ *is the exponent in (3.5).*

Proof: We note that since (A4) is satisfied, Theorem 3.1 holds. The proof then follows the same line as that of Theorem 5.2 in [20] for parallelograms. □

As mentioned previously, we have characterized the constant γ computationally, which will be the same over all the (affine-equivalent) elements.

4.4 Numerical Results

In this section we examine the performance of ST and MT1 on model problem SING (see Section 3.4.1). We are interested in both h- and p-refinement and also consider both smooth and near-singular solutions. We compare the results to the error bounds given above.

4.4.1 h-Refinement

We begin with ST using h-refinement on both a smooth and a near-singular solution. We see in Figure 4.2 that when the solution is smooth and $k = 2$, energy norm locking of $O(h)$ is observed as $\nu \to \frac{1}{2}$. This order of locking is predicted by (3.8) for $k = 3$ as well, although it does not appear for this model problem. Consistent with theory, we see no energy norm locking when $k = 4$.

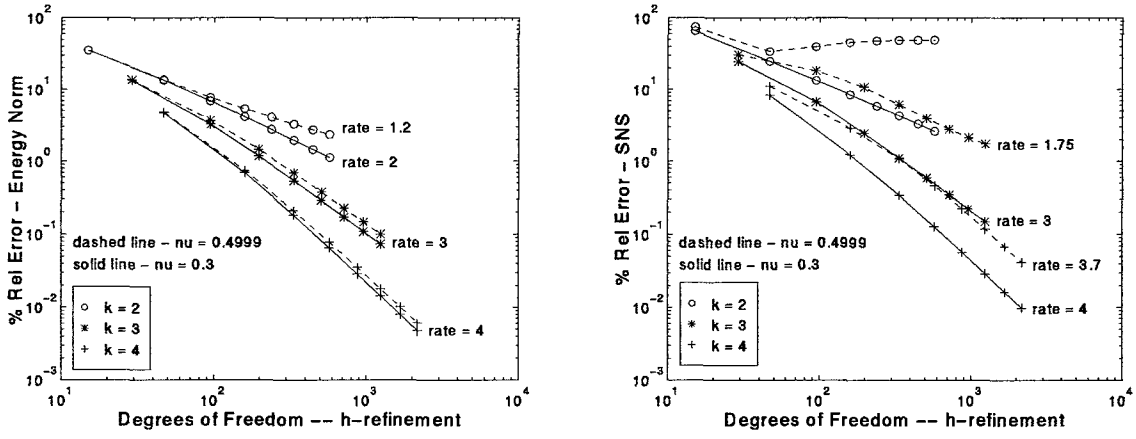

Figure 4.2: ST, h-refinement, Smooth Solution.

The SNS shows no convergence for $k = 2$ (i.e. $O(h^2)$ locking), and $O(h)$ locking

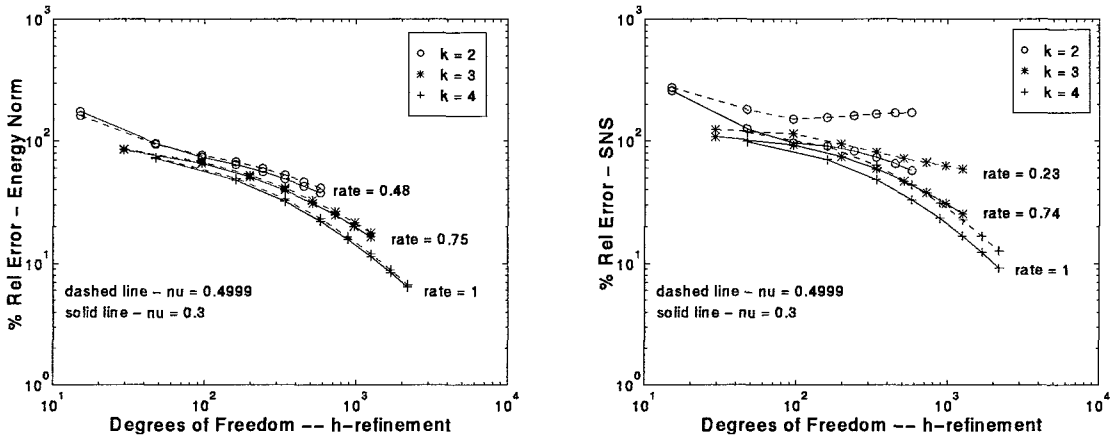

Figure 4.3: ST, h-refinement, Unsmooth Solution.

for $k = 3$. When $k = 4$, the SNS rate of convergence is unaffected as $\nu \to \frac{1}{2}$, but we see a locking ratio of about 4 that increases gradually as h decreases, see Table 4.4.1.

When the solution is near singular, we see in Figure 4.3 the rate of convergence in energy norm does not change as $\nu \to \frac{1}{2}$. This is consistent with (3.8), since the rate depends both on k and the regularity of the solution. For near singular solutions, the effective r is quite small, so the rate of convergence $\mu = \min\{k, r-1\}$ is dominated by r. The behavior for the pressure is qualitatively the same for the near-singular solution as for the smooth.

Next we use MT1 under h-refinement to solve SING with a smooth solution first, and then a near-singular one. In Figures 4.4 and 4.5 we see that the performance of MT1 is unaffected by the value of ν. Even the pressure approximation is unaffected as $\nu \to \frac{1}{2}$. As with ST, the regularity of the near-singular solution dominates the rate of convergence in Figure 4.5, so even for $k = 4$, the observed energy norm rate of

	N							
$k = 2$	15	47	95	159	239	335	447	575
$L_S(0.4999, N)$	1.14	1.37	2.97	5.39	8.17	11.35	14.94	18.95
	N							
$k = 3$	29	95	197	335	509	719	965	1247
$L_S(0.4999, N)$	1.24	2.71	4.40	5.56	6.74	8.11	9.75	11.66
	N							
$k = 4$	47	159	335	575	879	1247	1679	2175
$L_S(0.4999, N)$	1.34	2.36	3.21	3.61	3.86	4.03	4.16	4.27

Table 4.1: SNS Locking Ratios, ST, h-refinement, Smooth Solution, $k = 2, 3, 4$.

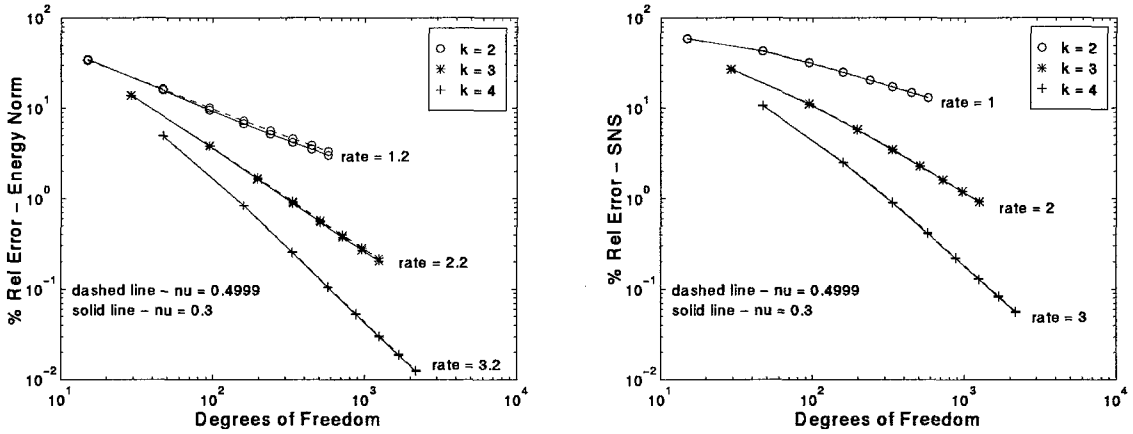

Figure 4.4: MT1, h-refinement, Smooth Solution.

convergence never exceeds $O(h^2)$.

Note that similar to MQ5, MT1 under h-refinement is locking free, yet the rate of convergence in both energy norm and SNS is $O(h)$ worse than the asymptotic rate of best approximation. This is due to the polynomial degree for p_N being 2 degrees lower than that for $\mathbf{u}_N$ (rather than 1 as in MT2).

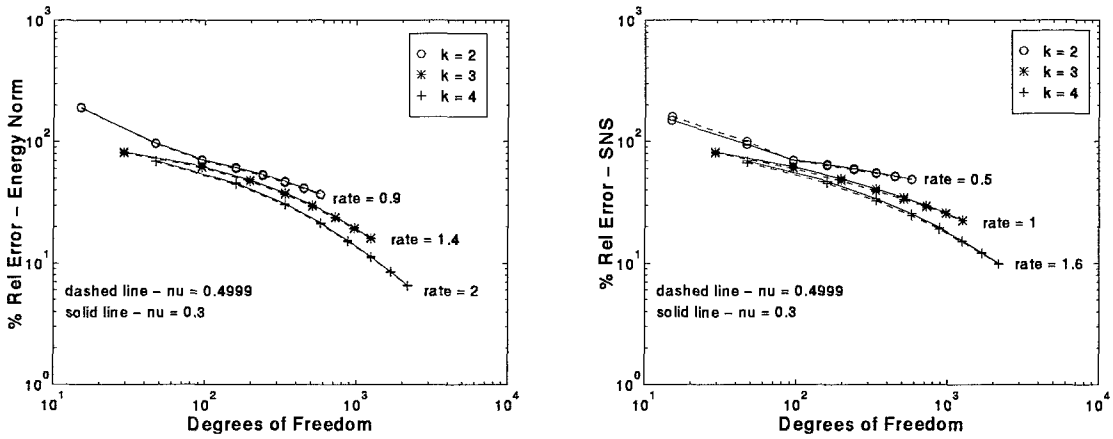

Figure 4.5: MT1, h-refinement, Unsmooth Solution.

4.4.2 p-Refinement

We see in Figures 4.6 and 4.7, that under p-refinement, ST performs very well on our model problem. The displacement approximation is essentially the same for both $\nu = 0.3$ and $\nu = 0.4999$. Only the pressures show a slight difference, with a nearly constant locking ratio of about 1.4 for the near-singular solution on 8 elements.

Even this small shift is avoided by MT1. We see in Figures 4.8 and 4.9 that the value of ν does not affect the performance of MT1.

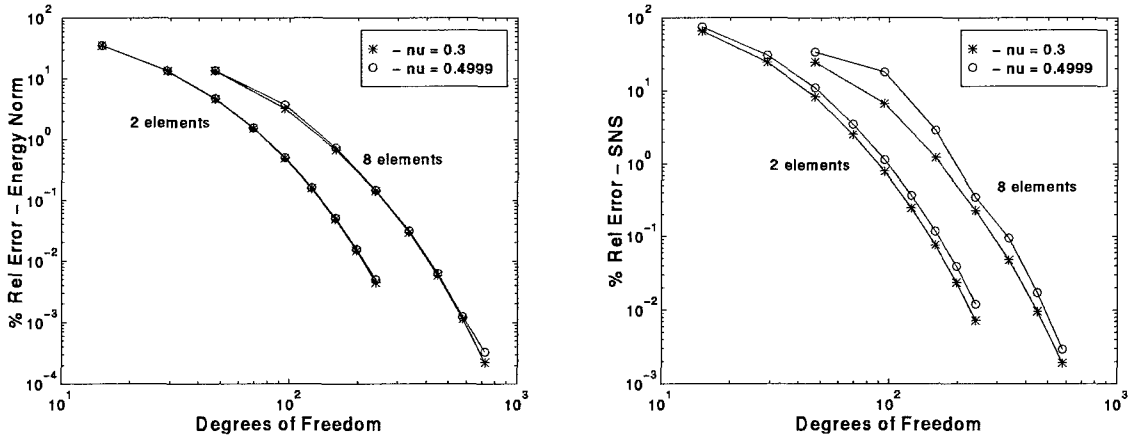

Figure 4.6: ST, p-refinement, Smooth Solution.

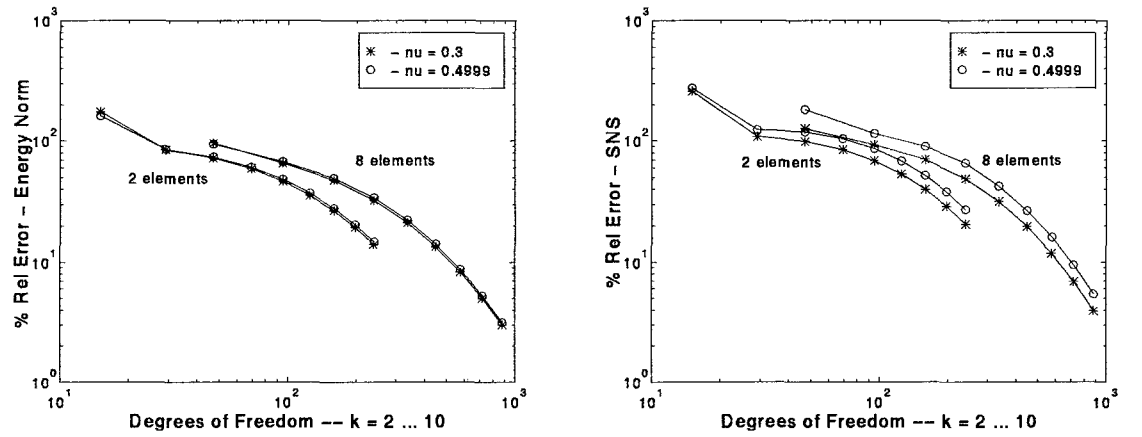

Figure 4.7: ST, p-refinement, Unsmooth Solution.

In summary, the numerical performance of ST and MT1 on our model problem is consistent with available theory. ST locks in the energy norm for low k under h-refinement, but is locking free if $k \geq 4$. As predicted, for the p version, it is locking-free in the energy norm but (somewhat surprisingly) almost locking-free in the pressures as well. Pressure locking is more pronounced in the h version. Here, no convergence

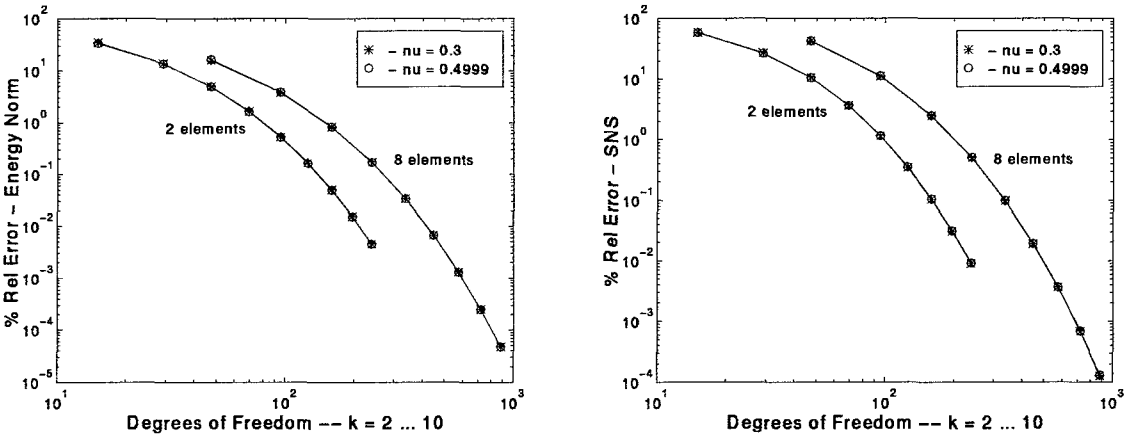

Figure 4.8: MT1, p-refinement, Smooth Solution.

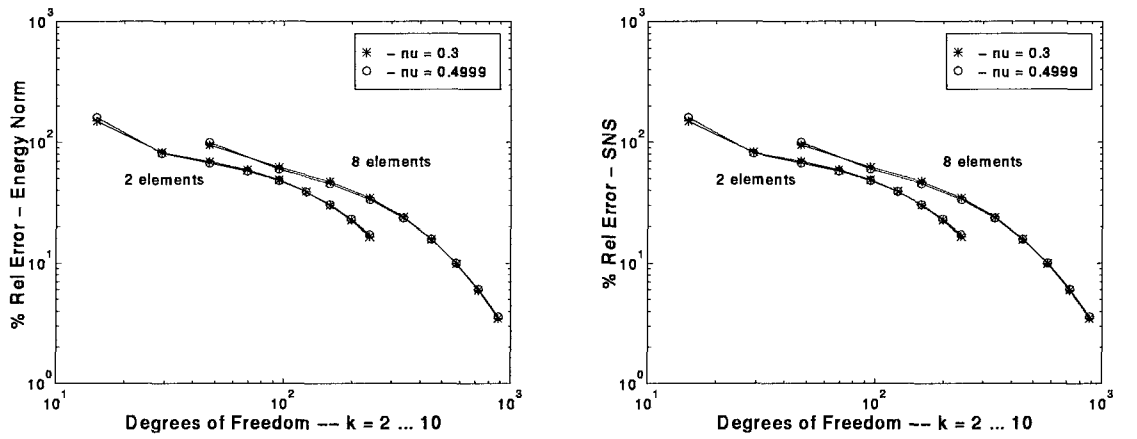

Figure 4.9: MT1, p-refinement, Unsmooth Solution.

is observed for $k = 2$ and $O(h)$ locking for $k = 3$, for both the smooth and near-singular solutions. When $k = 4$ no pressure locking occurs, although the locking ratio may be significant for smooth problems. The experiments indicate that MT1 under h-refinement is locking free for any reasonable k.

In light of these experiments, the lower bound on the inf $-$ sup constant for MT1

obtained analytically in [17] seems pessimistic. The inf-sup estimate of $k^{-0.3}$ for $k \leq 11$ suggested by the computations of Section 4.2 is reasonable since MT1 shows no SNS locking under p-refinement in that range. To test the apparent shift suggested by Figure 4.2, the p-refinement experiments of Figures 4.8 and 4.9 on MT1 would need to be run with higher values of k.

Chapter 5

Curvilinear Elements

Since curved elements are essential for p version meshes, in this chapter we investigate locking on curved elements, focusing primarily on p-refinement. We prove that on a single curved element, the displacement error is bounded by $(k-\alpha)^{-r}$ where α depends on the polynomial degree of the mapping from a reference element to the curvilinear element. We adapt the mixed methods from Chapters 3 and 4 to curved elements and show how the inf-sup constant can be estimated when these methods are used on curvilinear meshes. We use this result to compute $\inf - \sup$ constants for several mapped elements and show that these are stable for practical applications. We also show that modified versions of MQ1-6 can be proven to have the same stability behavior on curvilinear elements as on parallelogram elements.

When displacement is of interest, we show that the SFEM shows significant deterioration when curved elements are used on the boundary with p-refinement. In

addition, we show that the stress error is adversely affected under p-refinement by both curved boundary elements and elements with curved interior edges. We also perform experiments to show that the mixed methods of Chapters 3 and 4, when used on a curvilinear mesh, are robust for a model problem.

As a final test, in Section 5.5, we use a benchmark problem from [25] to investigate the performance of SFEM and a mixed method for computing point values of stresses. In [25], the SFEM is shown to be ineffective for computing point values of the sum of normal stress and a post processing method to overcome this shortcoming is proposed. We find that mixed methods with curvilinear meshes can be used to accurately extract these point values without any post processing.

5.1 Single Element Analysis

In this section we show that, on a *single* element, an invertible polynomial mapping does not affect the asymptotic *rate* of convergence under p-refinement, but can affect the relative error, resulting in a locking ratio greater than one. This shift is shown to depend on the degree of the polynomial map. This result is given for the case that $\hat{K}$ is the reference square.

Theorem 5.1 *Let $\mathcal{F}_K : \hat{K} \to K$ be an invertible polynomial map, $\mathcal{F}_K \in [Q_q(\hat{K})]^2$ and $\mathbf{u}_k \in [V_k(K)]^2$, where $V_k(K) = \{v : v = \hat{v} \circ \mathcal{F}_K^{-1}, \hat{v} \in Q_k(\hat{K})\}$. Let $\mathbf{u}$ satisfy (2.3)*

on K and $\mathbf{u}_k$ be the solution to (2.4). If $\hat{K}$ is the reference square then

$$\|\mathbf{u} - \mathbf{u}_k\|_{H^1(K)} \leq C(k-\alpha)^{-(r-1)}\|\mathbf{u}\|_{H^r(K)}, \tag{5.1}$$

where $\alpha = 3q - 2$.

Proof: It is well known (see Theorem 3.3 of [1]) that (5.1) follows if we can show it for the completely incompressible case. Thus we consider $\mathbf{u}$ such the div $\mathbf{u} = 0$, and let $\phi \in H^2(K)$ be such that $\mathbf{u} = \text{curl}\,\phi$ solves the limiting case ($\lambda \to \infty$) of (2.3).

Let the globally invertible polynomial map $\mathcal{F}_K : \hat{K} \to K$ be defined as $\mathbf{y} = \mathcal{F}_K\mathbf{x}$ where $\mathcal{F}_K \in [Q_q(\hat{K})]^2$. Let J_K be the Jacobian of $\mathcal{F}_K$ and d be the determinant of J_K. Then

$d = \frac{\partial y_1}{\partial x_1}\frac{\partial y_2}{\partial x_2} - \frac{\partial y_1}{\partial x_2}\frac{\partial y_2}{\partial x_1} \in \mathcal{P}_{2q-1,2q-2} \cup \mathcal{P}_{2q-2,2q-1} \subset Q_{2q-1}$. [1] Since $\mathcal{F}_K$ is smooth and invertible on K, $|d| \geq c > 0$ on $\hat{K}$ and for $\phi \in H^r(K)$ we have

$$C_1\|\phi\|_{H^r(K)} \leq \|\hat{\phi}\|_{H^r(\hat{K})} \leq C_2\|\phi\|_{H^r(K)}, \tag{5.2}$$

where $\hat{\phi} = \phi \circ \mathcal{F}_K$. Define $\hat{\psi} = \frac{\hat{\phi}}{d^2}$. For any l there exists $\hat{\psi}_l \in Q_l(\hat{K})$ such that for $0 \leq t \leq 2$, $r > 1$ (see [21])

$$\|\hat{\psi} - \hat{\psi}_l\|_{H^t(\hat{K})} \leq Cl^{-(r+1-t)}\|\hat{\psi}\|_{H^{r+1}(\hat{K})}. \tag{5.3}$$

Taking $\hat{\phi}_k = \hat{\psi}_l d^2$, and combining (5.2) and (5.3) with $t = 2$, we have

$$\begin{aligned} \|\phi - \phi_k\|_{H^2(K)} &\leq C\|\hat{\phi} - \hat{\phi}_k\|_{H^2(\hat{K})} \\ &\leq Cl^{-(r-1)}\|\hat{\phi}\|_{H^{r+1}(\hat{K})} \\ &\leq Cl^{-(r-1)}\|\phi\|_{H^{r+1}(K)}. \end{aligned} \tag{5.4}$$

[1] We define $\mathcal{P}_{k_1,k_2} = \text{span}\{x_1^{\alpha_1}x_2^{\alpha_2} : 0 \leq \alpha_1 \leq k_1, 0 \leq \alpha_2 \leq k_2\}$.

Now

$$\begin{aligned}\operatorname{curl}\hat{\phi}_k &= \left(\frac{\partial\hat{\phi}_k}{\partial y_2}, -\frac{\partial\hat{\phi}_k}{\partial y_1}\right)\\ &= \left(\left(\frac{\partial\hat{\psi}_k}{\partial x_1}\frac{\partial x_1}{\partial y_2} + \frac{\partial\hat{\psi}_k}{\partial x_2}\frac{\partial x_2}{\partial y_2}\right)d^2 + 2\hat{\psi}_k d\left(\frac{\partial d}{\partial x_1}\frac{\partial x_1}{\partial y_2} + \frac{\partial d}{\partial x_2}\frac{\partial x_2}{\partial y_2}\right),\right.\\ &\quad \left. -\left(\frac{\partial\hat{\psi}_k}{\partial x_1}\frac{\partial x_1}{\partial y_1} + \frac{\partial\hat{\psi}_k}{\partial x_2}\frac{\partial x_2}{\partial y_1}\right)d^2 - 2\hat{\psi}_k d\left(\frac{\partial d}{\partial x_1}\frac{\partial x_1}{\partial y_1} + \frac{\partial d}{\partial x_2}\frac{\partial x_2}{\partial y_1}\right)\right).\end{aligned}$$

Also

$$\begin{pmatrix} \frac{\partial x_1}{\partial y_1} & \frac{\partial x_1}{\partial y_2} \\ \frac{\partial x_2}{\partial y_1} & \frac{\partial x_2}{\partial y_2} \end{pmatrix} = \begin{pmatrix} \frac{\partial y_1}{\partial x_1} & \frac{\partial y_1}{\partial x_2} \\ \frac{\partial y_2}{\partial x_1} & \frac{\partial y_2}{\partial x_2} \end{pmatrix}^{-1} = \frac{1}{d}\begin{pmatrix} \frac{\partial y_2}{\partial x_2} & -\frac{\partial y_1}{\partial x_2} \\ -\frac{\partial y_2}{\partial x_1} & \frac{\partial y_1}{\partial x_1} \end{pmatrix}.$$

So

$$\begin{aligned}\operatorname{curl}\hat{\phi}_k = &\\ &\left(\left(-\frac{\partial\hat{\psi}_k}{\partial x_1}\frac{\partial y_1}{\partial x_2} + \frac{\partial\hat{\psi}_k}{\partial x_2}\frac{\partial y_1}{\partial x_1}\right)d + 2\hat{\psi}_k\left(-\frac{\partial d}{\partial x_1}\frac{\partial y_1}{\partial x_2} + \frac{\partial d}{\partial x_2}\frac{\partial y_1}{\partial x_1}\right),\right.\\ &\left. -\left(\frac{\partial\hat{\psi}_k}{\partial x_1}\frac{\partial y_2}{\partial x_2} - \frac{\partial\hat{\psi}_k}{\partial x_2}\frac{\partial y_2}{\partial x_1}\right)d - 2\hat{\psi}_k\left(\frac{\partial d}{\partial x_1}\frac{\partial y_2}{\partial x_2} - \frac{\partial d}{\partial x_2}\frac{\partial y_2}{\partial x_1}\right)\right).\end{aligned}$$

Now

$$\frac{\partial\hat{\psi}_k}{\partial x_1}\frac{\partial y_1}{\partial x_2}d \in \mathcal{P}_{l-1+q+2q-1,l+q-1+2q-1} = \mathcal{P}_{l+3q-2,l+3q-2} = Q_{l+3q-2}.$$

Similarly, every other term in curl $\hat{\phi}_k$ is in the same space. Letting $\alpha = 3q-2$ and $k = l+3q-2$, then $l = k-\alpha$. Then (5.4) implies

$$\|\mathbf{u}-\mathbf{u}_k\|_{H^1(K)} \le C(k-\alpha)^{-(r-1)}\|\mathbf{u}\|_{H^r(K)}. \tag{5.5}$$

□

Theorem 5.1 gives $\alpha = 1$ in the case of bilinear mappings. This has been experimentally observed in e.g. Figure 5.2 of [3], where the shift with other mappings is also computationally investigated.

Similar results are available if $\hat{K}$ is the reference triangle. In that case if $\mathcal{F}_K \in \mathcal{P}_q(\hat{K})$ and $\mathbf{u}_k \in [V_k(K)]^2$ where $V_k(K) = \{v : v = \hat{v} \circ \mathcal{F}_K^{-1}, \hat{v} \in \mathcal{P}_k(\hat{K})\}$, then $\alpha = \max\{0, 3q-4\}$. We have considered the simple case of a single element to avoid the complexities of more general meshes. Experimentally, the single element results carry over qualitatively to the multiple element case.

5.2 Curvilinear Mesh Analysis

We now consider meshes constructed with mapped elements. We show that Theorem 3.1 applies to MQ1-6 and MT1-2 on *regular* (defined below) curvilinear meshes provided condition (LS) holds. We show how to estimate the $\inf - \sup$ constant (in terms of k) for these mixed methods on mapped triangular and quadrilateral elements for certain types of maps. We show that several standard mappings produce stable methods and we provide a technique for examining the stability of additional maps.

Throughout this section, we assume we are given a family of partitions $\{\mathcal{C}_h\}$ of Ω, where $\Omega = \cup_{K \in \mathcal{C}_h} K$. We assume the mappings $\mathcal{F}_K : \hat{K} \to K$ are smooth and globally invertible on K. We let J_K denote the Jacobian of $\mathcal{F}_K$, and assume its inverse J_K^{-1} exists for any $\hat{x} \in \hat{K}$. We say that the curvilinear mesh $\{\mathcal{C}_h\}$ is *regular* [7] if, in addition to the conditions in Section 3.1, the following conditions hold.

i) Let $|J_K| = |\det J_K|$, then

$$\|J_K\|_\infty, \ \|J_K^{-1}\|_\infty, \ \sup_{\hat{x}\in\hat{K}} |J_K(\hat{x})|, \ [\inf_{\hat{x}\in\hat{K}} |J_K(\hat{x})|]^{-1} \leq \mathcal{K}, \tag{5.6}$$

where $\mathcal{K}$ is a constant independent of h.

ii) The mesh admits the existence of a "Clément operator" [8]; a continuous interpolate using averages of $\mathbf{v} \in [H^1(\Omega)]^2$ instead of point values.

Regular meshes can be constructed on many domains of interest.

To use Theorem 3.1 for our mixed methods on curvilinear meshes, we remark that although (A1) and (A2) hold, it is not known how to establish (A3) analytically. We therefore use condition (LS), by estimating the local stability condition computationally. In addition we must verify that (A4) applies for these mixed methods. The following lemmas establish (A4) for the case of triangular and quadrilateral elements respectively.

Lemma 5.1 *Let $\{\mathcal{C}_h\}$ be a family of regular partitions of Ω, and let $\mathcal{F}_K : \hat{K} \to K$ denote the smooth invertible map associated with K, with $\hat{K}$ the reference triangle. Then the pair $([\mathcal{P}_k(\Omega)]^2, \mathcal{P}_0(\Omega))$ is globally stable where $\mathcal{P}_k(\Omega) = \{v : v_{|K} = \hat{v} \circ \mathcal{F}_K^{-1}, \hat{v} \in \mathcal{P}_k(\hat{K})\}$.*

Proof: We let $\mathbf{V} = [H_0^1(\Omega)]^2$, $\mathbf{V}_h = [\mathcal{P}_2(\Omega)]^2$, and $Q_h = \mathcal{P}_0(\Omega)$. We use Proposition 4.1 from [6], which says it is sufficient to construct an operator $\Pi_2 : \mathbf{V} \to \mathbf{V}_h$ that has the following two properties:

$$\int_\Omega \operatorname{div}(\mathbf{v} - \Pi_2 \mathbf{v})\, q_h \, dx = 0 \quad \forall \mathbf{v} \in \mathbf{V} \text{ and } \forall \ q_h \in Q_h \tag{5.7}$$

and

$$\|\Pi_2\,\mathbf{v}\|_{1,K} \le C(h_K^{-1}\|\mathbf{v}\|_{0,K} + |\mathbf{v}|_{1,K}) \;\; \forall \mathbf{v} \in \mathbf{V} \;\text{ and }\; \forall K \in \mathcal{C}_h. \tag{5.8}$$

We define $\Pi_2\,\mathbf{v}_{|K}$ as follows:

$$\Pi_2\,\mathbf{v}_{|K} \in [\mathcal{P}_2(K)]^2,$$

$$\Pi_2\,\mathbf{v}_{|K}(M) = \mathbf{0} \quad \forall M = \text{ vertex of } K,$$

$$\int_e \Pi_2\,\mathbf{v}_{|K}\,ds = \int_e \mathbf{v}\,ds \quad \forall e = \text{ edge of } K. \tag{5.9}$$

Using (5.9), we establish (5.7) as follows:

$$\begin{aligned}\int_\Omega \operatorname{div}(\mathbf{v} - \Pi_2\,\mathbf{v})\,q_h\,dx &= \sum_{K\in\mathcal{C}_h}\int_K \operatorname{div}(\mathbf{v}_{|K} - \Pi_2\,\mathbf{v}_{|K})q_{h|K}\,dx \\ &= \sum_{K\in\mathcal{C}_h} q_{h|K}\int_{\partial K}(\mathbf{v}_{|K} - \Pi_2\,\mathbf{v}_{|K})\cdot\hat{n}\,ds = 0,\end{aligned}$$

where we have used the fact that q_h is constant over each K.

Now we establish (5.8). First, $\Pi_2(\mathbf{v}) = \mathbf{0}\;\; \forall \mathbf{v} \in [\mathcal{P}_0(K)]^2$. Also, $\|\Pi_2\mathbf{v}\|_1 \le C\|\mathbf{v}\|_1$ due to (5.9). Hence by the Bramble-Hilbert lemma we have $|\Pi_2\mathbf{v}| \le C|\mathbf{v}|_{1,K}$, or $\|\Pi_2\mathbf{v}\|_{0,K} \le C|\mathbf{v}|_{1,K}$. Also, by an inverse estimate, $|\Pi_2\mathbf{v}|_{1,K} \le h_K^{-1}\|\Pi_2\mathbf{v}\|_{0,K}$. Then

$$\begin{aligned}\|\Pi_2\mathbf{v}\|_{1,K} &\le \|\Pi_2\mathbf{v}\|_{0,K} + |\Pi_2\mathbf{v}|_{1,K} \\ &\le C|\mathbf{v}|_{1,K} + |\Pi_2\mathbf{v}|_{1,K} \\ &\le C|\mathbf{v}|_{1,K} + h_K^{-1}\|\Pi_2\mathbf{v}\|_{0,K} \\ &\le C|\mathbf{v}|_{1,K} + Ch_K^{-1}\|\mathbf{v}\|_{0,K} \\ &\le C(h_K^{-1}\|\mathbf{v}\|_{0,K} + |\mathbf{v}|_{1,K}).\end{aligned}$$

□

Lemma 5.2 *Let $\{\mathcal{C}_h\}$ be a family of regular partitions of Ω, and let $\mathcal{F}_K : \hat{K} \to K$ denote the smooth invertible map associated with K, with $\hat{K}$ the reference square. Then the pair $([\mathcal{Q}_k(\Omega)]^2, \mathcal{P}_0(\Omega))$ is globally stable where $\mathcal{Q}_k(\Omega) = \{\mathbf{v} : \mathbf{v}_{|K} = \hat{\mathbf{v}} \circ \mathcal{F}_K^{-1}, \hat{\mathbf{v}} \in \mathcal{Q}_k(\hat{K})\}$.*

The proof is similar to the proof of Lemma 5.1.

We see therefore that (A4) holds for curvilinear quadrilateral and triangular regular elements. Then if (LS) holds, the inf-sup constant is given by Theorem 3.1.

We investigate condition (LS) computationally as follows. Let $\mathcal{F}_K$ be an arbitrary smooth invertible mapping. To verify the local stability condition (LS) we should use the subspaces $\mathbf{V}_k(K) \cap \mathbf{H}_0^1(K)$ and $W_k(K) \cap L_0^2(K)$. However, instead of $W_k(K) \cap L_0^2(K)$, it turns out to be easier, both computationally and theoretically, to use $W_k(K) \cap \widetilde{L_0^2}(K)$ where

$$\widetilde{L_0^2}(K) = \{\psi : \psi = \hat{\psi} \circ \mathcal{F}_K^{-1}, \hat{\psi} \in L_0^2(\hat{K})\}.$$

Note that functions $\psi \in \widetilde{L_0^2}(K)$ satisfy $\int_K \psi \, |J_K^{-1}| \, dx = 0$ instead of $\int_K \psi dx = 0$. We therefore define ($\widetilde{\text{LS}}$), an alternative condition to (LS):

($\widetilde{LS}$) For every $K \in \mathcal{C}_h$, given $q^* \in W_k(K) \cap \widetilde{L_0^2}(K)$, there exists $\mathbf{v}^* \in \mathbf{V}_k(K) \cap [H_0^1(K)]^2$ such that (3.4) holds.

The above computational substitution can be justified on the basis of the following theorem.

Theorem 5.2 *Let the spaces $\mathbf{V}_N, W_N$ satisfy either (LS) or $(\widetilde{LS})$, and (A4). Then the global stability estimate (3.5) holds.*

Proof: The case (LS), (A4) is proven in [20].

Let $q \in W_N$ be arbitrary. Then for each $K \in \mathcal{C}_h$, $q_{|K} = \hat{q} \circ \mathcal{F}_K^{-1}$ where $\hat{q} = \bar{\hat{q}} + \hat{q}^* \in W_k(K)$, with $\bar{\hat{q}} \in \mathcal{P}_0(\hat{K})$ and $\int_{\hat{K}} \hat{q}^* d\hat{x} = 0$. Then $q_{|K} = (\bar{\hat{q}} + \hat{q}^*) \circ \mathcal{F}_K^{-1} = \hat{q} \circ \mathcal{F}_K^{-1} + \hat{q} \circ \mathcal{F}_K^{-1} = \tilde{q}_{|K} + q^*_{|K}$, where $\tilde{q}_{|K} \in \mathcal{P}_0(K), q^*_{|K} \in W_k(K) \cap \widetilde{L}_0^2(K)$. Then write $q = \tilde{q} + q^*$ with $\tilde{q}$ being the weighted L^2 projection of q onto the space of piecewise constants:

$$\tilde{W}_N = \{q \in W_N : q_{|K} \in P_0(K) \ \ \forall K \in \mathcal{C}_h\}.$$

From Lemmas 5.1 and 5.2, there is $\tilde{\mathbf{v}} \in \mathbf{V}_N$ such that

$$(\operatorname{div} \tilde{\mathbf{v}}, \tilde{q}) \geq C_3 \|\tilde{q}\|_0^2 \text{ and } |\tilde{\mathbf{v}}|_1 \leq C_4 \|\tilde{q}\|_0, \tag{5.10}$$

with positive constants C_3 and C_4 independent of $\tilde{\mathbf{v}}$ and $\tilde{q}$.

For each $K \in \mathcal{C}_h$, we have $q^*_{|K} \in W_k(K) \cap \widetilde{L}_0^2(K)$ and hence by $(\widetilde{LS})$ we can find $\mathbf{v}^* \in \mathbf{V}_N$ such that $\mathbf{v}^*_{|K} \in [H_0^1(K)]^2$ and

$$(\operatorname{div} \mathbf{v}^*, q^*) \geq C_1 k^{-\gamma} \|q^*\|_0^2 \text{ with } |\mathbf{v}^*|_1 \leq C_2 \|q^*\|_0. \tag{5.11}$$

Since $\mathbf{v}^*_{|K} \in [H_0^1(K)]^2$, it holds that

$$(\operatorname{div} \mathbf{v}^*, \tilde{q}) = 0. \tag{5.12}$$

Let now $\mathbf{v} = \delta \tilde{\mathbf{v}} + \mathbf{v}^*$. Using (5.10)-(5.12), the Schwarz inequality and the

arithmetic-geometric mean inequality we get

$$\begin{aligned}(\operatorname{div}\mathbf{v},q) &= \delta(\operatorname{div}\tilde{\mathbf{v}},\tilde{q}) + \delta(\operatorname{div}\tilde{\mathbf{v}},q^*) + (\operatorname{div}\mathbf{v}^*,\tilde{q}) + (\operatorname{div}\mathbf{v}^*,q^*)\\ &\geq \delta C_3\|\tilde{q}\|_0^2 - \delta|\tilde{\mathbf{v}}|_1\|q^*\|_0 + C_1k^{-\gamma}\|q^*\|_0^2\\ &\geq \delta C_3\|\tilde{q}\|_0^2 - (\delta/2\varepsilon)\|q^*\|_0^2 - (\delta\varepsilon/2)|\tilde{\mathbf{v}}|_1^2 + C_1k^{-\gamma}\|q^*\|_0^2\\ &\geq \delta(C_3 - (C_4\varepsilon/2))\|\tilde{q}\|_0^2 + (C_1k^{-\gamma} - (\delta/2\varepsilon))\|q^*\|_0^2\\ &\geq C_5k^{-\gamma}(\|\tilde{q}\|_0^2 + \|q^*\|_0^2)\\ &= C_5k^{-\gamma}\|q\|_0^2,\end{aligned}$$

where we first choose $\varepsilon = C_3/C_4$ and then $\delta = \varepsilon k^{-\gamma}/C_1$. Since we then also have

$$|\mathbf{v}|_1 \leq \delta|\tilde{\mathbf{v}}|_1 + |\mathbf{v}^*|_1 \leq \delta C_4\|\tilde{q}\|_0 + C_2\|q^*\|_0 \leq C\|q\|_0,$$

the assertion is proved. □

Since (A4) holds by Lemmas 5.1 and 5.2, the global stability condition (3.5) depends on either (LS) or ($\widetilde{\text{LS}}$). We have not established (LS) for curvilinear elements based on the mixed methods of Chapters 3 and 4, but we provide computatioal validation of ($\widetilde{\text{LS}}$) in the next section. We also verify ($\widetilde{\text{LS}}$) analytically for modified versions of our quadrilateral mixed method spaces in Section 5.4

Provided the global stability condition holds, the following theorem gives error bounds for the mixed methods.

Theorem 5.3 *Let* $\mathbf{V}_N(\Omega), W_N(\Omega)$ *be defined on regular meshes* $\{\mathcal{C}_h\}$ *consisting of curvilinear triangles and quadrilaterals. Let the global stability condition (3.5) hold*

with constant γ independent of h. Let (A5)-(A6) hold with $n \geq 0$ in (A6). Then for any $\varepsilon > 0$, there exists a constant C_ε independent of $\mathbf{u}, p, h$, and k, but dependent on $\mathcal{K}$ in (5.6), such that

$$\|\mathbf{u} - \mathbf{u}_N\|_1 \leq C_\varepsilon h^l k^{-s+1+\varepsilon}(\|\mathbf{u}\|_s + \|p\|_{s-1}) \tag{5.13}$$

$$\|p - p_N\|_0 \leq C_\varepsilon h^l k^{-s+1+\gamma+\varepsilon}(\|\mathbf{u}\|_s + \|p\|_{s-1}) \tag{5.14}$$

where

$$l = \min\{s-1, k-n\}.$$

See proof of Theorem 5.2 in [20]. For MQ1-4,6 and MT2, $n = 0$. For MQ5 and MT1, $n = 1$.

5.3 Computation Of Inf-Sup Condition

We begin with the results of computing the $\inf - \sup$ constant from $(\widetilde{\text{LS}})$ for the space MT1 on mapped triangular elements. We consider elements that have exactly one curved edge. The first map is a parabola, see Figure 5.1, ranging from the extreme concave edge with parallel tangents to a reasonable range of convex parabolic edges. The results are found in Figure 5.2. We see that as long as the case where the edges meet with parallel tangents is avoided, the $\inf - \sup$ constant has about the same decay rate as the unmapped reference triangle, where $\gamma \approx 1$.

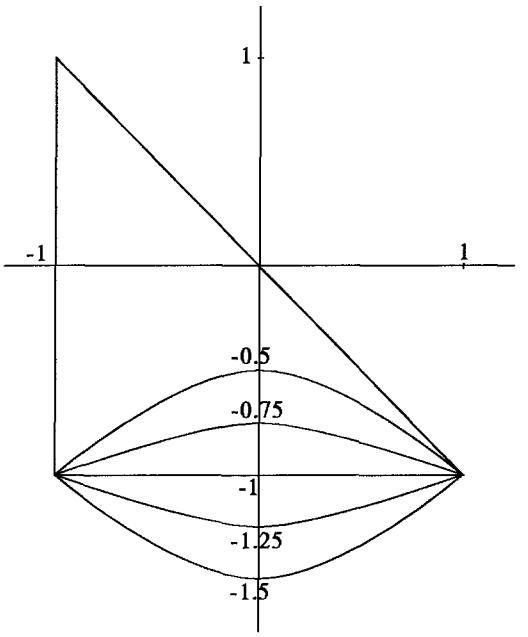

Figure 5.1: Curvilinear Triangles - Parabolic Edges

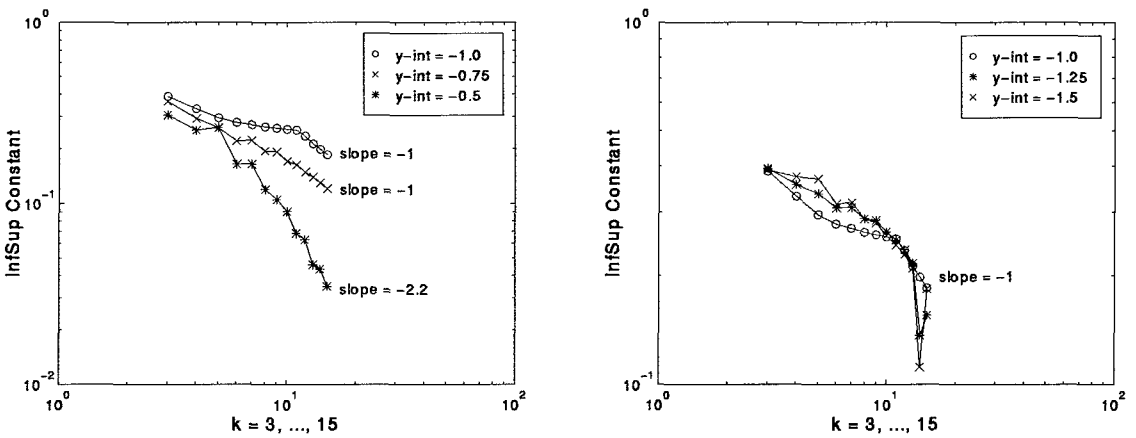

Figure 5.2: Inf-Sup Constants - Parabolic Triangles - Concave, Convex

The next case is for the circular maps shown in Figure 5.3. The range of maps considered is again from the case of concave parallel tangents to a reasonable range of convex circular edges. As with parabolas, as long as the case where edges meet with

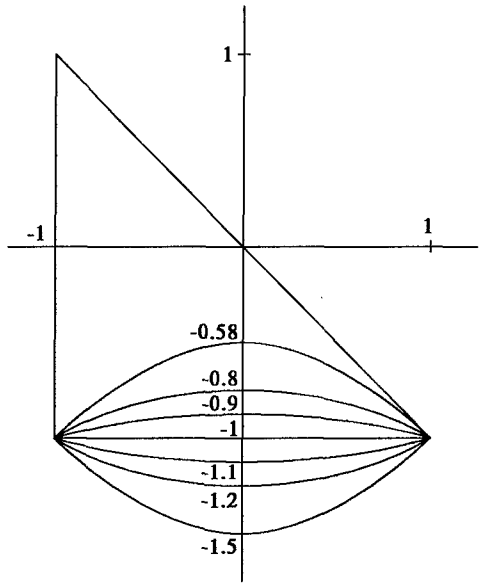

Figure 5.3: Curvilinear Triangles - Circular Edges

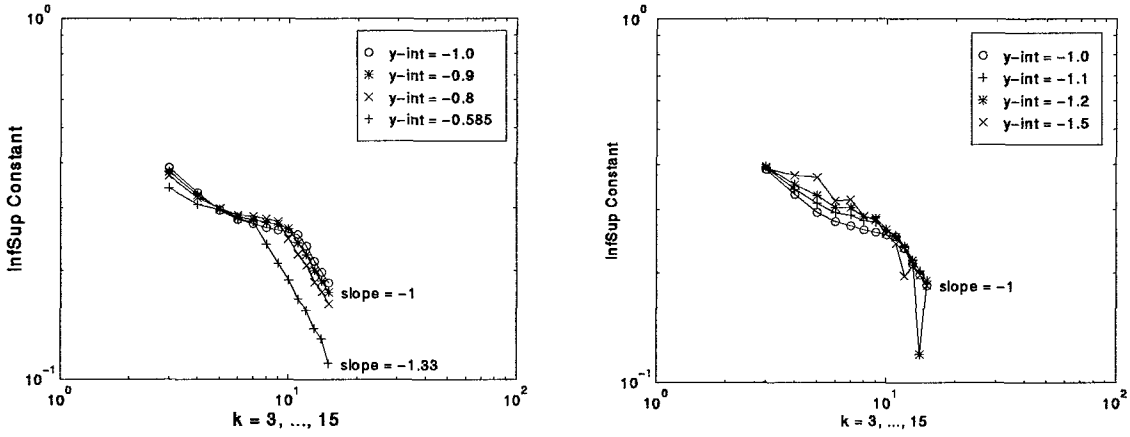

Figure 5.4: Inf-Sup Constants - Circular Triangles - Concave, Convex

parallel tangents is avoided, the decay rate γ is comparable to that of the unmapped element. This is consistent with our definition of regular mesh, which requires element interior angles be bounded away from 0 and π. These results are seen in Figure 5.4.

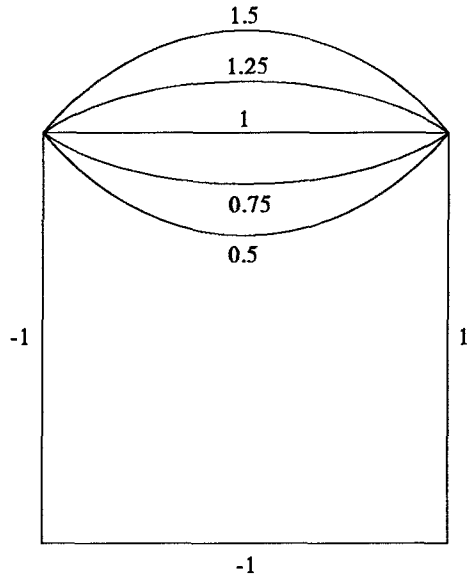

Figure 5.5: Curvilinear Quadrilaterals - Parabolic Edges

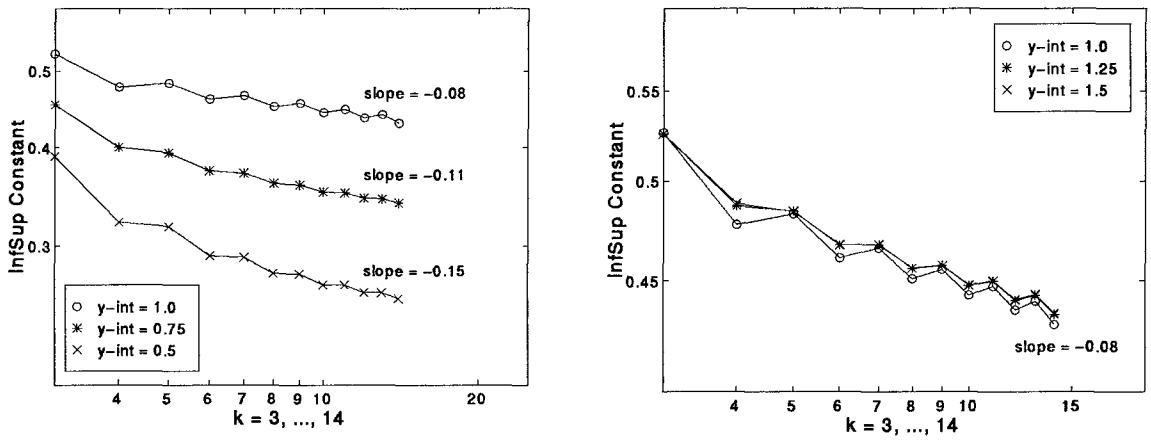

Figure 5.6: Inf-Sup Constants - Parabolic Quadrilaterals - Concave, Convex

We conclude that if triangular meshes are constructed so as to produce sufficiently regular elements, the resulting inf − sup constants are comparable to the linear case. We note that automatic mesh generators exist that produce regular meshes for most

practical Ω.

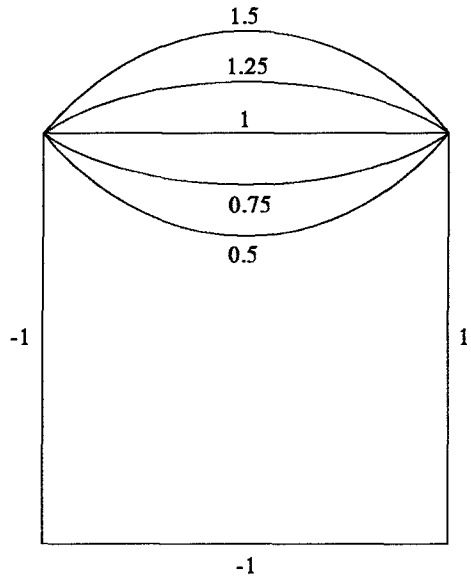

Figure 5.7: Curvilinear Quadrilaterals - Circular Edges

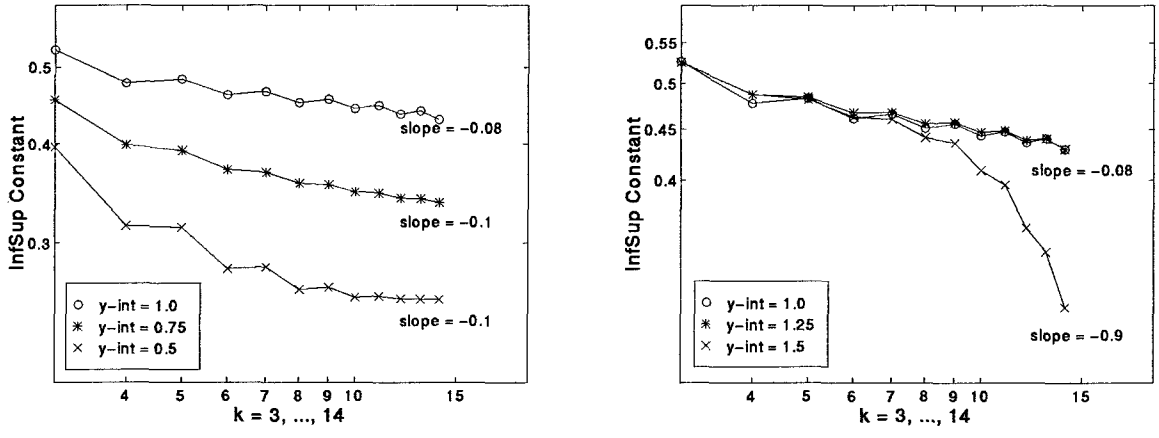

Figure 5.8: Inf-Sup Constants - Circular Quadrilaterals - Concave, Convex

We performed similar calculations for the curvilinear quadrilaterals in Figures 5.5 and 5.7, using MQ4. The results are given in Figures 5.6 and 5.8. We see that the k

tested are well within the pre-asymptotic range, since the rate is not close to $-\frac{1}{2}$.

5.4 A Stable Curvilinear Quadrilateral Element

The stability of mixed methods MQ1-6 depends on condition (LS) (or equivalently ($\widetilde{\text{LS}}$)) and the inf-sup constant for these methods depends on γ in (LS). So far we only have computational estimates of γ. In this section we define curvilinear elements for which a theoretical inf-sup constant of $Ck^{-\frac{1}{2}}$ can be established, identical to that for parallelogram elements (see Corollary 3.1).

To define these elements, use (3.2) to define V_N, W_N in terms of $V_k(K), W_k(K)$. For MQ1-6, we define $W_k(K)$ by (3.1). We define $V_k(K)$ as follows:

$$V_k(K) = \left\{ \begin{array}{ll} \mathbf{v} = \mathcal{L}_K(\hat{\mathbf{v}}) & : \hat{\mathbf{v}} \in \mathbf{V}_k^0(\hat{K}) \\ \mathbf{v} = \hat{\mathbf{v}} \circ \mathcal{F}_K^{-1} & : \hat{\mathbf{v}} \in \mathbf{V}_k(\hat{K}) \setminus \mathbf{V}_k^0(\hat{K}) \end{array} \right\}, \tag{5.15}$$

where $\mathbf{u} = \mathcal{L}_K(\hat{\mathbf{u}}) = |J_K|^{-1} J_K \hat{\mathbf{u}} \circ \mathcal{F}_K^{-1}$ is the Piola transformation of $\hat{\mathbf{u}}$ [6]. Since $\hat{\mathbf{v}} \in V_k^0(\hat{K}) \Rightarrow \mathbf{v} \in V_k^0(K)$, $\mathbf{V}_N$ is again conforming. We then have the following theorem.

Theorem 5.4 *Let $\mathbf{V}_N, W_N$ be defined by MQ1-6, (5.15) and (3.2). Then*

$$\inf_{q \in W_N} \sup_{\mathbf{v} \in \mathbf{V}_N \setminus \{0\}} \frac{(\operatorname{div} \mathbf{v}, q)}{\|\mathbf{v}\|_1 \|q\|_0} \geq Ck^{-\frac{1}{2}}, \tag{5.16}$$

where the constant C is independent of h, k and q, i.e. (3.5) holds.

Proof: We show that ($\widetilde{\text{LS}}$) holds with $\gamma = \frac{1}{2}$. The theorem then follows from Theorem 5.2.

Let $q^* \in W_k(K) \cap \widetilde{L_0^2}(K)$ be arbitrary and define $\hat{q}^* \in W_k(\hat{K}) \cap L_0^2(\hat{K})$ by $\hat{q}^* = q^* \circ F_K$ ($\hat{q}^* \in L_0^2(\hat{K})$ by definition of $\widetilde{L_0^2}(K)$). On the reference square, the continuous inf-sup condition holds. Hence, there exists $\hat{\mathbf{v}} \in [H_0^1(\hat{K})]^2$ such that

$$(\text{div}\ \hat{\mathbf{v}}, \hat{q}^*) \geq C\|\hat{q}^*\|_{0,\hat{K}}^2 \quad \text{and} \quad |\hat{\mathbf{v}}|_{1,\hat{K}} \leq \|\hat{q}^*\|_{0,\hat{K}}, \tag{5.17}$$

with C independent of $\hat{q}^*$ and $\hat{\mathbf{v}}$.

Define $\hat{\mathbf{v}}^* \in \mathbf{V}_k^0(\hat{K})$ by $\hat{\mathbf{v}}^* = \mathcal{T}_k\hat{\mathbf{v}}$. By (A2), (A3) and (5.17) we obtain (integrating by parts)

$$\begin{aligned}(\text{div}\ \hat{\mathbf{v}}^*, \hat{q}^*)_{\hat{K}} &= -(\hat{\mathbf{v}}^*, \nabla\hat{q}^*)_{\hat{K}} = -(\mathcal{T}_k\hat{\mathbf{v}}, \nabla\hat{q}^*)_{\hat{K}} \\ &= -(\hat{\mathbf{v}}^*, \nabla\hat{q}^*)_{\hat{K}} = (\text{div}\ \hat{\mathbf{v}}, \hat{q}^*)_{\hat{K}} \\ &\geq C\|\hat{q}^*\|_{0,\hat{K}}^2\end{aligned} \tag{5.18}$$

and

$$|\hat{\mathbf{v}}^*|_{1,\hat{K}} = |\mathcal{T}_k\hat{\mathbf{v}}|_{1,\hat{K}} \leq Ck^{\frac{1}{2}}\|\hat{\mathbf{v}}\|_{1,\hat{K}} \leq Ck^{\frac{1}{2}}\|\hat{q}^*\|_{0,\hat{K}}. \tag{5.19}$$

This proves the discrete inf-sup condition on the reference square.

Next, we let

$$\mathbf{v}^* = \mathcal{L}_K(\hat{\mathbf{v}}^*) = |J_K|^{-1}J_K\hat{\mathbf{v}}^* \circ \mathcal{F}_K^{-1}. \tag{5.20}$$

Then by (A1), $\mathcal{L}_K(\hat{\mathbf{v}}^*) \in \mathbf{V}_k(K) \cap [H_0^1(K)]^2$. Using the basic property of the Piola transformation [6], we have

$$(\text{div}\ \mathbf{v}^*, q^*)_K = (\text{div}\ \hat{\mathbf{v}}^*, \hat{q}^*)_{\hat{K}}. \tag{5.21}$$

By assumption of the requlrity of the elements, we have

$$\|q^*\|_{0,K} \cong C h_K^{\frac{1}{2}} \|\hat{q}^*\|_{0,\hat{K}} \quad \text{and} \quad |\mathbf{v}^*|_{1,K} \leq C h_K^{-\frac{1}{2}} |\hat{\mathbf{v}}^*|_{1,\hat{K}}. \tag{5.22}$$

Then $(\widetilde{LS})$ follows from (5.21) and (5.22), and the local conditions (5.18) and (5.19).

□

By Theorem 5.3, since (3.5) holds and (A5)-(A6) hold, therefore we get the convergence rates in (5.13) and (5.14). We have not used these modified spaces in our computations. However, the experiments in Section 5.5 reflect these rates of convergence.

We point out that to implement these spaces, one needs only a basis for $W_k(\hat{K})$ and $V_k(\hat{K})$, the mapping $\mathcal{F}_K$ and its Jacobian. In particular, the inverse mapping $\mathcal{F}_K^{-1}$ is not required.

5.5 Numerical Experiments

In the p-version, element size is fixed, so curvilinear elements must be used to accurately model the domain for most practical problems. We use the blending function method (see [24]) to match the domain exactly. We also study meshes which have interior edges that are curved. We study the standard and mixed methods on both curvilinear quadrilateral and triangular elements.

We limit our investigation to domains (meshes) that are typical in applications. This is of course a subjective restriction, but the curved domains seen in practice

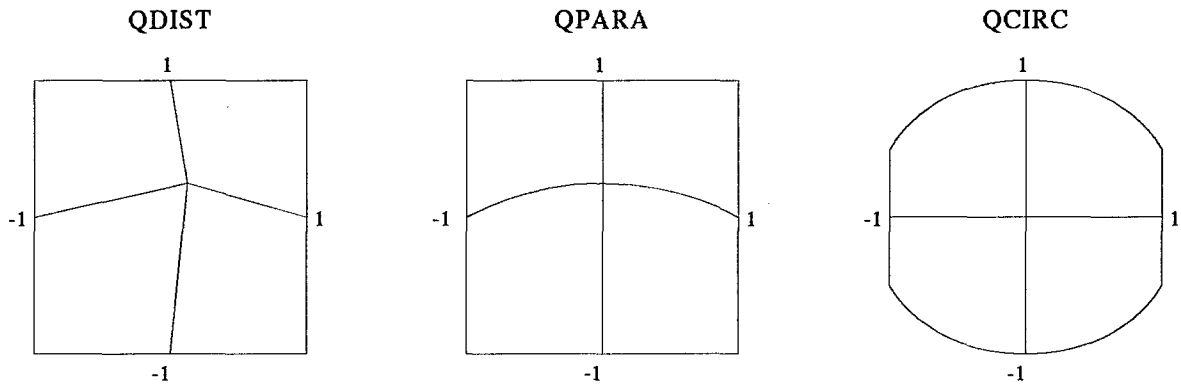

Figure 5.9: Curvilinear Quadrilateral Meshes

can often be parameterized using piecewise low degree polynomials or trigonometric functions (ellipses). These domains can be produced by mapping the reference domain with non-affine invertible mappings.

The quadrilateral meshes we use are given in Figure 5.9 and the triangular meshes are given in Figure 5.10. These meshes were chosen to include elements with edges that are parameterized by low-order polynomials (parabolas) and trigonometric functions (circles), with both interior and boundary curved edges.

5.5.1 Finite Element Spaces

In Chapters 3 and 4 we described several polynomial spaces defined on reference elements. When curvilinear elements are used, the finite element spaces are composed by applying non-affine invertible smooth mappings to reference polynomial spaces. The resulting spaces are not polynomials, but mapped images of these reference polynomial spaces. Recall that SQ : $V_k = Q'_k(\hat{K})$ and ST: $V_k = \mathcal{P}_k(\hat{K})$.

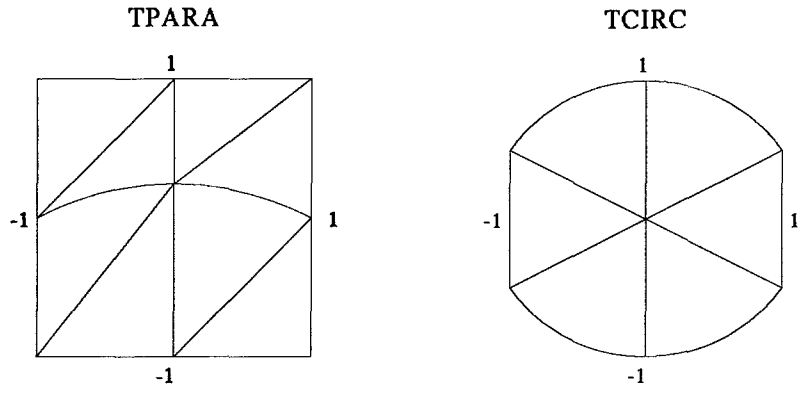

Figure 5.10: Curvilinear Triangular Meshes

We restrict our attention to MQ1: $V_k = Q_k(\hat{K}) \cap \mathcal{P}_{k+2}(\hat{K}), W_k = \mathcal{P}_{k-1}(\hat{K})$ and $MT1 : V_k = \mathcal{P}_k(\hat{K}), W_k = \mathcal{P}_{k-2}(\hat{K})$. A partition $\mathcal{C}_h$ of the domain Ω is constructed such that $\Omega = \cup_{K \in \mathcal{C}_h} K$ as indicated in Figures 5.9 and 5.10. For each K there exists a smooth invertible mapping $\mathcal{F}_K$ such that $K = \mathcal{F}_k(\hat{K})$, where $\hat{K}$ is either the reference triangle or square.

5.5.2 Computational Convergence Results

We restrict our attention to the p version and begin by examining SQ and ST on meshes with curvilinear quadrilateral and the triangular elements, respectively. We continue using energy norm and SNS to measure the error as discussed in Chapter 3. Throughout this section we solve model problem SING with a near-singular (unsmooth) solution.

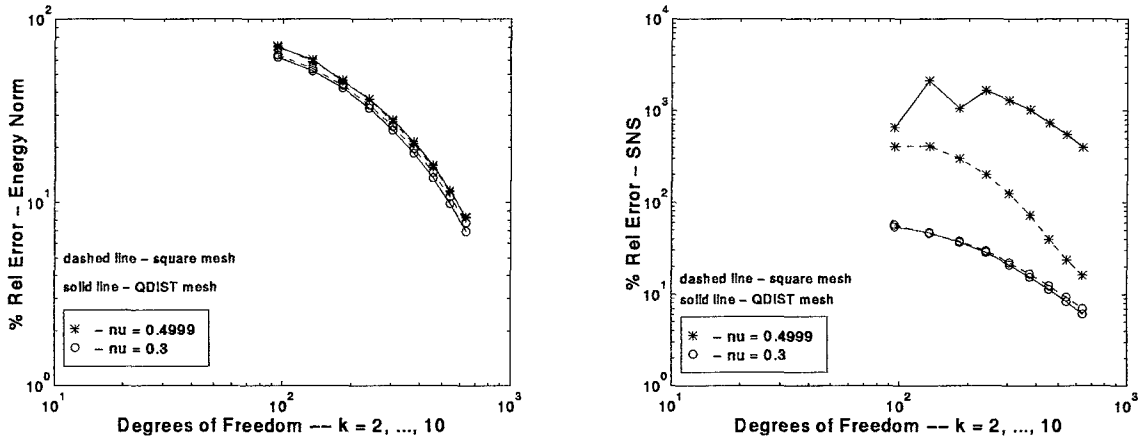

Figure 5.11: Method SQ, Square Mesh vs QDIST, Unsmooth solution.

SFEM on Quadrilateral Elements

We first look at method SQ on meshes with straight and curved interior boundaries. For this we solve problem SING on meshes QDIST and QPARA and also a mesh with four square elements. In Figures 5.11 and 5.12 we see that the error in energy norm is not sensitive to changes in ν, however this is not true for the SNS error. As $\nu \to \frac{1}{2}$ the relative error in SNS increases significantly on both QDIST and QPARA, much more so than it does for the square mesh. We conclude that method SQ has near optimal behavior for energy norm but that it locks in SNS when the mesh contains elements with curved interior edges. Table 5.5.2 shows that the locking ratios are significantly worse when curved interior edges are present.

The results for the model problem on mesh QCIRC are shown in Figure 5.13. We see that the error in both the energy norm and SNS increases significantly as $\nu \to \frac{1}{2}$. Thus we conclude that the standard method degrades significantly when curvilinear

	N							
	95	135	183	239	303	375	455	543
Square - L_S	7.12	8.85	7.85	6.71	5.63	4.33	3.19	2.53
QDIST - L_S	12.08	45.26	28.78	57.90	61.98	66.20	64.77	65.72
QPARA - L_S	35.93	23.70	57.73	64.52	65.49	74.49	78.79	81.54

Table 5.1: SNS Locking Ratios ($L_S(0.4999, N)$), SQ, Unsmooth Solution.

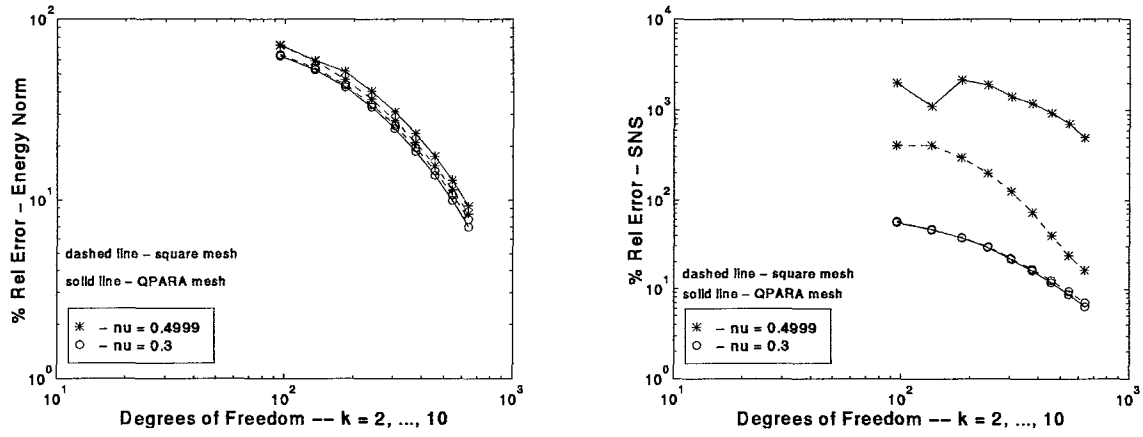

Figure 5.12: Method SQ, Square Mesh vs QPARA, Unsmooth solution.

elements are used to partition domains with curved boundaries. This energy norm locking was not observed for method SQ on straight sided elements.

SFEM On Triangular Elements

To evaluate the standard method on curvilinear triangular elements we use meshes TPARA and TCIRC shown in Figure 5.10. Mesh TPARA has curved interior edges,

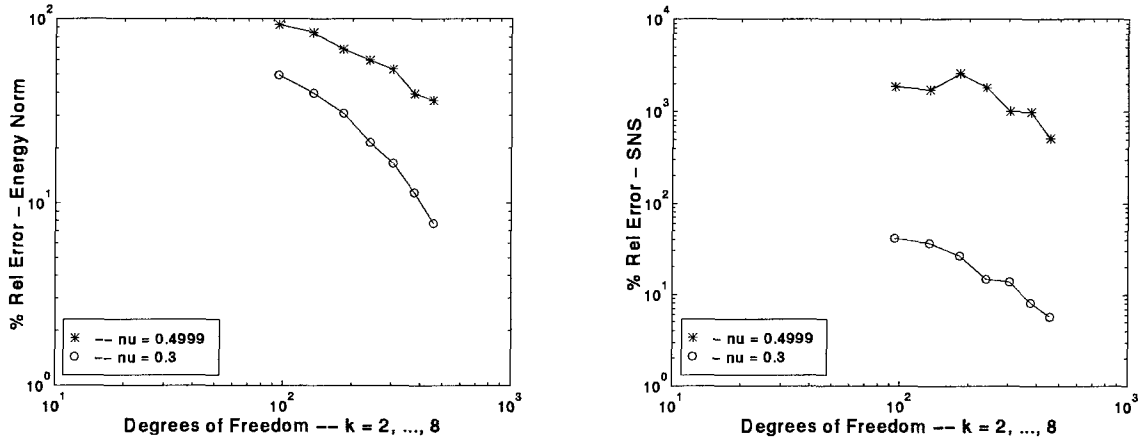

Figure 5.13: Method SQ, Mesh QCIRC, Unsmooth solution.

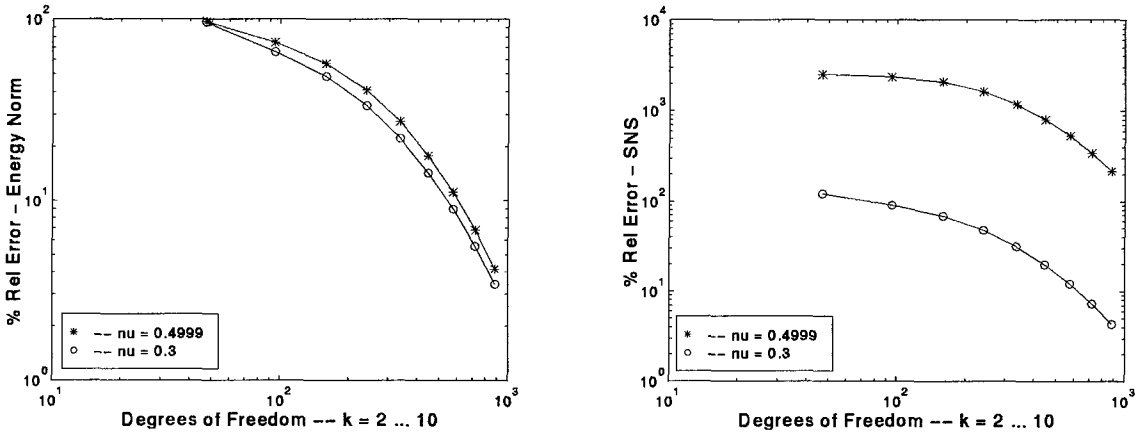

Figure 5.14: Method ST, Mesh TPARA, Unsmooth solution.

while TCIRC has curved elements on the boundary. As seen in Figures 5.14 and 5.15, method ST exhibits no energy norm locking on either mesh while SNS locking ratios are significant in both, as seen in Table 5.5.2.

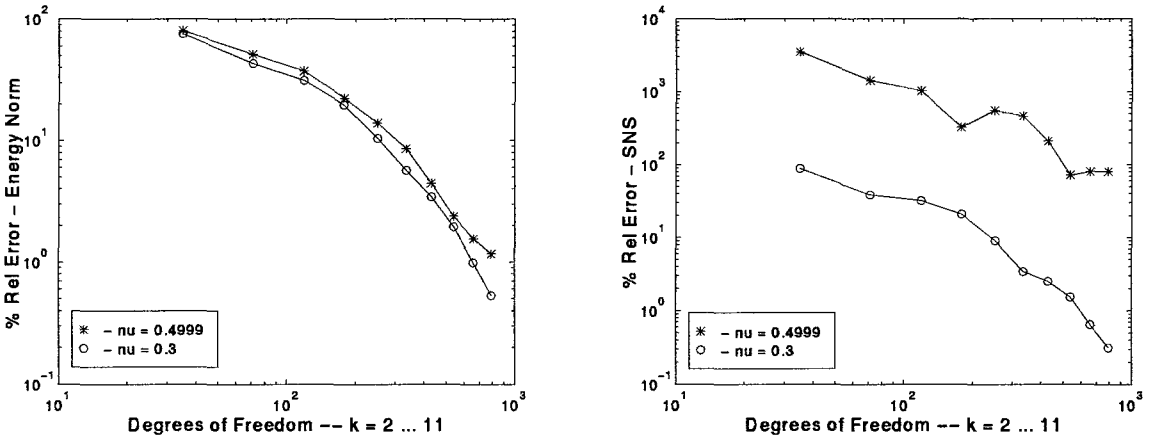

Figure 5.15: Method ST, Mesh TCIRC, Unsmooth solution.

	N								
	47	95	159	239	335	447	575	719	879
TPARA - L_S	20.82	26.10	30.50	34.10	37.40	40.72	44.04	47.32	50.29
	N								
	35	71	119	179	251	335	431	539	659
TCIRC - L_S	39.55	37.26	32.07	15.73	61.06	136.21	84.67	46.92	123.77

Table 5.2: SNS Locking Ratios ($L_S(0.4999, N)$), ST, Unsmooth Solution.

MFEM On Quadrilateral Elements

We now turn our attention to mixed finite element methods. We do the same sequence of experiments for the mixed methods as we did for the standard method. When curved

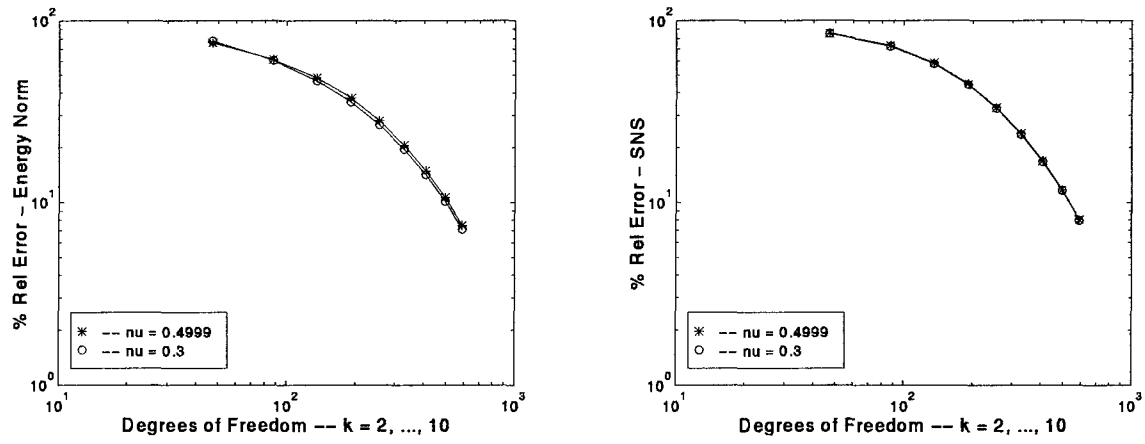

Figure 5.16: Method MQ1, Mesh QDIST, Unsmooth solution.

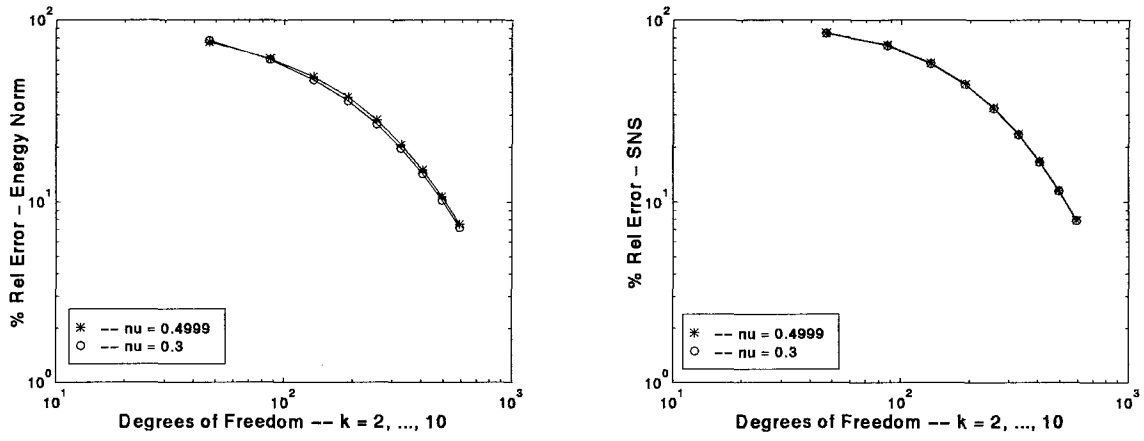

Figure 5.17: Method MQ1, Mesh QPARA, Unsmooth solution.

edges are in the mesh interior, as in QDIST and QPARA, the curves for $\nu = 0.3$ and for $\nu = 0.4999$ are essentially the same. Thus we see in Figures 5.16 and 5.17 that method MQ1 is very robust on meshes with curved interior edges. Similarly, on mesh QCIRC virtually no increase in the errors is observed, as seen in Figure 5.18.

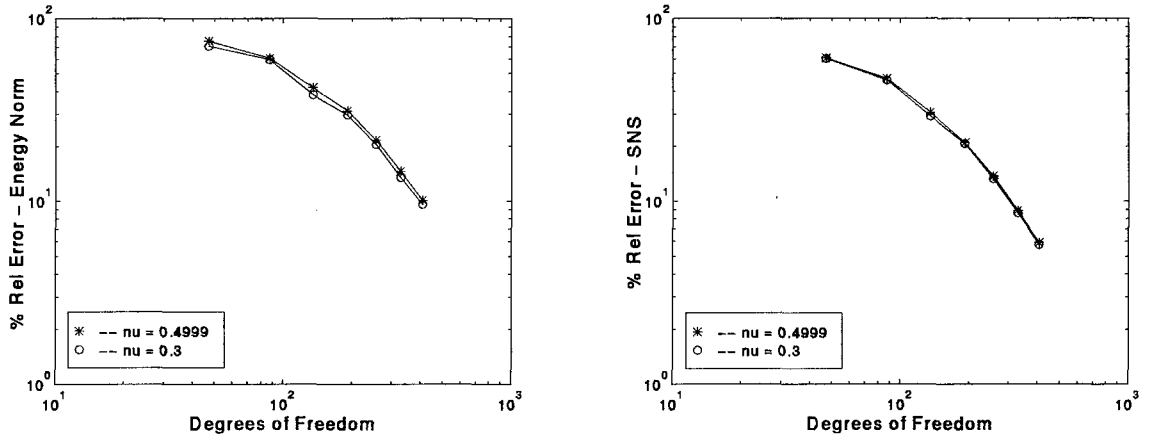

Figure 5.18: Method MQ1, Mesh QCIRC, Unsmooth solution.

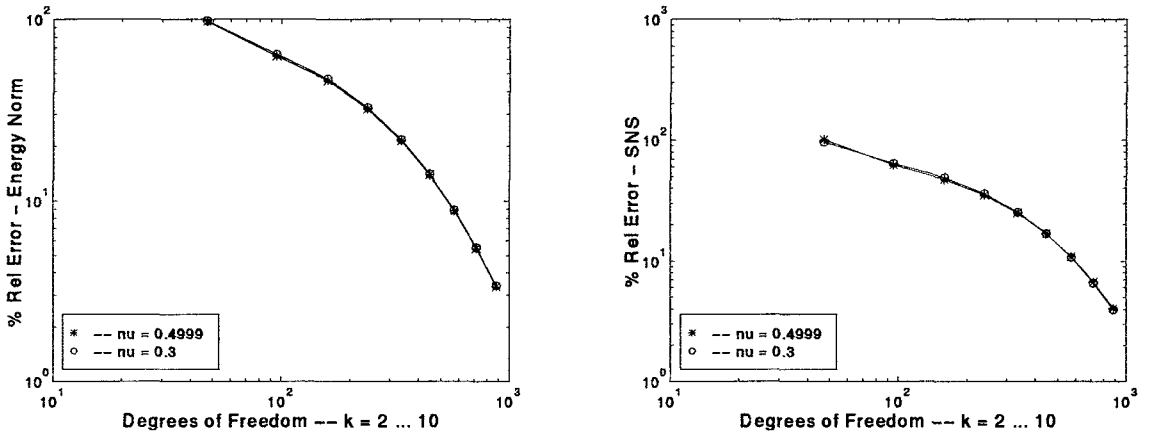

Figure 5.19: Method MT1, Mesh TPARA, Unsmooth solution.

MFEM On Triangular Elements

To study mixed methods on curvilinear triangular elements we use MT1 (which has the same displacement space as ST) to solve the model problem on mesh TPARA as an example of a mesh with curved interior edges and on mesh TCIRC as and example of a mesh with curved edges on the boundary. We see in Figures 5.19 and 5.20 the

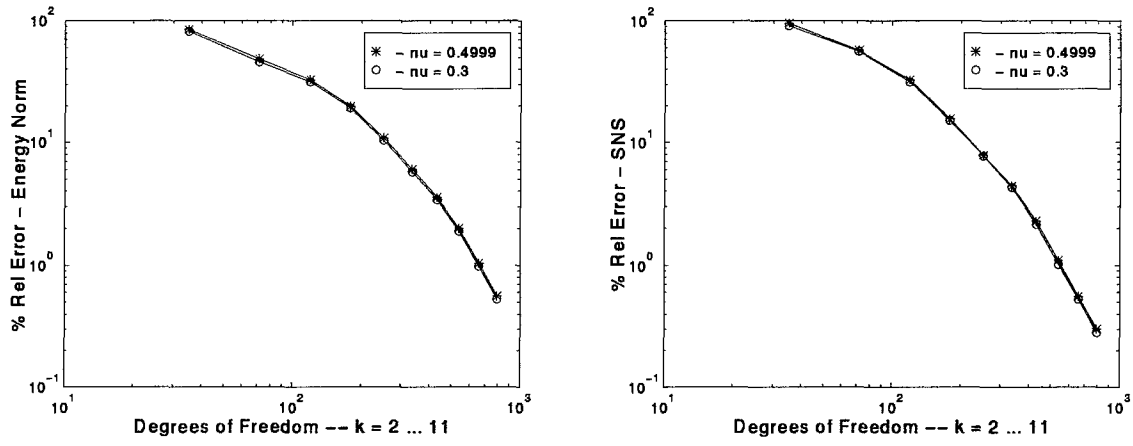

Figure 5.20: Method MT1, Mesh TCIRC, Unsmooth solution.

error is unaffected as $\nu \to \frac{1}{2}$.

In summary, when the curved edges are on the mesh *interior*, the standard method showed mild energy norm locking but significant SNS locking on both quadrilateral and triangular meshes. On the other hand, the mixed methods show essentially identical error curves for both quadrilateral and triangular meshes in both energy and SNS as $\nu \to \frac{1}{2}$.

Meshes with curved *exterior* boundaries influence both displacement and SNS locking, for the standard method. Some locking was seen in the energy norm on both quadrilateral and triangular meshes which was not present on straight sided elements. In addition, SNS locking was severe. For the mixed methods the rate of convergence was unaffected in the problems we studied, both for the energy norm and SNS, although minor locking ratios were observed in some cases.

5.6 Computing Point Values - A Benchmark Problem

In the engineering design process, often the objective is to identify regions of high stress and produce a design that distributes the stress more evenly throughout the body, producing lower maximum stress levels. This requires the analytical tool to accurately compute point values of stress and other quantities of engineering interest. To evaluate the point value extraction capability of the FEMs we are studying, we turn to a benchmark problem from [25] which we will refer to as the Rigid Circular Inclusion (RCI) problem.

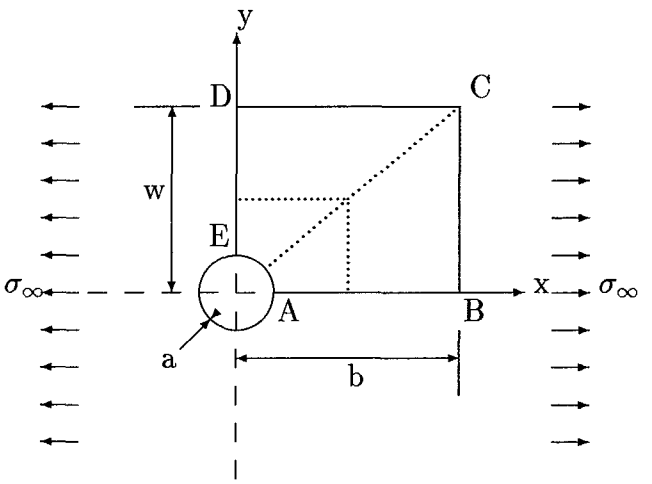

Figure 5.21: Rigid Circular Inclusion Problem and Quadrilateral Mesh.

This problem involves a rigid circular inclusion in an infinite plate, subject to unidirectional tension under plane strain conditions. The problem is illustrated in

Figure 5.21. The exact displacement components, found in [15], are:

$$\begin{aligned} u_r &= \frac{\sigma_\infty}{8Gr}\left\{(\kappa-1)r^2 + 2\gamma a^2 + \left[\beta(\kappa+1)a^2 + 2r^2 + \frac{2\delta a^4}{r^2}\right]\cos 2\theta\right\}, \\ u_\theta &= -\frac{\sigma_\infty}{8Gr}\left[\beta(\kappa-1)a^2 + 2r^2 - \frac{2\delta a^4}{r^2}\right]\sin 2\theta, \end{aligned}$$

and the exact stress components are:

$$\begin{aligned} \sigma_r &= \frac{\sigma_\infty}{2}\left[1 - \frac{\gamma a^2}{r^2} + \left(1 - \frac{2\beta a^2}{r^2} - \frac{3\delta a^4}{r^4}\right)\cos 2\theta\right], \\ \sigma_\theta &= \frac{\sigma_\infty}{2}\left[1 + \frac{\gamma a^2}{r^2} - \left(1 - \frac{3\delta a^4}{r^4}\right)\cos 2\theta\right], \\ \tau_{r\theta} &= -\frac{\sigma_\infty}{2}\left(1 + \frac{\beta a^2}{r^2} + \frac{3\delta a^4}{r^4}\right)\sin 2\theta, \end{aligned}$$

where $\kappa, \beta, \gamma, \delta$ are constants which depend on Poisson's ratio ν only. In the case of plane strain:

$$\kappa = 3 - 4\nu, \quad \beta = -\frac{2}{3-4\nu}, \quad \gamma = -\frac{2-4\nu}{2}, \quad \delta = \frac{1}{3-4\nu}.$$

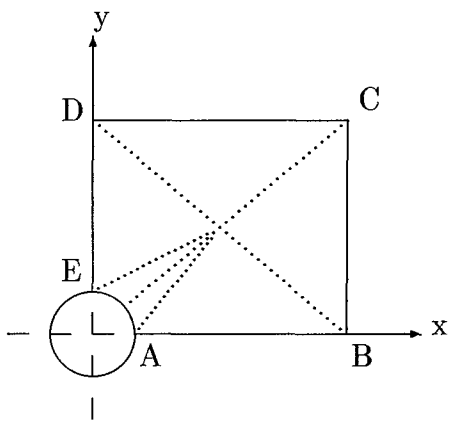

Figure 5.22: Rigid Circular Inclusion Problem - Triangular Mesh.

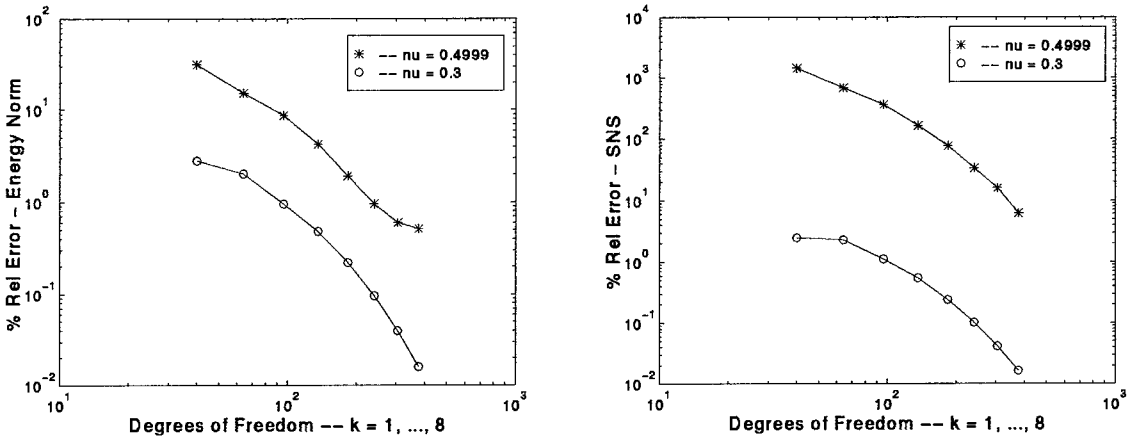

Figure 5.23: RCI problem, Method SQ, Quadrilateral elements.

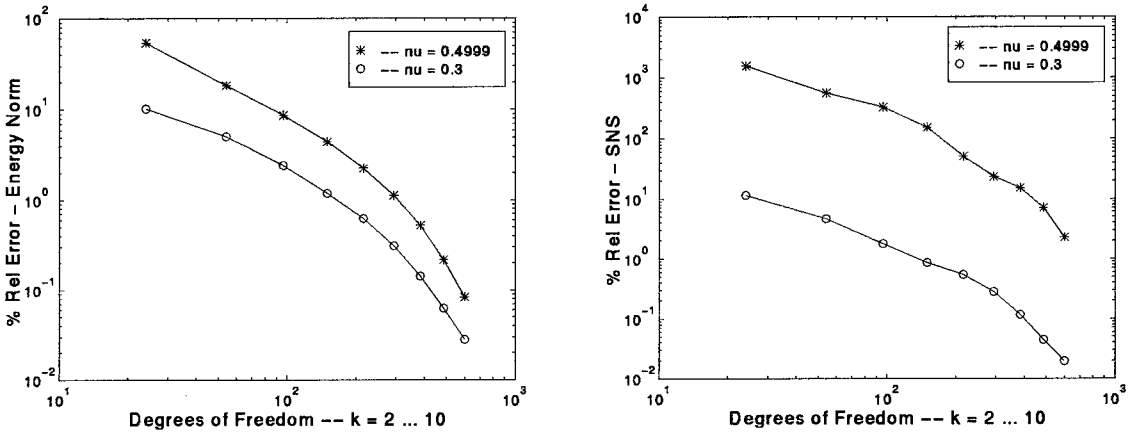

Figure 5.24: RCI problem, Method ST, Triangular elements.

Before we look at SNS point value extraction, we do the same error measurements we have done in previous chapters. The first two experiments are with SQ and ST using p-refinement on the RCI problem; the triangular mesh is shown in Figure 5.22. The results are shown in Figures 5.23 and 5.24. In Table 5.6 we see that both methods have significant locking ratios, although the rates of convergence appear unaffected as

$\nu \to \frac{1}{2}$. In general, the locking ratios for ST are smaller than those for SQ. In both methods, the locking ratios stay relatively constant over the range of k we tested.

	N							
SQ	40	69	96	136	184	240	304	376
L_E	11.21	7.52	9.14	8.84	8.67	9.95	15.05	32.24
L_S	585.28	296.40	326.04	303.42	318.91	329.10	382.76	377.50
	N							
ST	24	54	96	150	216	294	384	486
L_E	5.27	3.60	3.59	3.75	3.63	3.62	3.67	3.46
L_S	136.61	120.29	183.64	178.30	93.06	82.93	129.70	159.59

Table 5.3: Locking Ratios, SQ and ST, RCI Problem.

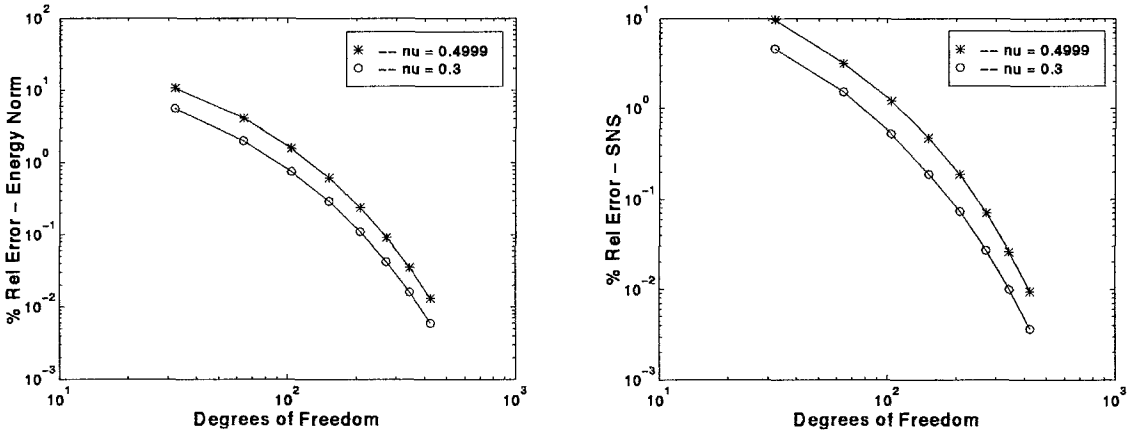

Figure 5.25: RCI problem, Method MQ1, Quadrilateral elements.

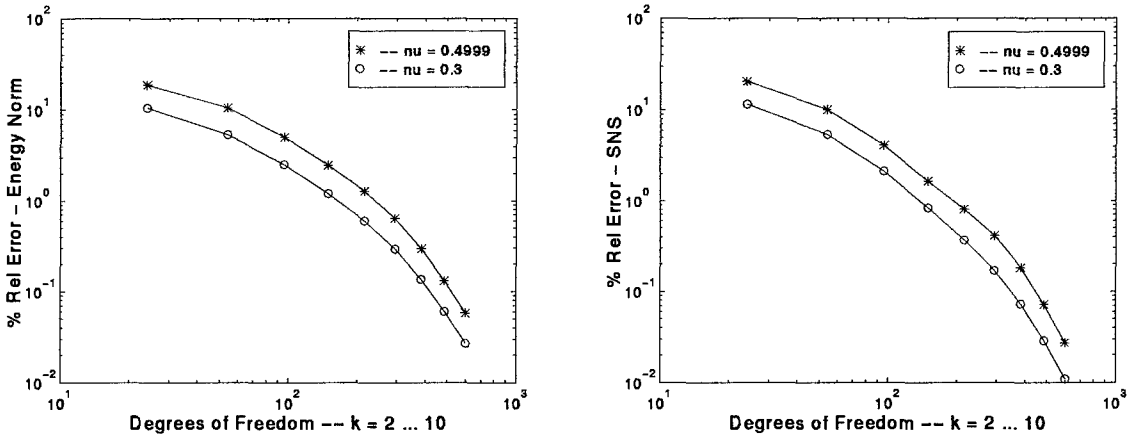

Figure 5.26: RCI problem, Method MT1, Triangular elements.

In both energy norm and SNS, MQ1 and MT1 produce locking ratios of about 2, as seen in Figures 5.25 and 5.26.

We conclude that mixed methods on meshes with curvilinear boundaries are subject to slight increase in error as $\nu \to \frac{1}{2}$ although the rate of convergence seems unaffected. On the other-hand, SFEM on meshes with curvilinear boundaries shows significant locking ratios, particularly in SNS. For this model problem, we also see non-trivial locking ratios in energy norm, which are significantly greater than those observed for the model problem of Section 5.3.

As mentioned above, an important capability of an FEM is point extraction of stress, which in SQ and ST may be done by differentiating the computed displacements. It is shown in [25] that $\sigma_x - \sigma_y$ and τ_{xy} can be accurately extracted this way, even as $\nu \to \frac{1}{2}$, but that $\sigma_x + \sigma_y = \text{SNS}$ cannot. (For the latter, at least in two dimensions, post-processing could be used - see [25].)

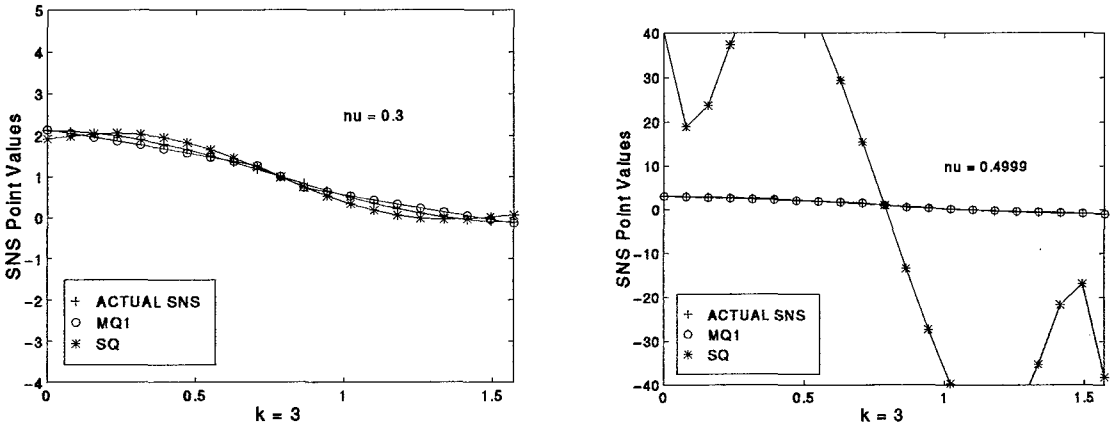

Figure 5.27: SNS Point Values MQ1 vs SQ, k = 3, $\nu = 0.3$ and 0.4999.

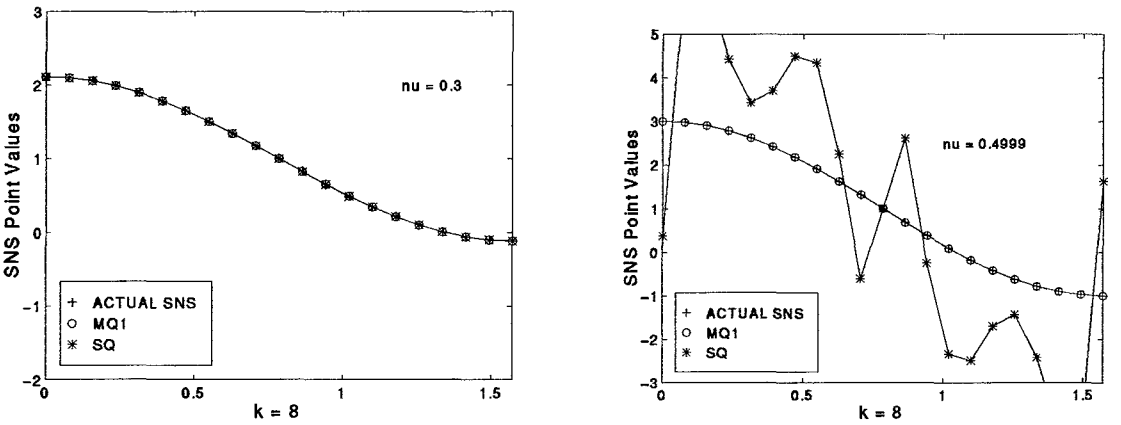

Figure 5.28: SNS Point Values MQ1 vs SQ, k = 8, $\nu = 0.3$ and 0.4999.

In Figure 5.27 and 5.28 we compare the point values of SNS along the arc AE (see Figure 5.21), computed using SQ (differentiation of the displacements) and MQ1. We note that when $\nu = 0.3$, both methods compute the actual SNS reasonably well even for $k = 3$; while for $k = 8$ they match the actual values very well. On the other hand, when $\nu = 0.4999$, we observe that even for $k = 3$, MQ3 still matches the exact solution

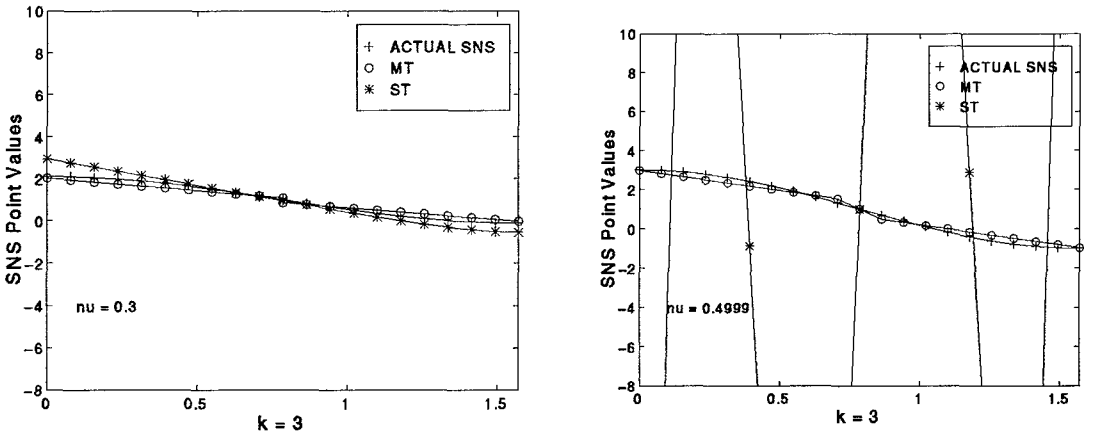

Figure 5.29: SNS Point Values MT1 vs ST, $k = 3$, $\nu = 0.3$ and 0.4999.

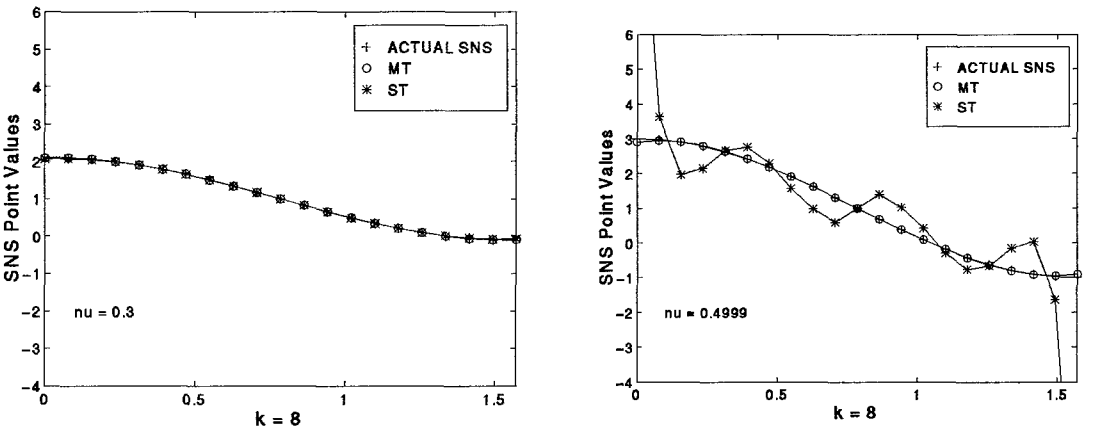

Figure 5.30: SNS Point Values MT1 vs ST, $k = 8$, $\nu = 0.3$ and 0.4999.

reasonably well, while SQ produces highly oscillatory results. The oscillations continue in SQ even for $k = 8$, while MQ3 and the exact solution are essentially identical for this k.

We performed the same set of experiments with ST and MT1 on a triangular mesh (see Figure 5.21) for RCIP with 6 elements. The results in Figures 5.29 and 5.30 are

qualitatively the same as with quadrilateral elements. MT1 performs well over the range of ν tested while ST produces good results for $\nu = 0.3$ but when $\nu = 0.4999$ the output from ST is oscillatory even for large k.

5.7 Summary

In this chapter, we have investigated the locking characteristics of several different FEMs. The performance of these methods is summarized in Table 5.7. A "Yes" means that the method converges at the asymptotic best rate, is locking-free, and has negligible locking ratios (≤ 4). "Rate" means the rate of convergence is less than optimal. "Lock" means the method locks to some degree. "LR" means the locking ratios are significant (> 4). The h version results refer to experiments on meshes with straight edges (Chapter 3 and 4 results). The p version results refer to meshes with straight edges as well as meshes with curved boundaries (Chapter 5 results).

No computations were done using MT2, although we expect it to perform similar to MQ1,2 and 4.

Method	h version		p version			
	Displacement	Stress	Displacement		Stress	
	Straight	Straight	Straight	Curve	Straight	Curve
SQ	Lock	Lock	Yes	Lock	LR	Lock
ST	Lock $k \leq 3$ Yes, $k = 4$	Lock $k \leq 3$ LR $k = 4$	Yes	LR	Yes	LR
MQ1,2,4	Yes	Yes	Yes	Yes	Yes	Yes
MQ3,5	Rate	Rate	Yes	Yes	Yes	Yes
MT1	Rate	Rate	Yes	Yes	Yes	Yes

Table 5.4: Convergence and locking properties of the different methods.

Chapter 6

An Application to Nonlinear Elasticity

The analysis of mechanical components and structures is most commonly performed on the basis of the linear theory of elasticity [12]. This approach gives excellent results for a large variety of problems and is based on the assumption that the strains and displacements are small. In the case of strains, "small" means much less than unity. In the case of displacements, "small" means that the original undeformed configuration and the final configuration of a body should not differ by much, so that enforcing equilibrium in the undeformed configuration is the same as enforcing equilibrium in the deformed configuration. In many important problems, for example when the limits of the load carrying capacity of a structure are of interest, the displacements are large enough that the equilibrium equations in the deformed configuration are

very different from those in the undeformed configuration. In order to obtain reliable results, a geometrically nonlinear analysis must be performed [16].

In [16], an iterative method is described for solving geometrically nonlinear problems in finite elasticity. It is based on a spatial formulation, which has some advantages over the traditional material formulation. These include: (a) the equilibrium equations are satisfied in the deformed configuration; (b) the displacement components are approximated by high-order polynomials and the blending function method is used to provide an accurate geometric description of the deformed configuration; (c) the discretization errors are controlled by p-refinement; (d) the simulation of nonconservative loads, such as follower loads, does not require any additional extensions in the formulation, nor does it destroy the symmetry of the resulting stiffness matrix; and (e) the extraction of stresses from the finite element solution is straightforward, since in this approach the equilibrium equations are expressed in terms of the Cauchy stresses. This formulation is a standard finite element displacement-based formulation. We use this spatial formulation to define a mixed method by introducing an independent variable for the "pressure".

6.1 Mixed Method - Spatial Formulation

Using the equilibrium equations of elasticity (2.1a) we multiply by a test function $\mathbf{v} \in \mathbf{V}$ and integrate to get the variational form of the equilibrium equations,

$$\int_\Omega (\sigma_x v_{1,1} + \sigma_y v_{2,2} + \tau_{xy}(v_{1,1} + v_{2,2}))\, dx = \int_\Omega f_i v_i\, dx + \int_{\Gamma_1} g_i v_i\, ds \quad \forall \mathbf{v} \in \mathbf{V}. \tag{6.1}$$

In the case of *plane strain*

$$\begin{bmatrix} \sigma_x \\ \sigma_y \\ \tau_{xy} \end{bmatrix} = \begin{bmatrix} 2\mu + \lambda & \lambda & 0 \\ \lambda & 2\mu + \lambda & 0 \\ 0 & 0 & \mu \end{bmatrix} \begin{bmatrix} \varepsilon_x \\ \varepsilon_y \\ \gamma_{xy} \end{bmatrix}. \tag{6.2}$$

The nonlinear strain tensor $\boldsymbol{\varepsilon}$ is

$$\boldsymbol{\varepsilon} = \begin{bmatrix} \varepsilon_x \\ \varepsilon_y \\ \gamma_{xy} \end{bmatrix} = \mathbf{a} - \mathbf{b} \tag{6.3}$$

where

$$\mathbf{a} = \begin{bmatrix} u_{1,1} \\ u_{2,2} \\ u_{1,2} + u_{2,1} \end{bmatrix} \tag{6.4}$$

is the linear part of $\boldsymbol{\varepsilon}$ and

$$\mathbf{b} = \begin{bmatrix} \frac{1}{2}(u_{1,1}^2 + u_{2,1}^2) \\ \frac{1}{2}(u_{1,2}^2 + u_{2,2}^2) \\ u_{1,1}u_{1,2} + u_{2,1}u_{2,2} \end{bmatrix} \tag{6.5}$$

is the nonlinear part. Substituting (6.2) into (6.1) we get

$$\int_\Omega (2\mu(\varepsilon_x v_{1,1} + \varepsilon_y v_{2,2}) + \mu\gamma_{xy}(v_{1,2} + v_{2,1}) + \lambda(\varepsilon_x + \varepsilon_y)(v_{1,1} + v_{2,2}))\, dx = \int_\Omega f_i v_i\, dx + \int_{\Gamma_1} g_i v_i\, ds \quad \forall \mathbf{v} \in \mathbf{V}. \tag{6.6}$$

Define

$$p = -\lambda(\varepsilon_x + \varepsilon_y), \tag{6.7}$$

and substitute (6.3) and (6.7) into (6.6). We move the nonlinear terms to the right hand side to get

$$2\mu \int_\Omega (a_1 v_{1,1} + a_2 v_{2,2} + \frac{1}{2} a_3(v_{1,2} + v_{2,1}))\, dx - \int_\Omega p(v_{1,1} + v_{2,2})\, dx = \int_\Omega f_i v_i\, dx + \int_{\Gamma_1} g_i v_i\, ds + 2\mu \int_\Omega (b_1 v_{1,1} + b_2 v_{2,2} + \frac{1}{2} b_3(v_{1,2} + v_{2,1}))\, dx. \tag{6.8}$$

Putting (6.7) into variational form, we get

$$\int_\Omega (a_1 + a_2) w\, dx + \lambda^{-1} \int_\Omega pw\, dx = \int_\Omega (b_1 + b_2) w\, dx \quad \forall w \in W. \tag{6.9}$$

The system of equations (6.8) and (6.9) is the variational form of our mixed method. We produce an iterative scheme as follows. Let $\Omega^{(0)}$ designate the reference configuration. Let upper indices "(i)" represent quantities associated with the i^{th} iteration. Then we have: $\mathbf{u}^{(i+1)}$ is the unknown displacement vector to be determined at the i^{th} iteration; $\mathbf{u}^{(i)}$ is the known displacement at the i^{th} iteration; and $\Omega^{(i)}$ and $\Gamma_1^{(i)}$ define the domain and the traction boundary of the deformed configuration at the i^{th} iteration.

Using (6.8) and (6.9) we define the iterative procedure

$$2\mu \int_{\Omega^{(i)}} (a_1^{(i+1)} v_{1,1} + a_2^{(i+1)} v_{2,2} + \frac{1}{2} a_3^{(i+1)} (v_{1,2} + v_{2,1}))\, dx^{(i)} \tag{6.10}$$
$$- \int_{\Omega^{(i)}} p^{(i+1)} (v_{1,1} + v_{2,2})\, dx^{(i)} = \int_{\Omega^{(i)}} f_i v_i\, dx^{(i)} + \int_{\Gamma_1^{(i)}} g_i v_i\, ds^{(i)}$$
$$+ 2\mu \int_{\Omega^{(i)}} (b_1^{(i)} v_{1,1} + b_2^{(i)} v_{2,2} + \frac{1}{2} b_3^{(i)} (v_{1,2} + v_{2,1}))\, dx^{(i)}$$

and

$$\int_{\Omega^{(i)}} (u_{1,1}^{(i+1)} + u_{2,2}^{(i+1)}) w\, dx^{(i)} + \lambda^{-1} \int_{\Omega^{(i)}} p^{(i+1)} w\, dx^{(i)} = \tag{6.11}$$
$$\frac{1}{2} \int_{\Omega^{(i)}} ({u_{1,1}^{(i)}}^2 + {u_{1,2}^{(i)}}^2 + {u_{2,1}^{(i)}}^2 + {u_{2,2}^{(i)}}^2) w\, dx^{(i)}.$$

We use the mixed method spaces MQ1 and first solve the discrete version of (6.10) and (6.11) for $\mathbf{u}_N^{(1)}$ by integrating on the reference configuration $\Omega^{(0)}$, which is the linear problem ($\mathbf{u}_N^{(0)} = \mathbf{0}$). This produces the displacement vector $\mathbf{u}_N^{(1)}$ such that $\Omega^{(1)} = \Omega^{(0)} + \mathbf{u}_N^{(1)}$. Using $\Omega^{(1)}$ we again solve the discrete form of (6.10) and (6.11) for $\mathbf{u}_N^{(2)}$ by integrating on $\Omega^{(1)}$. Continuing in this way, we produce a sequence of solutions $\{\mathbf{u}_N^{(i)}\}$ which converges to $\mathbf{u}_N$, the finite element approximation to the solution to (6.1). We also get p_N, an approximation to p.

At each iteration we have the following system of equations

$$\mathbf{A}\mathbf{u} - \mathbf{B}\mathbf{p} = \mathbf{R}_1 \tag{6.12}$$

$$\mathbf{B}^T\mathbf{u} + \mathbf{C}\mathbf{p} = \mathbf{R}_2. \tag{6.13}$$

On each element, we condense out the pressure by solving (6.13) for $\mathbf{p} = \mathbf{C}^{-1}(\mathbf{R}_2 - \mathbf{B}^T\mathbf{u})$ and substituting into (6.12), giving

$$(\mathbf{A} + \mathbf{B}\mathbf{C}^{-1}\mathbf{B}^T)\mathbf{u} = \mathbf{R}_1 + \mathbf{B}\mathbf{C}^{-1}\mathbf{R}_2. \tag{6.14}$$

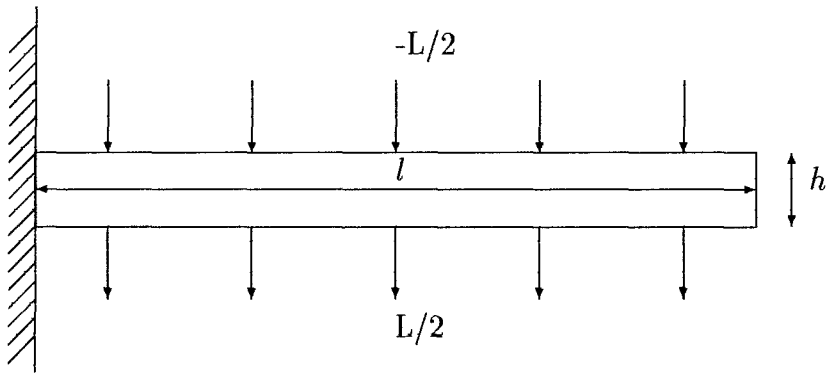

Figure 6.1: Cantilever Subject to Pressure Load

We then solve 6.14 for $\mathbf{u}$. By saving $\mathbf{C}^{-1}, \mathbf{R}_2$ and $\mathbf{B}$ on each element, we can recover $\mathbf{p}$.

Since each iteration involves integrating over a mapped domain, each element in the reference mesh becomes a curvilinear element with potentially no straight edges.

6.2 Numerical Results

We test the mixed method on the problem illustrated in Figure 6.1. A beam of length l and height h is fixed on one end and subject to a uniform pressure load $-L/2$ on top and $L/2$ on bottom. We set body forces $\mathbf{f} = \mathbf{0}$. In [16] this problem and several others are solved using the SFEM spatial formulation. Here, we are interested in the case where $\nu \to \frac{1}{2}$ which was not investigated in [16]. We want to approximate both the displacements and the sum of normal stresses, SNS which is related to p as before,

$$\text{SNS} = \frac{-2(\mu + \lambda)}{\lambda} p.$$

We compute the displacement and SNS for the case when $l = 10$, $h = 1$, modulus

of elasticity $E = 12000$, Poisson ratio $\nu = 0.3$ and 0.4999 and the load $L = 5$. We use SFEM with $V_k(\hat{K}) = Q_k(\hat{K})$ and our mixed method with MQ1; in both cases we use one quadrilateral element. The displacement results are given in Table 6.1.

	Standard Method		Mixed Method	
	$\nu = 0.3$	$\nu = 0.4999$	$\nu = 0.3$	$\nu = 0.4999$
$k = 2$	-2.4590	-0.2838	-2.6317	-2.4947
$k = 3$	-4.0682	-1.1477	-4.2534	-3.6171
$k = 4$	-4.8943	-2.0605	-4.9601	-3.9954
$k = 5$	-5.0443	-3.1704	-5.0731	-4.1209
$k = 6$	-5.0762	-3.6285	-5.0895	-4.1787
$k = 7$	-5.0949	-3.8592	-5.1037	-4.2243
$k = 8$	-5.1042	-4.0128	-5.1390	-4.3200

Table 6.1 Vertical Displacements of Point A.

The displacement for $\nu = 0.3$ is about the same for both methods, with the biggest difference when k is small. However, when $\nu = 0.4999$, the difference is significant, especially for small k. Assuming the results for $k = 8$ are reasonably close to the true solution, we see that the mixed method produces more accurate displacement approximations when k is small.

We are primarily interested in computing point values of SNS when the material is nearly incompressible. We use the standard formulation to extract SNS for ν =0.3

and 0.4999. The results are given in Figure 6.2 for various values of k. These results are qualitatively the same as those in Chapter 3, where the standard method produced highly oscillatory SNS point values as $\nu \to \frac{1}{2}$. We note that the scale for SNS when ν = 0.4999 is $O(10^4)$, 10 times the scale when $\nu = 0.3$. On the other hand, the mixed method produced the results shown in Figure 6.3. Even though the exact solution is not known, we see very intuitive distribution of SNS along the beam (with no qualitative change as $\nu \to \frac{1}{2}$); with a maximum at $x = 0$ smoothly decaying to 0 at the end ($x = 10$) of the beam.

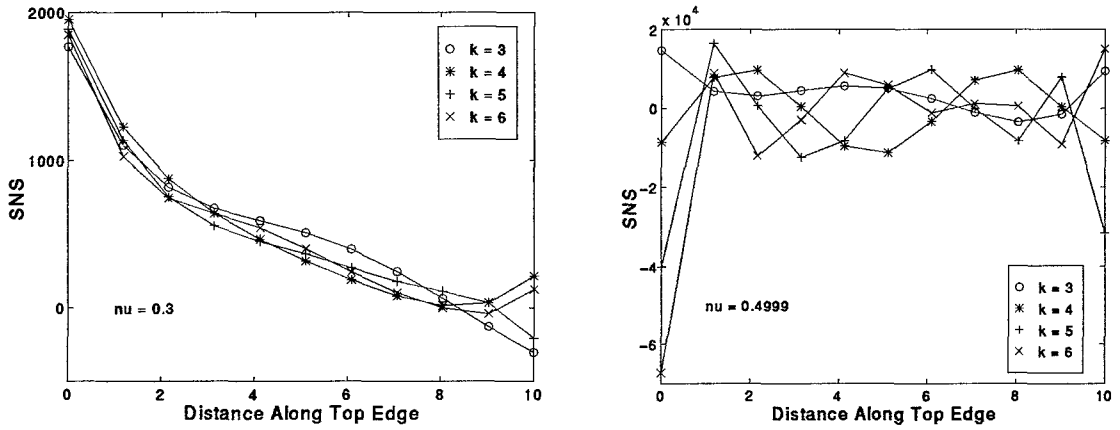

Figure 6.2: SNS on Top Edge, Standard Method

We conclude that mixed methods can effectively eliminate stress locking in some geometrically non-linear problems.

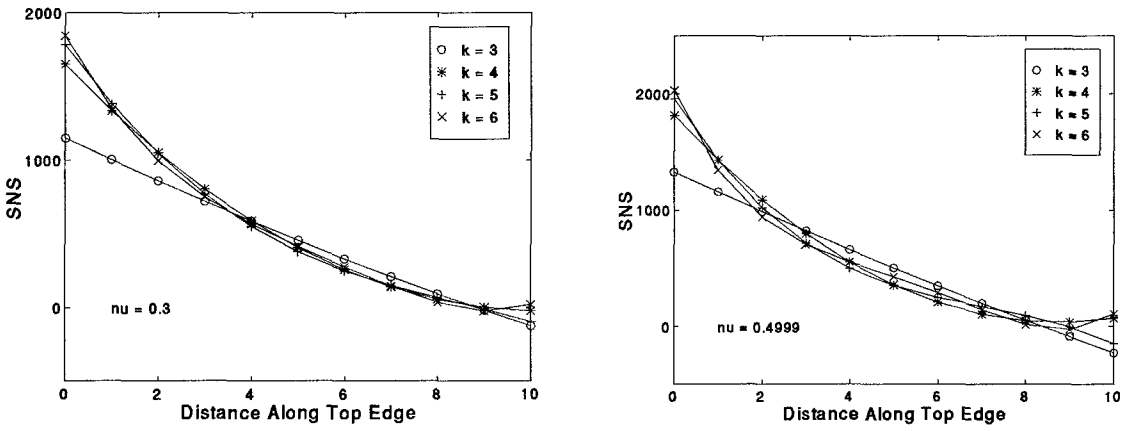

Figure 6.3: SNS on Top Edge, Mixed Method

Bibliography

[1] I. Babuška and M. Suri. Locking effects in the finite element approximation of elasticity problems. *Numer. Math.*, 62:439–463, 1992.

[2] I. Babuška and M. Suri. On locking and robustness in the finite element method. *SIAM J. Num. Anal.*, 29:1261–1293, 1992.

[3] I. Babuška and M. Suri. The p and hp versions of the finite element method, basic principles and proberties. *SIAM Review*, 36:578–632, 1994. No.4.

[4] C. Bernardi and Y. Maday. *Approximations Spectrales de Problemes aux Limites Elliptiques.* Springer-Verlag, New York, 1992.

[5] E. Boillat. On the right inverse for the divergence operator in spaces of continuous piecewise polynomials. M^3AS, 1996.

[6] F. Brezzi and M. Fortin. *Mixed and Hybrid Finite Element Methods.* Springer-Verlag, Berlin, Heidelberg, New York, 1991.

[7] P. G. Ciarlet. *The Finite Element Method For Elliptic Problems.* North-Holland, 1978.

[8] P. Clément. Approximation by finite element functions using local regularization. *R.A.I.R.O.*, 9:77–84, 1975.

[9] L. R. Herrmann. Elasticity equations for compressible and nearly incomprressible materials by a variational theorem. *AIAAJ*, 3:1896–1900, 1963.

[10] S. Jensen and M. Vogelius. Divergence stability in connection with the p-version of the finite element method. *Math. Modelling Numer. Anal.*, 24:734–767, 1990.

[11] P. Le Tallec and A. Patra. Non-overlapping domain decomposition methods for adaptive hp approximations of the stokes problem with discontinuous pressure fields. *TICAM, University of Texas at Austin, TX*, 1996. preprint.

[12] A. E. H. Love. *A Treatise on the Mathematical Theory of Elasticity.* Dover Publications, Inc., New York, 1944. fourth edition.

[13] R. H. MacNeal. *Finite Elements: Their Design and Performance.* Marcel Dekker, Inc., New York, Basel, Hong Kong, 1994.

[14] Y. Maday, A.T. Patera, and E.M. Ronquist. The $\mathbf{P}_N \times \mathbf{P}_{N-2}$ method for the approximation of the stokes problem. *Numer. Math.*, (1994).

[15] N. I. Muskhelishvili. *Some Basic Problems of the Mathematical Theory of Elasticity.* English translation of the 3rd edition by J. R. M. Radok: P. Noordhoff Ltd., Groningen, Holland, 1953. Published in Russian in 1933.

[16] A.T. Noël. Spatial formulation and numerical solution of geometrically nonlinear problems in finite elasticity. *Sever Institute of Washington University, St Louis MO*, 1996. DSc Dissertation.

[17] C. Schwab and M. Suri. Mixed *hp* methods for non-newtonian and stokes flows. to appear.

[18] L. R. Scott and M. Vogelius. Conforming finite element methods for incompressible and nearly incompressible continua. *In:Large Scale Computations in Fluid Mechanics. Lectures in Applied Mathematics*, 22:221–244, 1985. Part 2, AMS, Providence, RI.

[19] L. R. Scott and M. Vogelius. Norm estimates for a maximal right inverse of the divergence operator in spaces of piecewise polynomials. *Math. Modeling Num. Anal.*, 19:111–143, 1985.

[20] R. Stenberg and M. Suri. Mixed *hp* finite element methods for problems in elasticity and stokes flow. *Numer. Math.*, 72:367–389, 1996.

[21] M. Suri. The *p*-version of the finite element method for elloptic equations of order 2*l*. *Mathematical Modelling and Numerical Analysis*, 24:265–304, 1990.

[22] M. Suri. Analytic and computational assessment of locking in the *hp* finite element method. *Computer Methods in Applied Mechanics and Engineering*, 1995.

[23] T. Sussman and K. Bathe. A finite element formulation for nonlinear incompressible elastic and inelastic analysis. *Computers and Structures*, 26, 1/2:357–409, 1987.

[24] B. Szabo and I. Babuška. *Finite Element Analysis.* J. Wiley and Sons, New York, 1991.

[25] B. Szabo, I. Babuška, and B. K. Chayapathy. Stress computations for nearly incompressible materials by the *p*-version of the finite element method. *Int. J. Num. Meth. Eng.*, 28:2175–90, 1989.

[26] M. Vogelius. An analysis of the *p*-version of the finite element method for nearly incompressible materials - uniformly valid, optimal error estimates. *Numer. Math.*, 41:39–53, 1983.